

**DAMAGE MODELLING FOR PERFORMANCE-BASED EARTHQUAKE
ENGINEERING**

by

Abbas Javaherian Yazdi

B.Sc., University of Tehran, 2007

M.Sc., University of Tehran, 2010

A THESIS SUBMITTED IN PARTIAL FULFILLMENT OF
THE REQUIREMENTS FOR THE DEGREE OF

DOCTOR OF PHILOSOPHY

in

THE FACULTY OF GRADUATE AND POSTDOCTORAL STUDIES
(Civil Engineering)

THE UNIVERSITY OF BRITISH COLUMBIA
(Vancouver)

November 2015

© Abbas Javaherian Yazdi, 2015

ABSTRACT

The overarching objective in this work is to advance damage modelling for performance-based earthquake engineering. To achieve this objective, this thesis provides a new vision, technique, and software framework for the assessment of seismic damage and loss to building components. The advent of performance-based earthquake engineering placed a renewed emphasis on the assessment of damage and monetary loss in structural engineering. Assessment of seismic damage and loss for decision making entails two ingredients. First, models that predict the detailed damage to building components; second, a probabilistic framework that simulates damage and delivers the monetary loss for the reliability, risk, and optimization analysis. This motivates the contributions in this thesis, which are summarized in the following paragraphs.

First, a literature review is conducted on models, techniques and experimental studies that address component damage due to earthquakes. The existing approaches for prediction of the seismic damage, repair actions, and costs are examined. The objective in this part is to establish a knowledge bank that facilitates the subsequent development of probabilistic models for seismic damage.

Second, a logistic regression technique is employed for developing multivariate models that predict the probability of sustaining discrete damage states. It is demonstrated that the logistic regression remedies several shortcomings in univariate damage models, such as univariate fragility curves. The multivariate damage models are developed for reinforced concrete shear walls using experimental data. A search algorithm for model selection is

included. It is found that inter-story drift and aspect ratio of walls are amongst the most influential parameters on the damage.

Third, an object-oriented software framework for detailed simulation of visual damage is developed. The work builds on the existing software Rt. Emphasis is on the software framework, which facilitates detailed simulation of component behaviour, including visual damage. Information about visual damage allows the prediction of repair actions, which in turn improves our ability to predict the time and cost of repair.

PREFACE

Chapters 2 and 4 of this thesis are developed by the author of this thesis under supervision of Dr. Terje Haukaas. The same is the case for Chapter 3, which is the basis for a journal paper accepted for publication in *Earthquake Spectra*:

- Javaherian Yazdi, A., Haukaas, T., Yang, T.Y., Gardoni, P. “Multivariate Fragility Models for Earthquake Engineering”. DOI: 10.1193/061314EQS085M.

The above-mentioned paper is prepared in a collaborative effort with Dr. Terje Haukaas and Dr. Tony Yang from the University of British Columbia and Dr. Paolo Gardoni from the University of Illinois at Urbana-Champaign. The author of this thesis is responsible for the literature review, deriving equations, developing models, computer programming, data collection and process, performing analysis, and interpreting the results. This thesis is drafted by the author and finalized in an iterative process with the PhD research supervisor, Dr. Terje Haukaas. The author of this thesis is entirely accountable for preparing tables and figures.

TABLE OF CONTENTS

Abstract.....	ii
Preface.....	iv
Table of Contents	v
List of Tables	viii
List of Figures.....	x
Acknowledgments	xiii
Dedication	xv
Chapter 1: Introduction	1
1.1 Long-term Vision.....	1
1.2 Short-term Objectives	6
1.3 Motivation and Justification	7
1.4 Scope.....	8
1.5 Overview of Thesis and Contributions	9
1.5.1 Literature Review on Seismic Damage Models.....	9
1.5.2 Development of Multivariate Fragility Models	10
1.5.3 Software Framework for Simulation of Visual Damage	11
Chapter 2: Literature Review on Seismic Damage Models	12
2.1 Overview of Seismic Damage Modeling.....	12
2.1.1 Continuous Damage Measures	13
2.1.2 Discrete Damage Measures.....	20
2.2 Existing Models for Visual Damage.....	24

2.3	Existing Models for Repair Action	37
2.4	Existing Models for Cost of Repair	40
2.5	Existing Models for Time of Repair	45
Chapter 3: Multivariate Fragility Models for Earthquake Engineering.....		47
3.1	Approaches for Damage Modeling in PBEE	49
3.2	Approaches to Establish Fragility Functions	52
3.3	Approaches to Conduct Logistic Regression.....	56
3.4	Binomial Logistic Regression.....	58
3.5	Multinomial Logistic Regression.....	59
3.6	Illustrative Example	61
3.7	Damage Models for RC Shear Walls.....	64
3.8	Appraisal of Drift as Damage Indicator.....	70
3.9	Model Selection Procedure	77
3.10	Model Application	83
3.11	Conclusions.....	86
Chapter 4: Simulation of Visual Damage to Building Components		88
4.1	A New Building Component Concept	89
4.2	Library of Components.....	91
4.3	Model Development.....	94
4.3.1	RC Column Component.....	97
4.3.2	RC Shear Wall Component.....	103
4.4	Coordination of Repair	107
4.5	Demonstration Examples	110

4.5.1	Example 1: Push-over Analysis of Cantilevered RC Column	111
4.5.2	Example 2: Cantilevered RC Column Subjected to Cyclic Loading....	115
4.5.3	Example 3: Cantilevered RC Shear Wall Subjected to Lateral Load ...	117
4.5.4	Example 4: One Story Building Subjected to Lateral Load	119
4.6	Conclusions.....	123
Chapter 5: Conclusions and Future Work		124
5.1	Overview of the Research Approach	124
5.2	Future Research Directions.....	126
Bibliography		130
Appendix A Reinforced Concrete Shear Wall Database		150
Appendix B Communication of Component Class with Structural Analysis		156

LIST OF TABLES

Table 2-1. Range of Park and Ang's damage index versus seismic damage (Park <i>et al.</i> 1987).	16
Table 2-2. Damage states and damage factors in ATC-13 (Applied Technology Council 1985).....	27
Table 2-3. Visual damage scenarios for RC columns (Berry <i>et al.</i> 2004).....	30
Table 2-4. Visual damage, repair actions and damage predictors for bridge columns (Berry <i>et al.</i> 2008).	31
Table 2-5. Visual damage for bridge columns (Lehman <i>et al.</i> 2004).....	32
Table 2-6. Visual damage and repair actions for RC shear wall (Brown 2008).....	33
Table 2-7. Visual damage and repair actions for RC beam-column joint (Pagni and Lowes 2006).	35
Table 2-8. Report of damaging earthquakes for 2011 from CATDAT.	43
Table 3-1. Artificial data to illustrate problems with closed-form solutions.....	57
Table 3-2. Illustration of the data-format that is available in practical problems.....	58
Table 3-3. Set of artificially generated data for illustration exercise.....	62
Table 3-4. Damage state allocation for the observation in the first row of the table in the Appendix.....	70
Table 3-5. List of explanatory functions.....	72
Table 3-6. Statistics of the model parameters, given 2 drift-observations, θ_4 , θ_5 , and θ_6 have unit 1/MPa.....	75

Table 3-7. Statistics of the model parameters, given 5 drift-observations, θ_4 , θ_5 , and θ_6 have unit 1/MPa.....	75
Table 3-8. Model parameters for the final model.	82
Table 4-1. Visual damage scenarios versus repair actions for RC components.	96
Table 4-2. Mean value of parameters in Eq. (4-4) and Eq. (4-5).....	112
Table 4-3. Mean value of parameters and key strain variables in Eqs. (4-6) to (4-9).	117
Table 4-4. Repair actions and repair quantities at different drift ratios.	122
Table A-1. Database of test data for RC shear wall.....	150

LIST OF FIGURES

Figure 1-1. Reliability-based optimization analysis with multiple cost models.	3
Figure 1-2. From visual damage to repair cost.	4
Figure 1-3. Visualization of damage in Rts.	5
Figure 3-1. Fragility functions (Yang <i>et al.</i> 2009).	52
Figure 3-2. The logit function.	56
Figure 3-3. Backbone curve from cyclic testing (Pilakoutas and Elnashai 1995).	65
Figure 3-4. Reinforced concrete shear wall.	66
Figure 3-5. Damage states relative to backbone curve.	67
Figure 3-6. The visual damage observed during cyclic test of the wall whose hysteretic curve is shown in Figure 3-3 (Pilakoutas and Elnashai 1995).	68
Figure 3-7. Two observed drift-values for each damage state.	69
Figure 3-8. Five observed drift-values for each damage state.	69
Figure 3-9. Frequency diagram and PDF for drift.	71
Figure 3-10. Variation of damage probabilities with δ for a specific shear wall.	76
Figure 3-11. Confidence bands for damage probabilities: a) 2 δ -values in each damage state; b) 5 δ -values in each damage state.	77
Figure 3-12. Model selection algorithm.	80
Figure 3-13. Stepwise deletion process to obtain a parsimonious model.	81
Figure 3-14. Change in the residual deviance of the multinomial logistic regression models in each iteration of deletion process.	82

Figure 3-15. Variation of damage probabilities with δ for a specific shear wall.....	85
Figure 3-16. Variation of fragility probabilities with δ , h_w/l_w , f_{yl} , and ρ_{hw} for a specific shear wall.....	86
Figure 4-1. Traditional finite element versus building component class.....	90
Figure 4-2. Fragility specification for RC walls: basic identifier information (Applied Technology Council 2012).	92
Figure 4-3. Fragility specification for RC walls: parameters of log-normal fragility function, repair cost and time (Applied Technology Council 2012).....	93
Figure 4-4. Visual damage scenarios for RC components: (a) Concrete cracking; (b) Cover concrete spalling; (c) Cover concrete falling; (d) Reinforcement bar buckling/fracture (Berry <i>et al.</i> 2008; Pagni and Lowes 2006; Brown and Lowes 2007).....	95
Figure 4-5. Segments of RC column component for which visual damage is simulated; segments are numbered from bottom to top and counter clockwise.....	98
Figure 4-6. RC shear wall component; the segment mesh is shown by solid lines; the finite element mesh is shown by the dashed lines.....	105
Figure 4-7. Simulation of damage and assessment of earthquake cost in Rts.	109
Figure 4-8. Fibre-discretized cross-section for RC column component.	111
Figure 4-9. Snapshot of Rts: Push-over curve and visual damage for RC column component.	113
Figure 4-10. Push-over curve and visual damage on the four segments of the RC column component: compression and tension sides.	114
Figure 4-11. Rts snapshot: Cyclic loading versus visual damage in each segment.	115

Figure 4-12. Cyclic loading and visual damage on the four segments of the RC column component: East and west sides..... 116

Figure 4-13. The wall component dimensions and segments. 118

Figure 4-14. Visual damage to RC shear wall component: a) $\delta=1\%$; b) $\delta=1.5\%$; c) $\delta=2\%$. 119

Figure 4-15. Plan view of building. 120

Figure 4-16. Elevation view of building. 120

Figure 4-17. Visual damage on columns and shear walls at three inter-story drift ratios: a) $\delta=1\%$; b) $\delta=1.5\%$; c) $\delta=2\%$ 121

Figure B-1. Class map of Rts building analysis: the inheritance and composition relationship. 157

Figure B-2. The communication of RComponent class with structural analysis in Rts. 159

Figure B-1. Class map of Rts building analysis: the inheritance and composition relationship. 157

Figure B-2. The communication of RComponent class with structural analysis in Rts. 159

ACKNOWLEDGMENTS

I would like to express my profound gratitude to my supervisor, Dr. Terje Haukaas, for his extensive knowledge, his generosity with his time, constant support, and encouragement during my PhD studies. I am indebted to Dr. Haukaas for his outstanding guidance in this research and sharing his invaluable experience with me. I would also like to extend my appreciation to the members of my PhD supervisory committee: Dr. Ricardo Foschi for insightful discussions and comments during Reliability Seminars, Dr. Carlos Ventura for his encouragements and giving me the access to the database of the MATRIX project, and Dr. Tony Yang for teaching me several things about reinforced concrete structures and providing me the test database for shear walls.

I gratefully thank Dr. Paolo Gardoni from the University of Illinois at Urbana-Champaign for teaching me several things about earthquake engineering, his vast knowledge, and enlightening discussions about damage modelling. I graciously acknowledge the financial support from the Natural Science and Engineering Research Council of Canada (NSERC) and the Canadian Precast/Prestressed Concrete Institute (CPCI).

I would also like to appreciatively recognize my colleagues and fellow students at the Department of Civil Engineering for their help and joyful company. Many thanks go to Mojtaba, Majid, Sepideh, Sai, Alfred, Vasantha, Amir Hossein, Amin, Laura, Saeid, and Meraj. I am utterly thankful to my dear and very close friends. First and foremost I would like to thank Mohammad Sajjad and Ehsan, great friends who were my family here in Vancouver. Special thanks go to Navid, Shahram, Ardavan, Hossein, and Salman.

I am eternally indebted and grateful to my father, Jalal Javaherian Yazdi, and my mother, Zahra Rahighi Yazdi, for their unconditional love, support, and encouragement in every step of my life. Their unfaltering faith in me and calming words provided me with stamina to press forward whenever I felt exhausted and overwhelmed. Words cannot express my appreciation to them. Last but not least, I would like to gratefully thank my sisters, Maryam and Fatemeh, for their love and inspiration, which never diminished by the long distance between us.

DEDICATION

To my beloved mother and father

Chapter 1: INTRODUCTION

The overarching objective in this thesis is to improve damage modelling for performance-based earthquake engineering (PBEE). This objective is aligned with the long-term vision in this thesis, *i.e.*, simulation of the built environment, particularly the events that can occur in the lifespan of a building. Examples of such events include extreme loading, deterioration, earthquake damage, direct and indirect monetary losses, and environmental impacts of the constructions. The simulation of these events serves as a basis for the assessment of building performance, and it facilitates quantification and mitigation of risk. The focus in this thesis is earthquake damage.

1.1 LONG-TERM VISION

The vision behind this thesis includes the detailed simulation of buildings at the component level, encompassing a wide range of the performance indicators. These include construction cost, manufacturing cost, environmental impact costs, cost of earthquake damage, *etc.* The assessment of such performance indicators is rife with uncertainty. Therefore, probabilistic methods and models are utilized. In particular, the vision adopted in this thesis includes the use of reliability-based methods; hence, uncertainties are characterized by random variables and the models simulate physical responses, such as ground motions, structural responses, and costs.

That vision entails the development and implementation of several interacting models. Those models, and possibly their gradients, are repeatedly evaluated during the course of reliability and optimization analysis. The evaluation of each model demands trial

realization of input random variables and evaluation of “upstream” models whose responses are input for the downstream model. Algorithms for conducting reliability analysis in this manner with multiple interacting models are implemented in the computer program Rt (Mahsuli and Haukaas 2013). In this thesis, models for simulation of component response, component damage, and component repair cost are implemented in the second version of Rt, called “Rts”. The added “s” has two implications. First, it implies that Rts is the second version of Rt. Second, it signals the inclusion of structural analysis in the extended software. This chapter presents background information about Rts, while the simulation of damage to building components is explained in Chapter 4.

Figure 1-1 depicts the analysis that is envisioned in Rts. Rectangular boxes show the models that are evaluated during a reliability-based optimization analysis. Each arrow indicates a model output delivered to the downstream model. An important aspect of the analysis is that it accommodates several cost models. As a schematic example, there are three cost models in Figure 1-1: 1) Environmental impact model, which outputs the cost of emissions, c_e , to the environment in the lifespan of building; 2) Construction/manufacturing model, which outputs the cost of building construction and manufacturing cost, c_c ; and 3) Repair model, which outputs the repair cost, c_r , for damage that the building may sustain over its lifespan. The building components provide information needed for these cost assessments.

The total cost, c , which itself is a random variable, is delivered to the reliability model, where the probability of exceeding different thresholds, p , is computed. Essentially, this establishes the “loss curve,” *i.e.*, the complementary cumulative distribution function for the total cost. In turn, the risk model outputs a risk measure: the risk measure presented in

Figure 1-1 is the mean of the total cost, μ_c , which is the area under the loss curve (Der Kiureghian 2005; Yang *et al.* 2009). One could also consider other risk measures, as discussed by Haukaas *et al.* (2013). The last model in Figure 1-1 is the optimization analysis, which minimizes the risk measure, *e.g.*, μ_c .

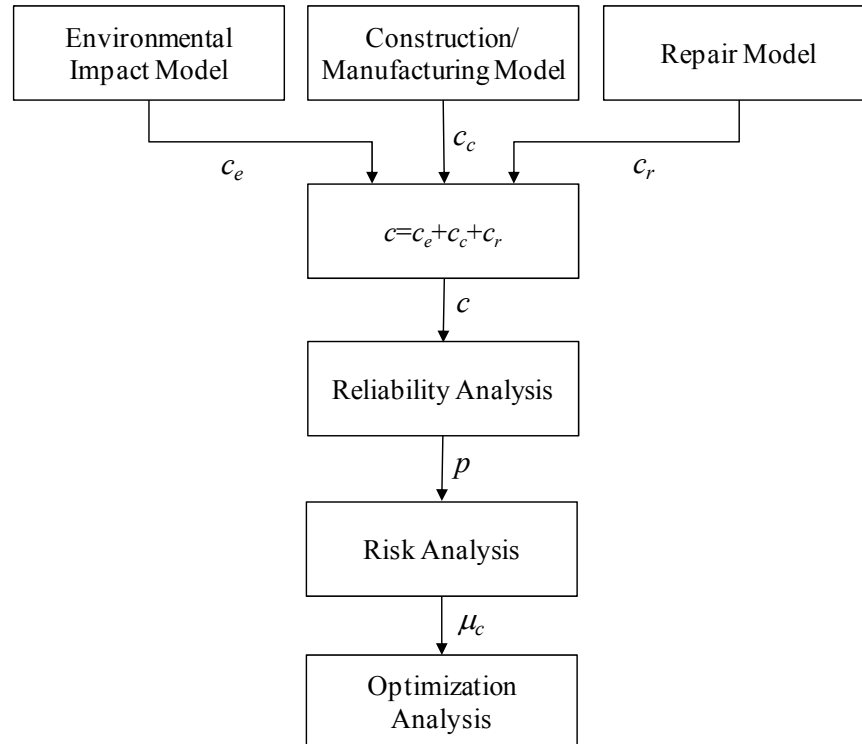


Figure 1-1. Reliability-based optimization analysis with multiple cost models.

In PBEE, the performance assessment of buildings and facilities is disaggregated into four models (Moehle and Deierlein 2004): ground motion model, structural response model, damage model, and loss model. In contrast with traditional code-based structural engineering, the forecasting of damage and monetary loss are in focus in PBEE. In fact, the invention of PBEE has placed a renewed emphasis on damage modelling. In PBEE, the output of damage models serves as input for loss models. Loss has three major constituents (Applied Technology Council 2012): 1) Casualties, which includes deaths and injuries that necessitate

hospitalization; 2) Repair cost, which includes the cost of repairing or replacing facilities and their contents; 3) Downtime, which implies the period of time in which a facility cannot be used or does not function properly as a result of damage.

To facilitate the prediction of loss, in this thesis a new vision for seismic damage assessment is adopted. Figure 1-2 depicts the sequence of damage and loss assessments in the new vision. In this paradigm it is recognized that the *repair action* is the key input for predicting cost and downtime associated with damage. In reality, all repair actions are determined based on the visual signs of damage. Hence, in this thesis the focus in the damage modelling is shifted to the prediction of visual damage. In turn, the repair cost is obtained from the repair action, simply summing the cost of material and labour to conduct the predicted repair action. Similarly, the cost due to interruption in functionality of the building is assessed from the time it takes to complete the predicted repair action.

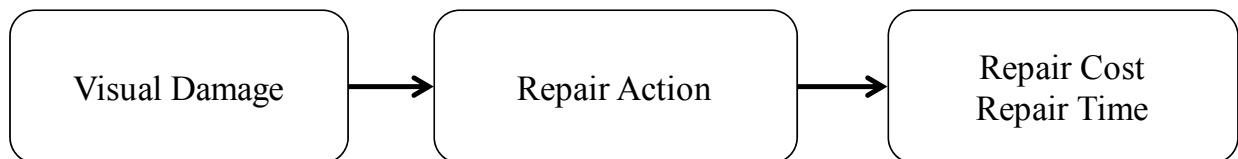


Figure 1-2. From visual damage to repair cost.

Visual signs of damage have been the basis for characterizing damage in several references (Applied Technology Council 2012; Federal Emergency Management Agency 2007; Krawinkler 1987; Park *et al.* 1987). The visual damage is different for different components. For a reinforced concrete (RC) shear wall, the visual damage is related to the severity of cracks, spalling of concrete, buckling of longitudinal reinforcement, and so forth (Applied Technology Council 2012; Park *et al.* 1987). Thus, the objective of a damage model

for that component should be to predict the severity of cracks and the possibility of reinforcement buckling during an earthquake. In contrast, for steel components the visual damage is defined as the local buckling of flange and web and the progress of cracks due to fatigue (Krawinkler and Zohrei 1983). On the other hand, for a non-structural component like a window, breaking of the glass is a possible realization for the visual damage.

Figure 1-3 is an excerpt from an Rts screenshot, which shows an example of detailed simulation of visual damage implemented in this thesis. In that figure, the damage to a reinforced concrete building is visualized. Although the detailed discussion of visual damage for reinforced concrete components is provided in the next chapters, it is noted that each color in Figure 1-3 indicates a particular visual damage in the segments of the reinforced concrete columns and core shear wall. This image symbolizes the long-term vision of this thesis.

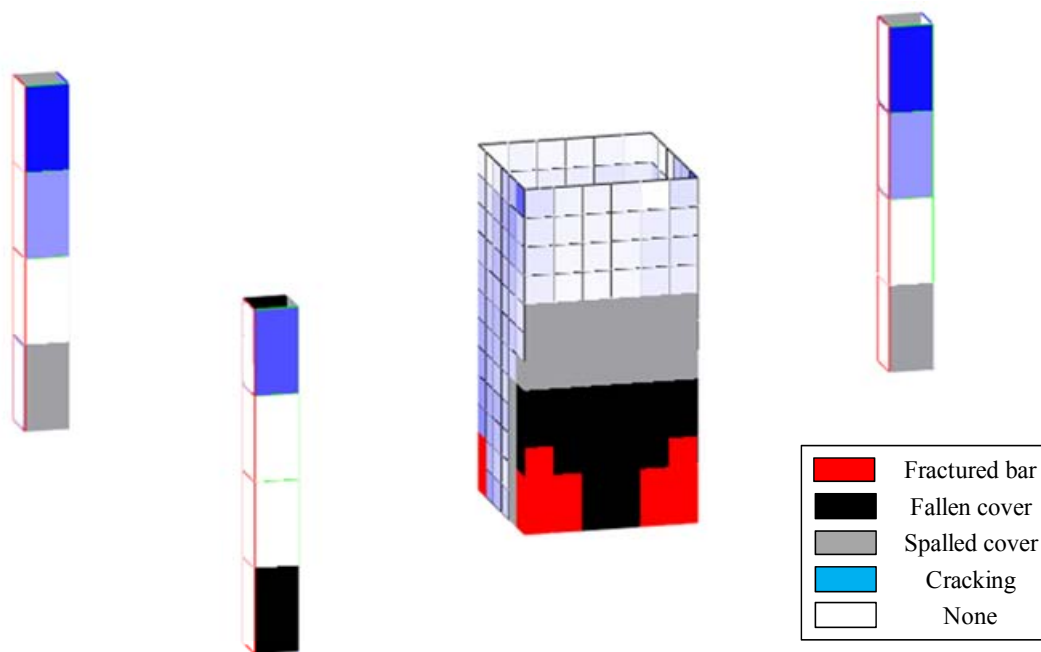


Figure 1-3. Visualization of damage in Rts.

1.2 SHORT-TERM OBJECTIVES

Damage modelling for two approaches in PBEE is conducted in this thesis. The first approach employs fragility functions, such as the methodology developed in the ATC-58 project (Yang *et al.* 2009). In this approach, fragility functions are used as damage model. These functions take a single structural response as input and output the probability of sustaining different discrete damage states. They are developed at the component-level in the ATC-58 project. The first short-term objective in this thesis is to extend the univariate fragility functions to a multivariate model. This is important because a multivariate model predicts the damage probabilities considering the effect of multiple variables that may all influence the level of damage, including structural responses, material properties, and geometry parameters.

The second approach for PBEE is the reliability-based scheme presented in the previous section, where the focus is on prediction of visual damage. Therefore, the second short-term objective in this thesis is to simulate visual damage to building components during an earthquake. This leads to several sub-objectives that are addressed in this study:

- Investigate the literature to examine which existing damage models can be employed for simulation of visual damage
- Explore the literature to identify existing models for repair actions, repair quantities, and repair cost
- Develop a software framework for simulation of visual damage to building components

- Formulate, in that software framework, a consistent model format for simulation of visual damage
- Implement, in the same software framework, models that predicts the repair actions and quantities to be repaired, again at the component-level

1.3 MOTIVATION AND JUSTIFICATION

The motivation in this study is multifold. The primary motivation is the need for enhancement and improvement of the state-of-the-art in models for PBEE. In contrast with the classical code-oriented approach, which tackles the uncertainties by conservative bias and safety factors, PBEE seeks the actual performance. The actual performance includes a broad range of earthquake consequences. These consequences have brought new measures, such as repair costs, down time, monetary loss, casualties, *etc.* into focus in earthquake engineering. The prediction of these measures requires robust predictive models. In fact, the introduction of PBEE has placed a renewed emphasis on damage modelling, and this serves as the key motivation for this work.

In PBEE, the uncertainties are not only present in the prediction of the occurrence and intensity of the ground motions but also in the assessment of damage. Furthermore, it is understood that the extent of seismic damage is affected by several structural parameters. These structural parameters introduce new uncertainty to the prediction of seismic damage. Consequently, there is a need for damage models and modelling techniques that candidly identify the influential variables and account for the uncertainties. The development of such damage models is in focus in this thesis.

Another motivation is the need for tools that help engineers quantify and mitigate the risk. The detailed simulation of seismic damage and ensuing costs are important ingredients in the risk-based analysis framework presented earlier as a long-term vision. From this viewpoint, the simulation of damage is essential to assess the direct and indirect cost of repair. This information is critical for risk-based design; however, it is not available in the current codified engineering design.

1.4 SCOPE

Because the context of this thesis is PBEE, seismic damage models are in focus. This excludes damage due to other events, *e.g.*, wind, traffic, deterioration, impact, corrosion, *etc.* As stated before, the objective is to simulate detailed seismic damage; therefore, all models and simulations are implemented at the building component-level. Thus, the global structural damage, *i.e.*, the structural stiffness reduction and strength degradation, collapse, and change in the structural dynamic characteristics, is outside the scope of this thesis.

In this thesis, “repair” is referred to as the series of actions to bring the damaged component to its undamaged state. In this context, repair does not include any action to retrofit and improve mechanical properties of the component.

In the assessment of earthquake cost, the cost of repair is directly linked to damage. However, there are several other earthquake consequences, such as downtime, casualty, business interruption due to repair, change in the availability of materials and workforce for repair, surge in demand for construction and accommodation, surge in inflation, *etc.* that impose additional cost. Such additional costs are often referred to as indirect costs. These consequences sometimes have more significant influence on the overall earthquake cost than

the direct repair cost. Also, they may affect the stakeholders' decision on the repair and demolition of the building. The assessment of indirect cost of earthquake consequences is not considered in this thesis.

1.5 OVERVIEW OF THESIS AND CONTRIBUTIONS

This section describes the organization of this thesis and explains how each chapter addresses the research objectives outlined above.

1.5.1 Literature Review on Seismic Damage Models

In Chapter 2, a review on the seismic damage models is conducted to investigate how the existing works support the new vision. Two damage models are examined: First, damage indices, which represent the extent of seismic damage in terms of a value from zero to one. Second, fragility functions, which represent the probability of damage given the value of a structural response. It is observed that majority of damage indices assess damage in deterministic manner by representing the ratio of some seismic demand to capacity. Also, it is seen that the fragility functions are univariate models that ignore the effect of structural parameters on the damage. To address this shortcoming, a method for developing multivariate fragility functions is outlined in Chapter 3. Several articles that address the visual damage to building components are explored. This entails the experimental studies that report visual damage and existing models that measure the visual damage at the component level. In that chapter, the articles that explore the repair actions are also explored. A large body of the literature focuses on the repair actions for reinforced masonry and concrete components. The repair cost and the cost of earthquake are reviewed in a separate section in Chapter 2. It is observed that several researchers have been estimating the cost of

repair as the ratio of repair cost to the replacement cost. Also, the repair cost is normally evaluated holistically for buildings and limited research conducted to estimate the cost of repair for each component. The last section in Chapter 2 explores the literature on the repair time. Researchers have found that the time of repair is the most challenging parts of performance assessments and several socioeconomic factors affect the time of repair. Similar to repair action, the time of repair is generally recorded and evaluated for buildings rather than components separately.

1.5.2 Development of Multivariate Fragility Models

A new method for developing multivariate damage models that predict the damage probability is suggested in Chapter 3. Specifically, the logistic regression is employed to extend the univariate fragility functions that are prevalent in PBEE to a multivariate model. The maximum likelihood method is utilized to estimate model parameters as well as several model inferences that are employed to evaluate the quality of the model. The multivariate damage models for reinforced concrete shear walls are developed using a database of 146 experiments. An algorithm for model selection is employed to evaluate the effect of different parameters on the damage. It is observed that the inter-story drift ratio and aspect ratio of the wall are amongst most influential parameters on the damage probability. That is, the wall with higher aspect ratio can tolerate more drift before sustaining damage. It is found that the multivariate damage models have several advantages and remove shortcomings that are seen in univariate model. A summary of these advantages is:

- The multivariate damage models can be developed with more limited number of tests in comparison with the univariate models

- In contrast with the lognormal fragility functions that may cross and lead to negative probability, the multivariate models do not predict negative probabilities
- With the multivariate models, the modeller is able to evaluate and expose different variables that affect the damage
- The multivariate models can readily be used in the ATC-58 framework (Yang *et al.* 2009) for PBEE analysis.

1.5.3 Software Framework for Simulation of Visual Damage

A new software framework for simulation of building components is developed. The framework is tailored to assess a wide range of component design costs. These costs include the cost of construction and manufacturing, environmental impacts, repairs and demolitions. The simulation of visual damage due to earthquake loading is conducted. The damage models are employed to simulate the possible visual damage scenarios in detail at different “segments” of the component. The repair action model receives the output of visual damage models and outputs the required repair actions for each component in building and the rigorous assessment of repair quantities. Four examples are provided to demonstrate the simulation of the visual damage to the reinforced concrete column and reinforced concrete shear wall components. The component entity is intended to develop a new library of building components. The new component library will include a wide range of component-specific refined models for assessment of the construction cost, environmental impacts, visual damage, repair actions, and quantities that should be repaired. The work builds on the existing computer program Rt and promotes the risk-based optimal design approach presented in this chapter.

Chapter 2: LITERATURE REVIEW ON SEISMIC DAMAGE MODELS

This chapter provides an overview of the literature on the seismic damage modelling. The objective is to identify the existing damage models, experimental studies, and repair methods that facilitate the prediction of visual damage envisioned in Chapter 1. In the following, existing damage models for discrete and continuous measures are first examined. Two major damage models are examined: Damage indices and fragility functions. Thereafter, the models, methods, and experimental data that address visual damage are explored. Finally, the existing literature on the cost of repair and the required time for restoration of buildings and facilities after an earthquake are investigated. It is noted that the assessment of damage, repair cost, and repair time are associated with substantial and inevitable uncertainty. Probabilistic models and methods are needed to estimate these measures in an unbiased manner. As a result, particular attention is placed on the consideration of uncertainties in the review conducted here.

2.1 OVERVIEW OF SEISMIC DAMAGE MODELING

Existing seismic damage models predict damage in terms of either discrete or continuous damage measures. Several published articles (Applied Technology Council 2012; Applied Technology Council 1985; Federal Emergency Management Agency 1997; Federal Emergency Management Agency 2000; Park *et al.* 1987; Stone and Taylor 1993) prescribe discrete damage states for characterizing the level of seismic damage. This is probably the most well-known approach for damage assessment. While the actual damage often occurs as a continuous function of structural responses (Applied Technology Council 2012; Singhal

and Kiremidjian 1996; Kircher *et al.* 1997), several reasons justify the prescription of discrete damage states. First, they are appealing for developing damage models that produce probability as output. Second, they facilitate loss predictions because although the actual damage is a continuum, the associated repair action is not a continuous function of damage (Applied Technology Council 2012). This is because when the severity of seismic damage exceeds certain thresholds the required repair action changes. Third, the discrete damage states facilitate damage assessment of facilities in the post earthquake reconnaissance, where experts are asked to evaluate the level of damage to facilities. The Applied Technology Council (1989) provided guidance on the safety evaluation of buildings after earthquake. According to this guideline, buildings are labeled by three different placards: A red placard means “unsafe,” implying that it should not be entered; a yellow placard means “restricted use,” implying that a clearly unsafe condition does not exist but the observed damage precludes unrestricted occupancy; and a green placard means “inspected,” implying that the building may be safely occupied. In the subsequent sections the damage models for continuous and discrete measures are reviewed.

2.1.1 Continuous Damage Measures

In this section the models that predict continuous damage measures are in focus. The framework formula adopted by the researchers in the Pacific Earthquake Engineering Research Center employs a continuous measure for damage (Cornell and Krawinkler 2000; Der Kiureghian 2005). This damage measure, dm , is one of four constituents in the formulation that has become known as the PEER equation:

$$G(dv) = \int_0^{\infty} \int_0^{\infty} \int_0^{\infty} G(dv | dm) \cdot f(dm | edp) \cdot f(edp | im) \cdot f(im) \cdot ddm \cdot dedp \cdot dim \quad (2-1)$$

In this equation, which is based on the theorem of total probability, G =complementary cumulative distribution function, f =probability density function, dv =decision variable, edp =engineering demand parameter, and im =intensity measure. All models in Eq. (2-1) are conditional probabilities except $f(im)$. In particular, the damage model is the probability that the damage measure is equal to dm , given a value of edp .

Another category of continuous measures of damage is referred to as damage indices. A damage index represents the severity of damage in terms of a value between 0, *i.e.*, no damaged, and 1, *i.e.*, collapsed. For concrete components, damage indices often represent a ratio of demand parameters to capacities. In contrast, the concept of low cycle fatigue has been in focus for developing damage indices for steel structural components (Krawinkler 1987). The weighted average of local indices and the change in the overall stiffness of the structure have been used to formulate damage index for global structures. Several damage indices are proposed in the literature and Williams and Sexsmith (1995) provided a comprehensive overview. In the following, a brief overview of the most commonly used damage indices is provided.

Powell and Allahabadi (1988) proposed a damage index, DI_p , based on the deformation demand and capacity

$$DI_p = \frac{u_{max} - u_y}{u_u - u_y} = \frac{\mu_{max} - 1}{\mu_u - 1} \quad (2-2)$$

where u_{max} =maximum deformation during an earthquake; u_y =yield deformation capacity under monotonic loading; u_u =ultimate deformation capacity under monotonic loading; μ_{max} =maximum deformation ductility demand during earthquake; μ_u =ultimate deformation ductility capacity under monotonic loading. The validity of the last equality in Eq. (2-2)

becomes apparent by dividing the numerator and denominator of the first fraction by u_y . It is observed that DI_P is zero when the displacement equals u_y , while DI_P is unity when the displacement equals u_u . However, as Mahin and Bertero (1981) discussed, the maximum deformation ductility cannot alone represent the cumulative effects of number of cycles of inelastic deformation and hysteretic energy dissipation demand. In fact, Kratzig and Meskouris (1997) demonstrated that μ_{max} is not a robust indicator of damage. Therefore, other demand parameters are considered in the damage indices reviewed below.

Fajfar (1992) developed a damage index based on dissipated hysteretic energy in elastic-perfectly-plastic systems. The developed damage index reads

$$DI_F = \frac{E_h}{E_u} \quad (2-3)$$

where E_h =total dissipated hysteretic energy under earthquake load and E_u =dissipated hysteretic energy under monotonic loading to the ultimate deformation ductility capacity. Hysteretic energy is also an important ingredient in the well-known and widely used damage index for reinforced concrete, developed by Park and Ang (1985). Their damage index reflects the effect of both maximum deformation and total hysteretic energy dissipation:

$$DI_{PA} = \frac{u_{max}}{u_u} + \frac{\beta}{F_y \cdot u_u} \cdot E_h \quad (2-4)$$

where β =a non-negative constant that depends on the history of inelastic response and structural characteristics and F_y =yield strength. De Leon and Ang (1994) calibrated the Park and Ang damage index based on the actual damage data reported from the 1985 Mexico City earthquake. Furthermore, Stone and Taylor (1994) made efforts to calibrate that damage index based on the study of reinforced concrete columns. Park *et al.* (1987) translated the

range of their index to actual seismic damage. The description of seismic damage for different DI_{PA} values is shown in Table 2-1.

Table 2-1. Range of Park and Ang’s damage index versus seismic damage (Park *et al.* 1987).

Range of DI_{PA}	Damage description
$DI_{PA} < 0.1$	None damage or localized minor cracking
$0.1 \leq DI_{PA} < 0.25$	Minor damage – minor cracking throughout
$0.25 \leq DI_{PA} < 0.4$	Moderate damage - severe cracking and localized spalling
$0.4 \leq DI_{PA} < 1$	Severe damage - crushing of concrete and exposure of reinforcing bars
$DI_{PA} \geq 1$	Collapse

For steel structural components, the damage index proposed by Krawinkler (1987) has been frequently used. Krawinkler (1987) employed the concept of low-cycle fatigue and the hypothesis of “linear damage accumulation” to develop his two-parameter damage index

$$DI_K = \sum_{i=1}^N \frac{1}{N_{fi}} = C \cdot \sum_{i=1}^N (\Delta u_{pi})^c \quad (2-5)$$

where N =number of cycles of inelastic deformation; N_{fi} =number of cycles to failure; Δu_{pi} =plastic deformation range of the cycle i ; C =structural performance coefficient that depends on the failure mode and detailing; and c =structural parameter that normally ranges from 1.5 to 2.0. The parameters in Eq. (2-5) necessitate two sets of experiments: First, the experiments to determine C and c ; second, the experiments to determine the individual plastic deformation Δu_{pi} and the number of inelastic cycles during an earthquake.

Damage indices are also proposed for global structures. In one approach, the weighted average of local indices is utilized to assess the overall extent of damage to one story. In this approach, the global damage index averages the damage indices for each component in a story considering its contribution to the total energy absorbed by components in that story. For a single story the weighted average damage index reads (Chung *et al.* 1990; Park *et al.* 1985; Kunnath *et al.* 1990)

$$DI_{story} = \frac{\sum DI_i E_i}{\sum E_i} \quad (2-6)$$

where DI_i =damage index at location i and E_i =absorbed energy at location i . Eq. (2-6) correctly highlights the effect of the components that absorb higher amounts of energy because they are more likely to experience higher level of damage and will have higher DI_i .

In another approach, Mehanny and Deierlein (2001) developed a damage index that basically tracks the cumulative inelastic deformations rather than dissipated energy on the composite moment frames during earthquake. This is done because the experimental data has demonstrated that the cumulative inelastic deformations are sufficient to capture failure mechanisms in ductile steel and reinforced concrete structures. The damage index of Mehanny and Deierlein (2001) accounts for the effect of loading sequence and cumulative damage, and it reads

$$DI_{MD}^+ = \frac{\left(\theta_p^+|_{\text{currentPHC}}\right)^\alpha + \left(\sum_{i=1}^{n^+} \theta_p^+|_{\text{FHC},i}\right)^\beta}{\left(\theta_{pu}^+\right)^\alpha + \left(\sum_{i=1}^{n^+} \theta_p^+|_{\text{FHC},i}\right)^\beta} \quad (2-7)$$

where DI_{MD}^+ =damage index in the positive direction of deformation; θ_p^+ =inelastic component deformation in the positive loading direction; θ_{pu}^+ =the associated capacity under monotonic loading; PHC stands for primary half cycle and refers to any half cycle with an amplitude that exceeds all previous cycles; FHC stands for follower half cycle and refers to all subsequent cycles of smaller amplitude; α , β are coefficients that should be calibrated by test data or detailed component analyses. Similar to DI_{MD}^+ , damage due to deformation in the negative direction is evaluated by DI_{MD}^- . Subsequently, a single index is defined combining DI_{MD}^+ and DI_{MD}^-

$$DI_{MD} = \sqrt[\gamma]{(DI_{MD}^+)^{\gamma} + (DI_{MD}^-)^{\gamma}} \quad (2-8)$$

where γ =calibration parameter and $DI_{MD} \geq 1.0$ denotes failure. Mehanny and Deierlein (2001) calibrated DI_{MD} against test data to primarily predict the component failure, therefore; its use for predicting different visual damage is limited.

A damage index for global structures considers the change in the structural stiffness before and after damage. Petryna and Kratzig (2005) evaluated the compliance matrix of the structure, \mathbf{K}^{-1} , using the structural eigenfrequencies, ω_i , and mode shapes

$$\mathbf{K}^{-1} = \mathbf{\Phi} \cdot \mathbf{\Omega}^{-1} \cdot \mathbf{m}^{-1} \cdot \mathbf{\Phi}^T \quad (2-9)$$

where $\mathbf{\Phi}$ =matrix of mode shapes; $\mathbf{\Omega} = \text{diag}\{\omega_i^2\}$; $\mathbf{m} = \mathbf{\Phi}^T \mathbf{M} \mathbf{\Phi}$; \mathbf{M} =mass matrix. Then, the maximum eigenvalue of the compliance matrix, λ_{\max} , is utilized as a representative of the global stiffness of the structure. This is the inverse of principal stiffness associated with the first mode of vibration. To this end, the damage index of Petryna and Kratzig (2005) is

formulated as the ratio of the maximum eigenvalue of the compliance matrix, λ_{\max} , for undamaged structure to the one for damaged structure

$$DI_{PK} = 1 - \frac{\lambda_{\max,0}^{-1}}{\lambda_{\max,r}^{-1}} \quad (2-10)$$

where the indices r and 0 denote the damaged and undamaged state of the structure, respectively.

Bozorgnia and Bertero (2003) addressed two drawbacks of the Park and Ang damage index in Eq. (2-4). First, for elastic responses, when $E_h=0$, the damage index should be zero, but in actuality it is not. Second, under monotonic loading when the deformation reaches to u_u the damage index should take the value 1, but in actuality it becomes greater than unity. To remove these drawbacks, Bozorgnia and Bertero (2003) proposed two modified damage indices for a generic inelastic single degree of freedom system:

$$DI_{BB1} = (1 - \alpha_1) \frac{\mu_{\max} - \mu_e}{\mu_u - 1} + \alpha_1 \frac{E_h}{E_u} \quad (2-11)$$

$$DI_{BB2} = (1 - \alpha_2) \frac{\mu_{\max} - \mu_e}{\mu_u - 1} + \alpha_2 \left(\frac{E_h}{E_u} \right)^{0.5} \quad (2-12)$$

where $0 \leq \alpha_1 \leq 1$ and $0 \leq \alpha_2 \leq 1$ are constant coefficients; $\mu_e = u_{\max}/u_y$, if $u_{\max} \leq u_y$, otherwise, $\mu_e = 1$.

Based on DI_{BB1} and DI_{BB2} , Bozorgnia and Bertero (2003) developed “damage spectra” for hundreds of horizontal ground motion records from the Landers earthquake in 1992 and the Northridge earthquake in 1994. A damage spectrum represents the variation of the damage index as function of the structural period for a series of single degree of freedom systems. The attenuation of the damage spectra due to the source-to-site distance and spatial distribution of damage spectra for the Northridge earthquake are examined in their work.

The assessment of seismic damage by damage indices is questioned in several articles (Williams and Sexsmith 1995; ATC-58 Project Task Report 2004; Federal Emergency Management Agency 2006). For example, the common assumption of elastic perfectly plastic behavior may not hold. It is also problematic in many cases to translate their value into actual damage. In addition to these drawbacks, damage indices are often based on simple structural models and they often characterize damage deterministically. This shortcoming is addressed in the following subsection.

2.1.2 Discrete Damage Measures

A transition from deterministic to probabilistic damage modelling has been pursued by several researchers, often in the form of fragility functions. Fragility functions normally express the probability that a system or component sustain failure, or exceed a certain level of damage, as function of some intensity or demand. The use of fragility functions as damage model is built on the premise of discrete damage states.

Fragility functions are omnipresent in state-of-the-art performance-based earthquake engineering. Several reasons support this trend. First, in contrast with damage indices, fragility functions inherently treat seismic damage in a probabilistic manner. Also, the simple format of the model is appreciated by engineers as a natural manner in which to express uncertainty in damage. Another reason is that damage modeling is inherently challenging, and it is often difficult to justify more complex models. Fragility functions were first used in conjunction with hazard curves, and integrated by means of the theorem of total probability to yield the failure probability (Cornell *et al.* 2002). Presently, fragility functions find use in many PBEE methodologies, such as that proposed by Yang *et al.* (2009) for seismic performance evaluation of facilities.

Several researchers (Hwang and Jaw 1990; Hwang and Huo 1994; Singhal and Kiremidjian 1996; Kircher *et al.* 1997; Beck *et al.* 1999; Shinozuka *et al.* 2000; Karim and Yamazaki 2001; Sasani and Der Kiureghian 2001; Porter *et al.* 2001; Beck *et al.* 2002; Gardoni *et al.* 2002; Cornell *et al.* 2002; Rosowsky and Ellingwood 2002; Porter *et al.* 2004; Wen *et al.* 2004; Wen and Ellingwood 2005; Lee and Rosowsky 2006; Kinali and Ellingwood 2007; Applied Technology Council 2012) made commendable effort to develop fragility functions. In the following, the approaches adopted by these researchers are explored and assessment of visual damage in each approach is examined.

One approach to develop fragility functions is to employ the nonlinear dynamic analysis of the structures. A number of researchers employed this analysis and used a damage index to characterize damage and develop fragility functions. For example, Singhal and Kiremidjian (1996) used the Park and Ang damage index to characterize the damage in the nonlinear structural analysis for an ensemble of ground motions. They selected the input random variables, *e.g.*, strength of concrete and steel, for nonlinear structural analyses using a Monte Carlo simulation. To identify damage, the ranges of the Park and Ang damage index are mapped to the damage states of minor, moderate, severe, and collapse. The damage probabilities are obtained by a Monte Carlo simulation. Because the observed damage data are limited (Singhal and Kiremidjian 1996), their damage probabilities were not verified with visual damage. The Other researchers such as Hwang and Huo (1994) and Karim and Yamazaki (2001) also utilized damage indices to characterize the seismic damage in nonlinear analysis. The shortcomings enumerated for damage indices hold for fragility functions developed using damage indices. Kinali and Ellingwood (2007) developed fragility functions for steel frames using nonlinear time history analysis. In their work, three

performance levels are defined: Immediate occupancy, life safety, collapse prevention. These performance levels are characterized by the interstory drift value at which the structural behavior changes during nonlinear dynamic analysis. The parameters of lognormal fragility functions are assessed for each performance level based on the results of analysis using ensembles of synthetic ground motions. Kinali and Ellingwood (2007) found that the mapping of the interstory drift values to the actual damage is a significant research issue in the structural engineering community.

Recently, a consortium of twelve European-Canadian research institutions has been established to develop new multi-hazard and multi-risk assessment methods for Europe. The result of their research is incorporated in the MATRIX project. In this project, a method for developing fragility functions using dynamic analysis is proposed (Réveillère 2012). In this method, a single-degree of freedom is analyzed against 1600 different combinations of one to twelve ground motions.. The parameters of lognormal fragility functions are computed using regression method and the maximum likelihood method.

The other approach to develop models for damage probabilities is to draw on the experience and judgment of specialists in earthquake engineering. This approach is adopted due to the lack of comprehensive post-earthquake damage data. The ATC-13 (Applied Technology Council 1985) provides the probability of being in a certain damage state at different ground motion intensity. The damage probabilities are tabulated in the so-called damage probability matrices. In that matrix, each column corresponds to certain ground motion intensity and each row corresponds to a certain damage state. Each element in that matrix shows the probability that the building sustains a certain damage state for corresponding intensity of ground motion. In the ATC-13, damage probability matrices for

78 classes of structures are developed. Following the ATC-13 approach, Ventura *et al.* (2005) divided buildings in British Columbia into 31 classes based on their material, lateral load resisting system, height, and use. The damage probability matrices for those building classes are developed. The lognormal fragility functions are fitted to discrete probability values for each damage probability matrix. In damage probability matrices, the damage levels are defined mainly based on the ratio of repair cost to the cost of replacement rather than visual damage. Also, the fragility functions developed based on expert opinion are criticized because their results are highly subjective (Lang 2002).

Fragility functions are best developed using experimental data. Using experimental data, Sasani and Der Kiureghian (2001) and Gardoni *et al.* (2002) developed capacity models for reinforced concrete shear walls and columns, respectively. The capacity models are used to establish a set of limit state functions. Each limit state function defines a failure event where the capacity is exceeded by a certain value of demand. The fragility probabilities are estimated by conducting reliability analysis with each limit state function. Their models are not verified against the observed visual damage to the component.

The other approach to develop fragility functions using experimental data has been proposed by researchers in the ATC-58 project (Applied Technology Council 2012). The ATC-58 method basically aims at computing the parameters of lognormal distributions using the recorded structural response at the onset of each damage state during test.

Fragility functions can be examined from several aspects. First, it is observed that fragility functions represent probability distribution for a capacity variable (Porter *et al.* 2001; Beck *et al.* 2002). From this viewpoint, in fragility functions, damage is defined as an event where the capacity variable is exceeded by demand. As a result, similar to damage

indices, fragility functions cannot be used to model the “detailed” visual damage at different segments of building components. Literature review conducted on the visual damage in the next section addresses this issue.

Second, fragility functions are a univariate model where the effect of different structural variables on damage is not considered. This effect is found to be important by several researchers. For example, Karim and Yamazaki (2003) found that the structural parameters such as height and over-strength ratio affect fragility probabilities. They linked the parameters of log-normal fragility functions to those structural parameters using regression methods. Also, Kiremidjian (1985) stated that the seismic damage is a function of structural parameters. To address this shortcoming, the multivariate models that relate damage probabilities to multiple variables are examined in Chapter 3.

2.2 EXISTING MODELS FOR VISUAL DAMAGE

In this section, first different approaches for the characterization of damage are examined. Thereafter, the models, methods, and test data that address visual damage are explored. The objective is to provide a basis for developing damage models that foster the vision proposed in Chapter 1.

Different criteria have been adopted by researchers for characterizing seismic damage. In one trend, the seismic damage is defined by visual signs of damage. Park *et al.* (1987) outlined series of damage states in a descriptive manner:

- None: Localized minor cracking
- Minor: Minor cracking throughout

- Moderate: Severe cracking and localized spalling
- Severe: Crushing of concrete and exposure of reinforcing bars
- Collapse

Earthquake Engineering Research Institute (1994) considers a broader range of earthquake consequences to define different damage levels. In that document, the damage to non-structural components, the risk of casualties, and downtime are considered to define five damage levels as

- None
- Slight: Minor damage to non-structural elements; building reopened in less than one week.
- Moderate: Mainly non-structural damage, little or no structural damage; building closed for up to 3 months; minor risk of loss of life.
- Extensive: Widespread structural damage; long term closure and possibly demolition required; high risk of loss of life.
- Complete: collapse or very extensive, irreparable damage; very high risk of loss of life

Although such characterization of damage is simple and intuitive employment of this approach for assessing the seismic performance is associated with some disadvantages. First, the descriptive words such as minor, little, severe, and high do not strictly indicate the level of damage. As a result the amount of items that are needed to be repaired cannot be determined. For example, it is not clear which width or length of crack is considered as

“minor” or “severe”. Second, these words may lead to discrepant interpretations for the level of damage as they describe damage subjectively rather than quantifying it objectively. In particular, the transition points from one damage state to other are not clear. This leads to confusions particularly, for the damage levels that lie to a transmission point between two levels of damage (Williams and Sexsmith 1995).

Bracci *et al.* (1989) and Stone and Taylor (1993) focused on the repairability of damage for defining their damage levels:

- Undamaged or minor damage
- Repairable
- Irrepairable
- Collapsed

This characterization of damage is more helpful for approximate loss estimation. However, the repair action, which plays central role for loss estimation in PBEE, cannot be determined by such characterization. More importantly, this characterization of damage does not differentiate the broad range of repairable damage scenarios that needs repair.

Federal Emergency Management Agency (1997; 2000) adopted four damage levels, mainly based on the seismic risk of life and serviceability of buildings:

- Operational: Backup utility services maintain functions; very little damage.
- Immediate occupancy: The building is safe to occupy and receive green tag inspection rating; any repairs are minor.
- Life safety: Structure remains stable and has significant reserve capacity; hazardous non-structural damage is controlled.

- Collapse prevention: The building remains standing, but only barely; any other damage or loss is acceptable.

In another approach, the monetary loss is the basis for defining the damage levels. In the ATC-13 (Applied Technology Council 1985), seven damage states are defined directly based on the range of “damage factor”. The damage factor is the ratio of dollar loss to replacement cost. Table 2-2 lists those damage states and the corresponding ranges of the damage factors (Applied Technology Council 1985).

Table 2-2. Damage states and damage factors in ATC-13 (Applied Technology Council 1985)

Damage state	Description	Damage factor range (%)
None	No damage	0
Slight	Limited localized minor damage not requiring repair	0-1
Light	Significant localized damage of some components generally not requiring repair	1-10
Moderate	Significant localized damage of many components warranting repair	10-30
Heavy	Extensive damage requiring major repairs	30-60
Major	Major widespread damage that may result in facility being demolished or repaired	60-100
Destroyed	Total destruction of the majority of the facility	100

The ATC-13 damage levels provide a suitable tool for estimation of approximate monetary loss due to earthquake. It will be more appealing to characterize the damage levels that facilitate the prediction of repair action. The aforementioned drawbacks for Park’s damage state hold for those damage states.

The ATC-58 project report (Applied Technology Council 2012) provides detailed description of the visual damage to more than 700 structural and non-structural components. The data is provided in the form of “fragility specification”. For each component, the fragility specification provides the description of visual damage, pictures of damaged component, required repair actions for each damage level, cost and time of repair, and parameters of lognormal fragility functions.

This section reviews the existing models and experimental data that address visual damage. The visual damage is not considered in all damage models. For example, Simoen *et al.* (2013) identified damage as the change in the mode shapes, mode frequencies, and the stiffness of the structure. Also, Li *et al.* (2013) characterized the seismic damage to RC structures as the stiffness degradation. In contrast with those models, several damage models are intended to predict the visual damage. For example, Broms (1965) proposed a simple model for calculating the average crack width, w_c , and crack spacing in reinforced concrete (RC) members

$$w_c = 2 \cdot t \cdot \varepsilon_s \quad (2-13)$$

where t =cover thicknesses, ε_s =tensile strain in reinforcement bar. Broms (1965) compared the calculated crack width with test results for tension and flexural members. Based on his studies, the maximum crack width for flexural and tension members are 1.66 and 2.08 times larger than w_c , respectively. More sophisticated models for crack width in RC beams subjected to monotonic loading are proposed by Oh and Kim (2007). Lovegrove and El Din (1982) and Balaguru and Shah (1982) proposed models for crack width in RC beams subjected to repeated loading considering the number of applied load cycles. Oh and Kang (1987) conducted five tests on the RC beams and developed a new model for the maximum

crack width in flexural RC members. Their model is presented in Chapter 4 and implemented in Rts.

Several researchers conducted test on the RC beams and reported the crack width and spacing. For instance, Chi and Kirstein (1958) and Mathey and Watstein (1960) conducted tests on flexural concrete members and reported the crack width. Adebar and Van Leeuwen (1999) tested twenty one large scale beams and reported the vertical and diagonal crack width versus longitudinal strain and shear stress. Hognestad (1962), Kaar and Mattock (1963), Kaar and Hognestad (1965), Clark (1956), and Riisch and Rehm (1963) reported 967 observations for crack width for the flexural RC members and Gergely and Lutz (1968) performed statistical study of those data. The result of that study led to the Gergely-Lutz formula for crack width. It is noted that these models often predict the flexural crack width, which is different from the maximum residual crack width that is observed after an earthquake.

A database of the cyclic tests of RC columns is established by Berry *et al.* (2004). The data base provides the maximum recorded drift, δ_{damage} , prior to the first observation of visual damage on the specimens. 274 tests on the rectangular and 160 tests on the spiral columns are included in the database. The visual damages reported in that data base are given in Table 2-3. It is noted that not all of the visual damage scenarios listed in Table 2-3 are reported for each test. This database can be used to develop models for visual damage based on the drift ratio.

Table 2-3. Visual damage scenarios for RC columns (Berry *et al.* 2004).

Damage state	Visual damage
Onset of spalling	First observation of spalling
Onset of significant spalling	Observation of ‘significant spalling, <i>i.e.</i> , spall height equal to at least 10% of the cross-section depth
Onset of bar buckling	Observation of the first sign of longitudinal bar buckling
Longitudinal bar fracture	Observation of the first sign of a longitudinal bar fracturing
Transverse reinforcement fracture	Observation of the first sign of the transverse reinforcement fracturing, or becoming untied.
Loss of axial-load capacity	Observation of loss of axial-load carrying capacity of the column
Column failure	The first occurrence of one of the following events: buckling of a longitudinal bar, fracture of transverse reinforcement, fracture of a longitudinal bar, or loss of axial-load capacity

Also, Berry *et al.* (2008) recommended various repair actions for RC bridge columns based on the extent of visual damage. In their work, each extent of visual damage is associated with a repair action. The structural response that can be used as the predictor of visual damage is also recommended. They concluded that the minor damage to RC columns is primarily determined by the maximum deformation demand, as opposed to the cumulative, cyclic deformation demands. Table 2-4 shows the damage level, visual damage scenario, recommended repair actions and the structural response, with which the visual damage can be predicted.

Table 2-4. Visual damage, repair actions and damage predictors for bridge columns (Berry *et al.* 2008).

Damage level	Visual damage	Repair action	Damage predictor
Negligible	Maximum residual crack width < 0.6 mm	None	Bar tensile strain
Minimum	Maximum residual crack width > 0.6 mm	Epoxy injection of cracks	Bar tensile strain
Minimum	Spalling of cover concrete	Patching of concrete cover and epoxy injection of cracks	Compressive strain in cover concrete
Moderate	Significant spalling of cover	Replacement of concrete cover and epoxy injection of cracks	Compressive strain in core concrete
Significant	Buckling of longitudinal bar, fracture of longitudinal bar, extensive damage to core	Replacement of section	Maximum tensile strain reduced for cyclic demand

Experimental study on the RC bridge columns was also conducted by Lehman *et al.* (2004). They tested ten circular-cross-section specimens. The details of the specimens were same as the typical bridge columns constructed in the regions of high seismicity in the United States. The visual damage was rigorously recorded during tests. They suggested the repair actions required for observed visual damages. In Table 2-5, the structural responses that can be used for predicting the visual damage are listed. Also, the repair action and the serviceability of the bridge under each extent of visual damage are provided.

Table 2-5. Visual damage for bridge columns (Lehman *et al.* 2004).

Visual damage	Structural response	Repair action	Serviceability
Hairline cracks	Longitudinal bar tensile strain	Limited epoxy injection of required	Fully serviceable
Open cracks Concrete spalling	Concrete compressive strain	Epoxy injection Concrete patching	Limited service, emergency vehicles only
Bar buckling/fracture Core crushing	Concrete compressive strain	Replacement of damaged section	Compressive strain in cover concrete

Lehman *et al.* (2004) concluded that the crack width is correlated with maximum tensile strain of bar while concrete spalling is correlated with the concrete maximum compressive strain. It was not clear in their work whether the maximum compressive strains or the maximum tensile strains have greater effect on the bar buckling. As a result, the bar buckling/fracture is arbitrarily identified by the point where the lateral-load strength drops by more than 20 percent of its peak value. However, Moyer and Kowalsky (2003) previously found that maximum tensile strain has significant effect on the bar buckling.

Takahashi *et al.* (1988) developed regression models to predict the crack width and length on the RC shear walls subjected to seismic loadings. They conducted cyclic tests on two shear wall specimens with different failure modes. One specimen was designed for flexural-shear failure mode and the other one was designed for flexural failure mode. The crack length, crack width and the number of cracks were recorded during tests at the maximum lateral displacement and when the lateral load was removed. Using recorded crack width and length, the regression models are developed to establish a link between those quantities and lateral displacement of the wall.

Brown (2008) first defined visual damage and suggested repair actions for RC shear walls. Table 2-6 lists the visual damage and repair actions for RC shear walls. He collected a large array of test data on RC shear walls that show the visual damage and drift ratio at which the component indicates the visual damage. The articles that report the visual damage from experimental studies are listed in the next paragraph. Brown (2008) examined the correlation of visual damage with different structural responses, *i.e.*, the interstory drift, number of load cycles, displacement ductility, and plastic rotation. He concluded that the drift ratio is the best predictor of the damage and developed lognormal fragility functions using drift ratios.

Table 2-6. Visual damage and repair actions for RC shear wall (Brown 2008).

Visual damage	Repair action	Description
First occurrence horizontal crack	Cosmetic repair	Replace and repair finishes
First occurrence of diagonal crack, yield of extreme reinforcement	Epoxy injection	Inject cracks with epoxy and replace finishes
Initial spalling of concrete cover	Patching	Patch spalled concrete, epoxy inject cracks, and replace finishes
Crushing in the web	Replace concrete	Remove and replace damaged concrete, replace finishes
Buckling/failure of longitudinal reinforcement	Replace reinforcement	Replace damaged reinforcing steel, remove, replace concrete, and replace finishes

The experimental studies that reported visual damage for RC shear walls are more limited than the experiments for other RC components (Brown 2008). A number of researchers that report the visual damage listed in Table 2-6 to RC walls are listed below:

- Pang (1991) tested thirteen full-size reinforced concrete panels and reported the crack width versus applied shear stress.

- Adebar *et al.* (2007) conducted cyclic test on a large RC shear wall and reported crack with and spacing on the both sides of the wall.
- Wang (1975) tested two one-third scale wall specimens to investigate the hysteretic behaviour of the walls. The visual damage is reported for both specimens.
- Oesterle *et al.* (1979) tested seven barbell shape specimens to examine the effect of flexural reinforcement.
- Oesterle *et al.* (1976) examined the impact of flexural reinforcement and transverse reinforcement in the boundary and loading on the response of slender and squat walls.
- Vallenias *et al.* (1979) tested four one-third scale wall specimens. They found that the out-of-plane instability causes failure in the slender rectangular walls.
- Lefas *et al.* (1990) tested thirteen walls to examine the impact of slenderness ratio, concrete strength, axial load ratio, and horizontal reinforcement on the wall response.
- Pilakoutas (1991) tested six specimens to validate analytical models for shear wall responses.
- Zhang and Wang (2000) tested four specimens to examine the influence of the “shear ratio” and axial load ratio on the wall response. The results of their work demonstrate that the axial load ratio has significant impact on the crack propagation on the wall.
- Sittipunt *et al.* (2001) tested four specimens to study the effect of diagonal reinforcement on the seismic response of the walls. They concluded that the diagonal reinforcement has significant effect on the performance of the walls.
- Thomsen and Wallace (2004) tested two specimens to examine the effect of transverse reinforcement in the boundaries of the wall.

For RC beam-column joints, Pagni and Lowes (2006) and Brown and Lowes (2007) studied visual damage and required repair actions.

Table 2-7 presents the visual damage and associated repair actions for RC beam-column joints. Using test data, the lognormal fragility functions for each visual damage scenario are developed considering different structural responses such as interstory drift ratio, number of cycles, and shear strain in joints.

Table 2-7. Visual damage and repair actions for RC beam-column joint (Pagni and Lowes 2006).

Visual damage	Repair action	Description
Maximum crack width < 0.5 mm	Cosmetic repair	Replace and repair finishes
Maximum crack width > 0.5 mm Beam longitudinal reinforcement yields	Epoxy injection	Inject cracks with epoxy and replace finishes
Spalling of more than 30% of joint surface	Patching	Patch spalled concrete, epoxy inject cracks, and replace finishes
Spalling of more than 80% of joint surface, cracks extend into the beam/column	Replace concrete	Remove and replace damaged concrete, replace finishes
Failure: Buckling of column longitudinal reinforcement, pull-out of beam longitudinal reinforcement	Replace joint	Replace damaged reinforcing steel, remove, replace concrete, and replace finishes

Several researchers have conducted test on the beam-column joints; however, only a limited number of them reported the visual damage during the experiments. In the following a number of researchers who reported visual damage during tests are listed:

- Meinheit and Jirsa (1977) studied the effect of transverse reinforcement on the response of beam-column joints. The visual damage is reported only for one of the eleven specimens that they tested.
- Pessiki *et al.* (1990) tested beam-column joints and concluded that the amount of reinforcing steel in the joint affects the failure mechanism. The visual damage is reported for seven specimens.
- Joh *et al.* (1991a; 1991b) conducted experimental studies to evaluate the effect of transverse reinforcement and beam eccentricity on the joints response.
- Walker (2001) and Alire (2003) examined the effect of shear stress and loading history on the seismic performance of the joints. They recorded visual damage during tests.
- Beckingsale (1980) tested three specimens to investigate the response of joints to earthquake loading. The visual damage was reported for all three specimens.
- Durrani and Wight (1982) conducted cyclic tests on six full scale joints to evaluate the impact of transverse reinforcement and slabs on the joints. From those specimens, three were in connection with continuous slabs. The visual damage is completely recorded during tests.
- Endoh *et al.* (1991) tested four joint specimens to study the anchorage of reinforcement in the beam and the shear strength of the joint.
- Hayashi *et al.* (1994) conducted experimental study on eleven specimens in order to develop a model for anchorage of reinforcement in the beam. Visual damage was reported only for one specimen.

- Milburn and Park (1982) studied the effect of distance of plastic hinges from the column and transverse reinforcement on the joint response. Visual damage was reported for all specimens.
- Park and Ruitong (1988) tested four specimens to investigate the effect of reinforcement diameter and transverse reinforcement on the joint response. Visual damage was reported for all four specimens.
- Zaid *et al.* (2001) investigated the shear strength, bond strength in beam and the effect of joint transverse reinforcement on the response of joints. Four specimens were tested and visual damage was reported.
- Briss (1978) conducted test on two specimens to propose a design method for beam-column joints. The visual damage was reported for both specimens.
- Teraoka *et al.* (1990) conducted a series of tests on the joints to validate a model for the response of this component. The visual damage was reported for eleven specimens.

Recently, the Earthquake Engineering Research Institute established an online database for damaged concrete buildings. At this time, the data base includes the case studies for more than 50 RC buildings from 12 countries and features a search criteria interface. For each building, the detail of structural system, earthquake, and pictures of visual damage to different components are provided. The data base is available online at db.concretcoalition.org and is a baseline for future research.

2.3 EXISTING MODELS FOR REPAIR ACTION

Repair action is a range of activities that are conducted in order to restore a damaged building or facility to its pre-earthquake condition. According to this definition, demolition followed

by reconstructing is a form of repair action. In the literature, limited research has been conducted on the probabilistic models that predict repair actions for building components. Most of the existing literature (Applied Technology Council 2012; Brown 2008; Pagni and Lowes 2006; Brown and Lowes 2007) aims to deterministically link the possible visual damage to the repair actions. This trend essentially relies on the professionals' experience from past earthquakes and does not account for the variation in the selected repair actions. The consideration of this variation is important because it is observed that the extent of the damage that triggers a certain repair action has been substantially variable (Pagni and Lowes 2006). Examples of this variation are the extent of hairline cracks on the surface of RC components that leads to cosmetic repair of finishes and demolition of buildings after an earthquake.

It is noted that several published articles (Rodriguez and Park 1991; Bett *et al.* 1988; Kuroiwa and Kogan 1980; Saadatmanesh *et al.* 1997) considered “strengthening” of the structures as part of “repair”. However, in this thesis, the term “repair” does not address any action that involves retrofitting or strengthening. Rather, repair addresses necessary actions for bringing a building back to its functionality without changing the strength of the structural parts against earthquake.

When addressing repair of building components, it is of importance to identify the point at which repair is extremely costly or impossible. Park *et al.* (1985) recognized the irreparable damage as the value of their damage index exceeds 0.4. Lehman *et al.* (2004) concluded the onset of spalling of the concrete as a point at which the repair is more time-consuming, costly and disruptive. Several published articles (Lehman *et al.* 2004; Brown 2008; Pagni and Lowes 2006; Frangou *et al.* 1995; Hanson and Comartin 2000; Kam and

Pampanin 2011) identified the fracture and buckling of the reinforcement as the point that the component should be replaced. The official website of the City of New York prescribes the demolition of a building if its foundation is shifted off or its structure is unstable; however, Ghobarah (2001) recognized that the identification of non-repairable damage is a challenge in PBEE.

For steel structures, there is limited literature on the repair of earthquake damaged buildings. Mahin (1998) mentioned some of repair actions for steel beam-column connections.

Most mentions of repair in the PBEE literature are intended to support the damage models, *e.g.*, Yang *et al.* (2009) stated that each damage state should be defined to signal a repair action. In the next paragraphs, a number of references that explain repair actions for earthquake damaged buildings are enumerated.

BRANZ, an independent company that provides research, testing, and consulting for the building industries, provides specific information for repair of earthquake damaged buildings after Canterbury earthquake. The information is published in several documents that are available online at www.branz.co.nz/EQ#general. These documents describe the repair of foundations, walls, and several building components in detail.

The federal emergency management agency (1999) provided practical guidance for the repair of damaged masonry and RC wall buildings. That document categorizes the repair in three categories: 1) Cosmetic repairs; 2) Structural repairs; 3) Structural enhancements. In each category, a number of repair actions are defined. For each repair action, the required materials and equipments are listed and the implementation of the repair is described. In addition, relevant references for each repair action are provided.

The ministry of business, innovation and employment of New Zealand provides several documents that describe the repair of buildings after Canterbury earthquake. The document details repair methods for foundations, chimney, wall bracing, wall and roof connections, concrete block masonry walls, interior walls, *etc.* to building owners and technicians. Those documents are available online at www.dbh.govt.nz.

The Consortium of Universities for Research in Earthquake Engineering (2010) provided general guidelines for the process and details of assessment and repair of damage in wood frame buildings. The repair actions for several building contents and components are explained in detail and photographs of visual damage are provided.

2.4 EXISTING MODELS FOR COST OF REPAIR

The estimate of economic impact of earthquakes is a challenging task (Jaiswal and Wald 2013). This is because of the inherent complexity in the estimation of direct and indirect losses to infrastructures and institutions. For example, the estimate of the economic impact of the 1994 Northridge earthquake grew in a decade. That is, the economic impact was initially estimated to be 40 billion dollars in 1997 (Eguchi *et al.* 1998), however, this amount increased to 57 billion dollars in 2004 (Seligson and Eguchi 2005). The change in that estimation was mainly due to the cost of business interruption and the change in the insured losses.

The existing research on the repair cost for building components is limited; therefore, this section mainly explores a few articles for assessing the cost of earthquakes. In this regard, Jaiswal and Kishor (2013) proposed a method for developing models that estimate the total direct monetary loss due to an earthquake in a region. The model inputs are earthquake intensity, the spatial distribution of population, the gross domestic product, and the economic

loss data from past earthquakes. In their method, first the loss ratio is defined as the ratio of the direct monetary loss to the value of exposed assets to the earthquake. Afterwards, the loss ratio is predicted by the lognormal cumulative function of intensity measure. The total gross domestic product is used to estimate the value of exposed assets to the earthquake. The total gross domestic product for each region is estimated by the product of the population of region and per capita gross domestic product. In turn, the value of exposed assets is estimated by the product of the total gross domestic product and a country-specific factor that accommodates the variation between value of assets and per capita gross domestic product. The parameters of lognormal cumulative distribution function are estimated using the loss data from past earthquakes and a least square method.

Chan *et al.* (1998) also used the gross domestic product and population to estimate the earthquake monetary loss to regions. In the absence of a detailed inventory database of the structures and facilities in regions, they suggested the gross domestic product to represent the value of assets in a region. In their method, the monetary loss to a region is calculated by the product of three variables: 1) The gross domestic product of the region; 2) The probability of earthquake intensity in the region; 3) The vulnerability of region to the earthquake intensity.

Reitherman (1985) reviewed and contrasted 37 methods for the assessment of damage and consequences of earthquake. For each method, the required data, the required analysis, output of the method, *etc.* are summarized. The monetary loss, power outage, and life safety are amongst the output of several review methods. It is concluded that the majority of these methods are of limited value in practical applications.

For assessment of repair cost for buildings, Hasselmen and Wiggins (1982) used a financial index, defined as the ratio of the repair cost to the replacement cost. They assumed that, on a log-log plot, the index is linearly related to the inter-story drift. Their financial index is further employed by Paultre and Mitchell (1991). Paultre and Mitchell (1991) first conducted a series of nonlinear structural analyses. The relationship between the drift ratio and the financial index proposed by Hasselman and Wiggins (1982) is utilized to estimate the cost of damage. Also, it is concluded from their work that the structure designed with higher ductility sustains less damage.

Gunturi and Shah (1992) concluded that the cost of earthquake to the building has three components: 1) The cost of damage to the structure, which is correlated to the ductility demand and energy absorption so is a function of the Park and Ang damage index; 2) The cost of damage to architectural, electrical, and mechanical components, which is assumed to be a function of inter-story drift; 3) The cost of damage to the building contents, which is a function of peak story acceleration.

Kappos *et al.* (2007) studied monetary loss to buildings due to the 1999 Athens earthquake using analytical methods and compared the results with the statistical data that show the repair costs. They concluded that the ground motions used for the analytical studies are the main factor contributing to the discrepancies between analytical and statistical results. Mackie *et al.* (2007) utilized the Pacific Earthquake Engineering Research Center framework to evaluate the cost of repair for different design options. In their work, the cost of repair is estimated per unit of quantity. Ramirez *et al.* (2012) studied the repair costs for 30 archetype reinforced concrete frame buildings. The buildings vary in height from one to twenty stories representing office buildings with special RC moment frame. Ramirez *et al.* (2012)

concluded that the height, architectural details, and structural design parameters significantly affect the cost of repair. Dowrick (1991) described an analysis of cost of damage to houses in the 1987 New Zealand. In his study, it is shown that cost of repair is log normally distributed.

The online data base of CATDAT provides a comprehensive report on the damaging earthquakes around the world. The data base reports the cost of 6500 earthquakes since 1900 (Daniell *et al.* 2010). In their annual report, number of damaging earthquakes, fatalities, homeless, economic loss, and total insured losses are provided. Table 2-8 shows a typical annual report of damaging earthquakes for the year of 2011 from the website.

Table 2-8. Report of damaging earthquakes for 2011 from CATDAT.

Number of damaging earthquakes	121+
Number of casualty-bearing earthquakes	60+ with at least 24 fatal
Country with the most damaging earthquakes	Japan, 27; China, 19; New Zealand, 17
Earthquake consequence	Estimate
Total fatalities	Between 20068 and 20480
Total injuries	1335
Total homeless	1.108 million
Total monetary losses	\$503.4 billion to \$749.54 billion (Median=\$623.50 billion)
Total monetary losses (excluding Fukushima nuclear)	\$394.41 billion to \$587.54 billion (Median=\$488 billion)
Total monetary losses (excluding Tohoku)	\$24.41 billion to \$39.54 billion (Median=\$29 billion)
Total insured losses	\$43.32 billion to \$67.49 billion (Median=\$52.86 billion)

Vranes and Pielke (2009) reported monetary loss from 80 earthquakes in the United States since 1900 and normalized them to 2005 dollars considering the inflation, increases in wealth and changes in population.

Graf and Lee (2009) presented a simple framework for the evaluation of repair cost using spectral acceleration, design base shear coefficient, *i.e.*, the ratio of design base shear to the weight of structure, response modification factor, height, and framing system. In the absence of actual repair cost of earthquakes, they used the applied technology council (1985) data base for model calibration.

For the estimation of fatalities in buildings, Porter (2009) suggested a technique to calculate mean rate as a function of spectral acceleration. The technique uses the data and methods in HAZUS (Kircher *et al.* 1997).

Non-structural components carry particular significance in the estimation of monetary loss for an earthquake. This type of components represents about 75 percent of the building cost (Kircher *et al.* 1997; Taghavi and Miranda 2003). Thaghavi and Miranda (2003) first collected a large database of non-structural components in commercial buildings. They presented a new taxonomy for those components. The database includes the damage description and repair actions together with a library of damaged components images. In addition, fragility functions that represent the damage as a function of structural response are provided. The performance of components in previous earthquakes together with structural response and structural systems are examined. That database provides the cost of typical components including the cost of construction and materials.

2.5 EXISTING MODELS FOR TIME OF REPAIR

Downtime is the period of time in which a building or facility cannot function as a result of earthquake damage. This period of time is needed to finance, plan, and complete the repair of seismic damage. Downtime includes two components (Comerio 2006): 1) Rational component, which includes construction costs and time; 2) Irrational component, which is the time needed for mobilization for repairs and includes financing, workforce availability, regulatory changes, relocation of functions, and economic uncertainty. The estimation of downtime is important because it indicates the indirect cost of damage.

Estimation of downtime is the biggest challenge in PBEE and risk management (Krawinkler and Miranda 2004). It is because of high uncertainties in the availability of workforce, materials, and finance after occurrence of an earthquake. In addition, there are limited amounts of data on building closure and downtime from past earthquakes (Comerio 2006), which is a hindrance for downtime modelling. Comerio (2006) studied the downtime of buildings with three different occupancies: educational buildings; commercial buildings and residential buildings. She studied the downtime for these buildings after the Loma Prieta and Northridge earthquakes. In her study, it is stated that myriad issues affect the ability of an owner to repair a damaged facility and irrational components have significant effect on the time of closure after an earthquake. In another study, Comerio (2013) explored the recovery of housing in Chile after the 2010 earthquake. It is found that the government program for repair and rebuild of buildings succeeded. The program's success is attributed to several factors ranging from the expertise of staffs and labors to community leadership and political will.

To overcome the complexity of factors that affects recovery time, Chang and Shinozuka (2004) and Miles and Chang (2006) developed a conceptual model. Their conceptual models demonstrate the relationship between households, businesses, lifeline networks, and neighborhoods. The evaluation of irrational components of downtime is outside the scope of this thesis and readers are referred to the aforementioned references.

Porter *et al.* (2001) proposed a methodology to estimate the time of repair for building components considering solely the effect of the rational components. In their methodology, the repair time to restore a certain damaged building component to its undamaged state is considered as a random variable. This random variable is multiplied by the number of damaged components of that type and divided by the number of crews and the number of working hours per day. Mitrani-Reiser (2007) extended the proposed methodology by Porter *et al.* (2009) with considering the time for the mobilization in addition to the rational time of repair. The time of mobilization is estimated by a “virtual inspector”, *i.e.*, a computer model that probabilistically estimates the building safety (Applied Technology Council 1989) using damage analysis. In that model, first a rough assessment of damage is conducted. This assessment evaluates the structural integrity of the building and the probability of a red, yellow, or a green tag being posted. The mobilization time is estimated based on the tag colour and added to the rational time of repair.

As a summarizing remark for this chapter, it is observed that thus far a little research has been done to develop probabilistic models for repair action. It is also seen that repair time is the biggest challenge in PBEE and more research is needed to probabilistically model the time of repair.

Chapter 3: MULTIVARIATE FRAGILITY MODELS FOR EARTHQUAKE ENGINEERING

The principal objective in this chapter is to improve the prediction of damage in performance-based earthquake engineering (PBEE) and consequence-based engineering (CBE). More precisely, the aim is to extend the univariate fragility functions that are prevalent in contemporary practice to multivariate models. This is done in recognition of the fact that damage is generally caused by multiple structural demands and that it normally depends on an array of material and geometry parameters. An important impetus for the work is that the advent of PBEE and CBE has drastically increased the importance of damage modeling in structural engineering. In fact, the prediction of damage is a cornerstone of PBEE and CBE because it facilitates the forecasting of future repair costs, which in PBEE is regarded as a key measure of structural performance, and in CBE is fundamental information to predict the expected consequences of natural hazards.

Although the consideration of damage is at the core of contemporary design, damage modelling already has a long history in structural engineering. One approach has been to characterize damage by means of damage indices. Park and Ang (1985) presented a damage index that was particularly popular before the turn of the century and Williams and Sexsmith (1995) provided a review of several others. The body of literature on various damage indices is substantial and beyond the scope of this chapter. However, it is emphasized that while damage indices are usually continuous, conversion tables are often provided to link their value to discrete damage states (Bai *et al.* 2009). This is not done because damage is discrete;

actual damage, such as cracking of concrete, is often continuous. Rather, the notion of discrete damage states has become a mainstay of contemporary damage modelling because the repair action, and thus the ensuing cost, is discrete. Moreover, the probabilistic approach has become widely accepted to account for uncertainties, which means that modern damage models essentially aim to express the probability that a structure or a component is in a particular damage state.

In PBEE, damage probabilities are often expressed in terms of univariate fragility functions, possibly with the only exception of the bivariate fragility models proposed by Gardoni *et al.* (2002). For instance, fragility functions are an important basis for the ATC-58 approach (Yang *et al.* 2009; Applied Technology Council 2012), which is a pioneering initiative in PBEE that serves as context for this chapter. While the use of univariate fragility functions has facilitated a renaissance in damage modelling, their use has several limitations. As described later, they predict damage by means of only one structural response; they ignore the effect of material properties and geometry parameters on damage; they may cross, which leads to negative probabilities; and ultimately they do not identify the parameters that actually affect damage. The models put forward in this chapter remedies these shortcomings.

In the following, approaches for damage modeling in PBEE are first described, prompting a description of the popular univariate fragility functions. Thereafter, different approaches to establish such fragility functions are reviewed, leading to the idea of using logistic regression. Next, two different techniques for conducting logistic regression are outlined, leading to the conclusion that the most straightforward method, found in elementary statistics textbooks, is inappropriate for this modeling problem. The remainder of the chapter describes the selected modelling approach and applies it to reinforced concrete shear walls.

The models show that the walls with higher aspect ratio and horizontal web reinforcement ratio are less susceptible to damage. Conversely, the walls subjected to higher axial load ratio are more susceptible to damage. However, further development of the research will convey the effect of loading protocol on the damage thus enlarging the use of the developed models in practice.

3.1 APPROACHES FOR DAMAGE MODELING IN PBEE

To provide context for the subsequent developments, different approaches to model damage in contemporary PBEE is first examined. Several research centers, such as the Pacific Earthquake Engineering Research Center (PEER) and the Mid-America Earthquake Center (MAE Centre), have conducted relevant work. For example, research carried out in PEER in the early 2000's was coordinated with reference to the “framing equation” (Der Kiureghian 2005; Cornell and Krawinkler 2000)

$$G(dv) = \int_0^{\infty} \int_0^{\infty} \int_0^{\infty} G(dv | dm) \cdot f(dm | edp) \cdot f(edp | im) \cdot f(im) \cdot ddm \cdot dedp \cdot dim \quad (3-1)$$

where G =complementary cumulative distribution function, f =probability density function (PDF), dv =decision variable, dm =damage measure, edp =engineering demand parameter, im =intensity measure, and vertical bars means that the distribution is conditioned on the outcome of the parameter after the bar. Although a detailed discussion of Eq. (3-1) is outside the scope of this chapter, it is noted that damage in the PEER approach is characterized by the *continuous* random variable dm . Thus, the damage model in Eq. (3-1), namely $f(dm|edp)$, is not a fragility function, but rather a probability distribution for a continuous random

variable (which can be obtained from a fragility function). It is also noted that Eq. (3-1) is based on the theorem of total probability (e.g., Ang and Tang 2007).

Total probability integration is also adopted in the CBE approach developed by the MAE Centre (Abrams 2002). However, in consequence-based engineering the probability of a *discrete* limit-state, LS , is sought (Wen and Ellingwood 2005; Kinali and Ellingwood 2007):

$$P(LS) = \int_0^{\infty} P(LS|edp) \cdot f(edp) \cdot dedp \quad (3-2)$$

The conditional probability $P(LS|edp)$ in Eq. (3-2) can be interpreted as the damage model in the consequence-based approach. In contrast with dm in Eq. (3-1), LS in Eq. (3-2) is an event, such as exceeding a certain EDP threshold. As a result, $P(LS|edp)$ is often referred to as a “fragility” (Wen and Ellingwood 2005).

The fragility concept is also employed in approaches that model the damage of individual building components; see, e.g., Porter *et al.* (2001), Ramamoorthy *et al.* (2006; 2008), Zhu *et al.* (2006), Applied Technology Council (2012), Bai *et al.* (2009; 2011) and Yang *et al.* (2009). These approaches classify the building components into assemblies or performance-groups, and several damage states are defined for each group. The assembly-based approach proposed by Porter *et al.* (2001) is extended by the researchers in the ATC-58 project (Yang *et al.* 2009). In the ATC-58 approach a sampling-based scheme is employed to make the realization of structural response with a limited number of structural analyses. This is done to avoid the computational cost due to a large number of dynamic structural analyses that was needed in the assembly-based approach (Porter *et al.* 2009). In both approaches, damage is described by a discrete random variable. The probability that a

component is in a particular damage state is expressed by fragility functions. Haukaas and Javaherian Yazdi (2013) examined damage modelling approaches that employ discrete and continuous random variables to describe damage.

A generic form of fragility functions are displayed in Figure 3-1. This figure shows a typical situation with four damage states. Figure 3-1 is also instructive as a means of understanding how to utilize fragility functions as damage models; each curve displays the probability that the damage state is equal to or greater than the associated state. Thus, the probability that a component is in damage state number j is (Bai *et al.* 2009)

$$P(DS = ds_j) = P(DS \geq ds_j) - P(DS \geq ds_{j+1}) \quad (3-3)$$

where DS =damage state, which is a discrete variable for characterizing the seismic damage.

One disadvantage of the damage model in Figure 3-1 is that it takes only one input parameter, edp . Some researchers have recognized that this is a simplifying assumption (Porter *et al.* 2001). For example, Karim and Yamazaki (2003) recognized that height and over-strength ratio affect the damage of highway bridges, in addition to structural response. This suggests that certain structural components that differ only in the value of a material and geometry parameters require different fragility functions. As a result, numerous fragility functions are needed to express the damage probability of all possible material and geometry configurations of a specific structural component. Additional issues are described in the following.

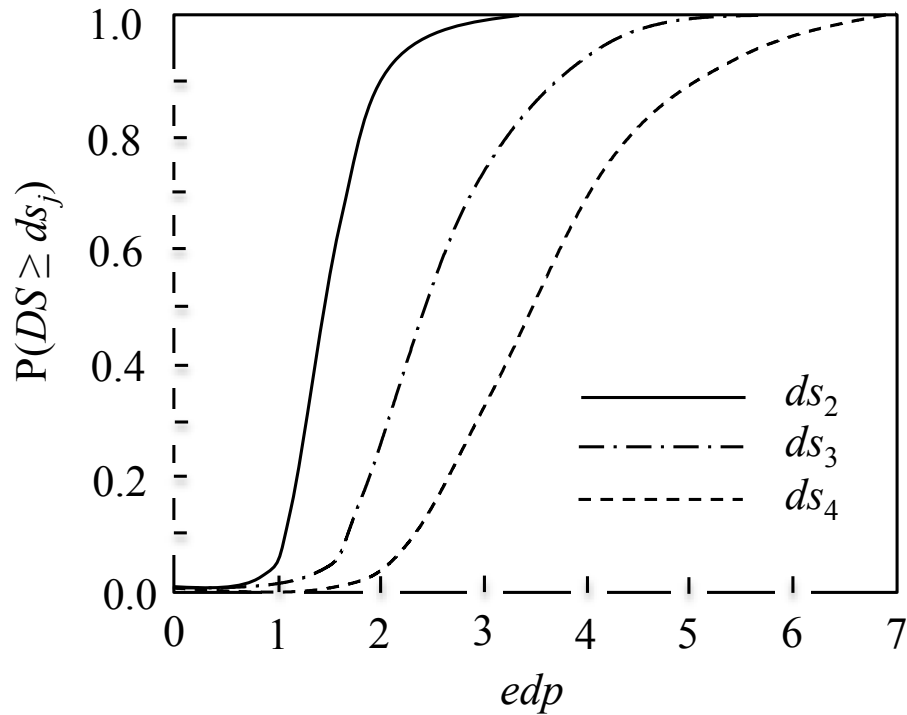


Figure 3-1. Fragility functions (Yang *et al.* 2009).

3.2 APPROACHES TO ESTABLISH FRAGILITY FUNCTIONS

Fragility functions were originally employed to model the conditional probability of failure for a given earthquake intensity (Gardoni *et al.* 2002; Cornell *et al.* 2002; 2003). Conversely, in PBEE, fragility functions represent the probability that a component has reached some damage state or worse. As such, the fragility functions in Figure 3-1 are not probability distributions for the continuous random variable edp . Nonetheless, a fragility function has the same properties as a cumulative distribution function (CDF). In fact, a fragility function can be interpreted as the probability distribution for the underlying capacity of the component to resist entering some damage state. As a result, researchers such as Shinozuka *et al.* (2000) and Singhal and Kiremidjian (1996) have employed the lognormal probability distribution to represent fragility functions. Several studies have estimated the parameters of this

distribution (Hwang and Jaw 1990; Hwang and Huo 1994; Karim and Yamazaki 2001; Kinali and Ellingwood 2007; Padgett and DesRoches 2008; Ryu *et al.* 2011; Jalayer *et al.* 2007). Importantly, lognormal fragility functions are also adopted by the ATC-58 project, generically written as (Yang *et al.* 2009; Applied Technology Council 2012)

$$P(DS \geq ds_j | edp) = \Phi \left(\frac{1}{\sigma_j} \cdot \ln \left(\frac{edp}{\mu_j} \right) \right) \quad (3-4)$$

where Φ =standard normal cumulative distribution function, μ_j =median value of the *edp* at which ds_j first occurs, and σ_j =standard deviation of the logarithm of that *edp*-value. This formulation implies that the fragility curves will cross at extreme *edp*-values for curves with different σ_j . As a result, damage probabilities computed by Eq. (3-3) can come out negative, which is another issue with fragility functions that is addressed in this chapter. It is noted, however, that in practice σ_j does not necessarily differ from one fragility model to other. This is because σ_j represents not only the statistical uncertainties in the test data but also the uncertainty from several sources, some of which is not easily quantified. As a result, the determination of σ_j involves qualitative judgment that, in practice, may not warrant different values for each fragility curve.

Another approach to establish fragility functions is to develop probabilistic capacity and demand models and then conduct a reliability analysis to estimate the probability that the demand exceeds the corresponding capacity. Gardoni *et al.* (Gardoni *et al.* 2002; 2003) employed a Bayesian approach to develop such models from experimental and virtual data.

The above-mentioned models are univariate and do not identify and expose the variables that may affect the damage. The identification of these variables is important

because normally the damage is a function of a range of structural characteristics and responses (Karim and Yamazaki 2003; Kiremidjian 1985). Hence, a multivariate modeling technique will help the modeller to interpret and characterize the importance of these variables and convey them to the users of the model. Furthermore, multivariate damage models enable the practicing engineers to recognize how the change in the design parameters at their discretion may affect the damageability of components. Also, in light of multivariate damage models, set of test data that shows observed damage to a generic component with different geometry and characteristics can be used for model development. The latter is further discussed in the next section.

In the literature, a few multivariate regression models for predicting probability are available. The idea in these models is to map the value of probability from zero to one to a real number from negative to positive infinity. This mapping is conducted by the use of a “link” function to develop multivariate models for $P(DS \geq ds)$. The most commonly used link function is called logit function and the multivariate model is called logistic regression model. The logistic regression model for “ordinal data”, *i.e.*, the data that has a natural ordering, is used for damage modeling in this paper. It is because of the fact that different damage states normally occur in order. Although logistic regression has not been employed extensively in engineering, the idea is not new. Koutsourelakis (2010), for example, explored the use of logistic regression in the context of earthquake engineering, but that study aimed at quantifying the effect of different earthquake intensity measures, and only binary problems were considered. In contrast, fragility functions for components with multiple damage states are developed in the following.

First consider the generic regression model

$$z = h(\mathbf{x}, \boldsymbol{\theta}) \quad (3-5)$$

where z =continuous output parameter, h =linear or nonlinear function, \mathbf{x} =regressors, such as material, geometry, and structural response parameters, and $\boldsymbol{\theta}$ =model parameters. A typical example of Eq. (3-5) is the linear regression model

$$z = \theta_1 + \theta_2 \cdot x_2 + \cdots + \theta_m \cdot x_m + \varepsilon \quad (3-6)$$

where ε =model error and the model is said to be linear because it is linear in the model parameters, θ_i , $i=1,2,\dots,m$. Bayesian linear regression models have been employed in a variety of engineering disciplines; for example, Gardoni *et al.* (2002) employed models of the form

$$z = \theta_1 + \theta_2 \cdot h_2(\mathbf{x}) + \cdots + \theta_m \cdot h_m(\mathbf{x}) + \varepsilon \quad (3-7)$$

where h =explanatory functions formulated in terms of the basic regressors to model the capacity of reinforced concrete columns. The word Bayesian means that the model parameters are random variables. Logistic regression differs from ordinary regression in two aspects. First, the right-hand side excludes the model error, ε , but can otherwise be linear or nonlinear like above. More importantly, the left-hand side is the logit function:

$$\ln\left(\frac{p}{1-p}\right) = \theta_1 + \theta_2 \cdot h_2(\mathbf{x}) + \cdots + \theta_m \cdot h_m(\mathbf{x}) \quad (3-8)$$

where $p=P(DS \leq ds)$ =probability of a certain damage *or less* (McCullagh and Nelder 1989). That is, the probability in Eq. (3-8) is the *complement* of the fragility function in Eq. (3-4). The logit function, $z=\ln(p/(1-p))$, is sketched in Figure 3-2 to emphasize that p varies from

zero to unity, while z varies from minus infinity to plus infinity. As a result, a regression model of the form in Eq. (3-8) can be employed to model probability values, such as the probability that a structural component is in a specific damage state. More precisely, Eq. (3-8) is employed to model the probability that a component is in damage state j or less. The two key advantages of logistic regression are: 1) that the proposed change can be readily implemented in the ATC-58 analysis procedure, and 2) that this can facilitate the development of multivariate damage models.

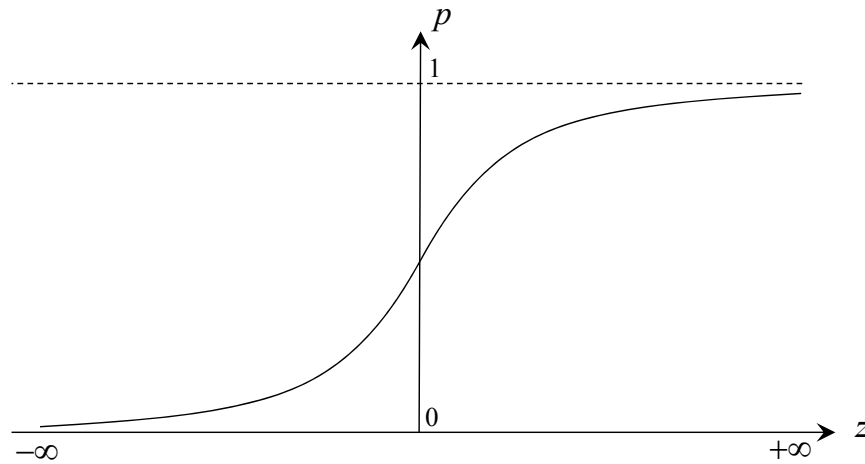


Figure 3-2. The logit function.

3.3 APPROACHES TO CONDUCT LOGISTIC REGRESSION

The development of logistic regression models is described in several textbooks (McCullagh and Nelder 1989; Agresti 1996; Ryan 2008; Hosmer and Lemeshow 2000) and two different techniques emerge. One technique is applicable to cases where observations of the probability, p , are available. In other words, the data gives the probability of different damage states for specific regressor-values. In this case, Eq. (3-8) is essentially an ordinary linear regression model with a simple transformation in the left-hand side. The artificial data

in Table 3-1 illustrates this situation for a problem with two damage states, ds_1 and ds_2 ; the data gives $P(DS=ds_1)$ for observed values of the regressors, x_2 and x_3 . In this case the logistic regression analysis is straightforward because the values of the left-hand side are computed from the values of p by means of the logit function, followed by ordinary linear regression with the model in Eq. (3-7). As a result, closed-form expressions for the statistics of θ in Eq. (3-8) are available in this situation (Stone 1996).

Table 3-1. Artificial data to illustrate problems with closed-form solutions.

P	x_2	x_3
0.27	19.44	33.76
0.58	111.92	23.22
0.74	73.33	33.05
0.08	57.93	91.47
0.83	44.08	51.22

Unfortunately, observations like in Table 3-1 are rarely available in practical engineering problems. This is because numerous experiments on identical specimens (*i.e.*, the same \mathbf{x} -values) must be conducted under identical conditions to estimate the probabilities like those in Table 3-1. Instead, the data format shown in Table 3-2 must be considered. Here, each row represents the observed damage state for a single test conducted on a single specimen. For the artificial data provided in Table 3-2, the first row states that a component with $x_2=19.44$ and $x_3=33.76$ has been observed to be in Damage State 2. With this type of data, which is far more realistic than the type of data illustrated in Table 3-1, closed-form solutions are no longer available, as described in the following section.

Table 3-2. Illustration of the data-format that is available in practical problems.

Damage State	Binary Variable	x_2	x_3
2	0	19.44	33.76
1	1	111.92	23.22
1	1	73.33	33.05
2	0	57.93	91.47
1	1	44.08	51.22

3.4 BINOMIAL LOGISTIC REGRESSION

An important objective in this chapter is to explain to engineers conducting PBEE and CBE how to develop multivariate models for $P(DS \geq ds)$ by means of Eq. (3-8). For pedagogical purposes it is therefore useful to start with binomial logistic regression, where only two damage states are considered. Suppose n observations are made, and that the regressor values and the corresponding damage state have been recorded in each experiment in the form in Table 3-2. Furthermore, let the binary variable $y = \{0, 1\}$ denote the damage state, where the outcomes 0 and 1 corresponds to the damage states 2 and 1, respectively.

A technique for estimating the model parameters in Eq. (3-8) is to maximize the likelihood function, which represents the probability of observing the data. Provided independent observations, the likelihood function can be written as (Ramamoorthy *et al.* 2006)

$$L(\boldsymbol{\theta}) = \prod_{i=1}^n \left[p_i^{y_i} \cdot (1 - p_i)^{1 - y_i} \right] \quad (3-9)$$

because when $y=0$ the bracketed expression in Eq. (3-9) evaluates to $1-p$, and when $y=1$ it evaluates to p . Thus, it correctly evaluates the probability of observing the data. The best

model is the one that maximizes $L(\boldsymbol{\theta})$. However, rather than working with $L(\boldsymbol{\theta})$ it is common to maximize its natural logarithm, which means that the following equation must be solved:

$$\frac{\partial \ln(L(\boldsymbol{\theta}))}{\partial \boldsymbol{\theta}} = \mathbf{0} \quad (3-10)$$

This is a popular and straightforward approach for the determination of point estimates for the model parameters. The covariance matrix can then be computed as the inverse of the Hessian of the negative of the log-likelihood function evaluated at the maximum likelihood point (Hosmer and Lemeshow 2000). Once the statistics for the model parameters are determined, the probability of damage state ds_1 is determined from Eq. (3-8), and the probability of damage state ds_2 is one minus that value.

3.5 MULTINOMIAL LOGISTIC REGRESSION

The difference between binomial and multinomial logistic regression is that the latter allows more than two damage states. The following notation is employed:

$$p_j = P(DS \leq ds_j) \quad (3-11)$$

where $j=1, 2, \dots, k-1$, where k is the number of damage states. This implies that the sought fragility probabilities are

$$P(DS \geq ds_{j+1}) = 1 - p_j \quad (3-12)$$

where the above definition of j is maintained to ensure a consistent numbering of the damage states. The generic format for multinomial logistic regression models adopted in this chapter is (McCullagh and Nelder 1989)

$$\ln\left(\frac{p_j}{1-p_j}\right) = \theta_{ds_j} + \theta_2 \cdot h_2(\mathbf{x}) + \theta_3 \cdot h_3(\mathbf{x}) + \dots + \theta_m \cdot h_m(\mathbf{x}) \quad (3-13)$$

Importantly, the first model parameter in the right-hand-side, *i.e.*, the intercept parameter, is the only model parameter that changes from the model for one damage state to the model for another. As a result, the problem with crossing of fragility functions is eliminated by imposing the constraint

$$\theta_{ds_1} \leq \theta_{ds_2} \leq \dots \leq \theta_{ds_{k-1}} \quad (3-14)$$

In short, each model is a shifted version of the model for the first damage state, and the shift is modulated by the intercept parameter. For a situation with four damage states the complete set of model parameters for the three logistic regression models is:

$$\boldsymbol{\theta} = (\theta_{ds_1}, \theta_{ds_2}, \theta_{ds_3}, \theta_2, \theta_3, \dots, \theta_m) \quad (3-15)$$

In accordance with the maximum likelihood approach, point estimates for the model parameters are obtained by solving Eq. (3-10), where

$$L(\boldsymbol{\theta}) = \prod_{i=1}^n \left(\prod_{j=1}^k p_{ij}^{y_{ij}} \right) \quad (3-16)$$

where $y_{ij}=1$ if observation i is in damage state j , otherwise $y_{ij}=0$, and p_{ij} is the probability that observation i is in damage state j predicted by Eq. (3-13). Note that in the formulation in Eq. (3-16) it is assumed that observations are statistically independent. Analogous to Eq. (3-3), the probability of a particular damage state is readily obtained from the model in Eq. (3-13) by

$$P(DS = ds_j) = p_{j+1} - p_j \quad (3-17)$$

and the probability of last damage state, ds_k is

$$P(DS = ds_k) = 1 - p_{k-1} \quad (3-18)$$

3.6 ILLUSTRATIVE EXAMPLE

A comprehensive data set for damage of shear walls are employed later in this chapter. Here, a simple illustration example is provided to allow the reader to follow the detailed steps of a basic logistic regression exercise. Table 3-3 shows an artificial but typical data set. In that table, 25 sets of variables x_2 , x_3 , and x_4 are artificially generated by uniformly distributed random number generators in MATLAB®. The random variables x_2 , x_3 , and x_4 are in the range between 0 and 150. Using linear regression model of the form in Eq. (3-6), the random variable r is calculated for each set of \mathbf{x} , assuming normal distribution for random variables θ_1 , θ_2 , θ_3 , θ_4 , and ε . Each set of data is marked by the variable $y_i = \{1, 2, 3, 4\}$, denoting damage states 1, 2, 3, and 4, respectively, based on the value of r . That is, if $r_i \leq 700$, $ds_i = 1$; if $700 < r_i \leq 800$, $ds_i = 2$; if $800 < r_i \leq 1000$, $ds_i = 3$; otherwise $ds_i = 4$. It should be noted here that the variable r and its underlying relationship with random variables \mathbf{x} is arbitrary. In fact, r serves as an auxiliary intervening variable to make a rational way for labeling each data set by ds_1 , ds_2 , etc.

Table 3-3. Set of artificially generated data for illustration exercise

ds_i	R	x_2	x_3	x_4
1	363.65	19.44	33.76	52.5
1	404.51	111.92	23.22	21.59
1	429.36	73.33	33.05	33.93
1	474.94	57.93	91.47	25.03
1	562.45	125.76	25.13	75.33
1	639.52	3.77	62.16	109.71
1	640.34	53.48	81.96	52
1	670.13	95	93.6	49.19
2	716.79	101.38	37.34	71.37
2	721.92	16.62	61.12	132.61
2	733.17	14.39	112.13	112.28
2	742.29	126.16	53.18	64.51
2	761.17	23.36	122.85	93.74
2	790.8	18.6	70.61	128.53
2	796.54	46.86	87.68	124.49
3	805.62	137.6	24.24	107.35
3	913.89	124.78	121.54	83.55
3	917.79	102.79	136.42	91.63
3	991.83	34.95	139.87	114.49
4	1014.41	111.05	103.92	123.61
4	1024.77	134.31	87.38	87.41
4	1035.21	80.79	148.76	113.28
4	1064.96	113.27	111.36	124.67
4	1128.71	140.42	102.48	144.32
4	1157.55	90.3	128.58	148.24

To predict the model parameters, $\theta^T = (\theta_{ds_1}, \theta_{ds_2}, \theta_{ds_3}, \theta_2, \theta_3, \theta_4)$, of the multinomial logistic regression models, the maximum likelihood method is utilized. To establish $L(\theta)$, first, for each data set in Table 3-3, p_{ij} in Eq. (3-16) for $j=1, 2, 3$, and 4 is predicted using multinomial logistic regression formula in Eq. (3-13). For instance, p_{12} reads

$$p_{12} = \frac{\exp(\theta_{ds_2} + 19.44 \cdot \theta_2 + 33.76 \cdot \theta_3 + 52.5 \cdot \theta_4)}{1 + \exp(\theta_{ds_2} + 19.44 \cdot \theta_2 + 33.76 \cdot \theta_3 + 52.5 \cdot \theta_4)} \dots \dots \dots \frac{\exp(\theta_{ds_1} + 19.44 \cdot \theta_2 + 33.76 \cdot \theta_3 + 52.5 \cdot \theta_4)}{1 + \exp(\theta_{ds_1} + 19.44 \cdot \theta_2 + 33.76 \cdot \theta_3 + 52.5 \cdot \theta_4)} \quad (3-19)$$

Defining y_{ij} for each data set, the likelihood function of the form in Eq. (3-16) is evaluated in a MATLAB code. To find the vector θ that maximizes $L(\theta)$, the MATLAB® subroutine *fmincon(.)* is employed to find θ that minimizes $-L(\theta)$ considering the constraint $\theta_{ds_1} \leq \theta_{ds_2} \leq \theta_{ds_3}$. In fact, the minimum of $-L(\theta)$ coincides with the maximum of $L(\theta)$. The multinomial logistic regression models read

$$\ln\left(\frac{p_1}{1-p_1}\right) = 30.15 - 0.12 \cdot x_2 - 0.085 \cdot x_3 - 0.2 \cdot x_4 \quad (3-20)$$

$$\ln\left(\frac{p_2}{1-p_2}\right) = 37.72 - 0.12 \cdot x_2 - 0.085 \cdot x_3 - 0.2 \cdot x_4 \quad (3-21)$$

$$\ln\left(\frac{p_3}{1-p_3}\right) = 42.12 - 0.12 \cdot x_2 - 0.085 \cdot x_3 - 0.2 \cdot x_4 \quad (3-22)$$

The direct minimization of $-L(\theta)$ using *fmincon(.)* is quite inefficient and may fail to estimate the model parameters accurately, particularly when the number of observations or the number of explanatory variables in the data set increases. In this chapter a MATLAB® subroutine for multinomial logistic regression is introduced and utilized later. The subroutine

is called *mnrfit* and employs iteratively reweighted least square method with the Newton-Raphson numerical algorithm to solve Eq. (3-10). The algorithm in the subroutine *mnrfit* is provided in the textbook by McCullagh and Nelder (1989).

3.7 DAMAGE MODELS FOR RC SHEAR WALLS

Reinforced concrete shear walls are key components in the lateral force resisting system of certain building types. Seismic damage to these walls is therefore an important concern in earthquake engineering, and new damage models for these components are developed in the following. The developments employ a database of experiments on reinforced concrete shear walls that is collected from several published articles (Zhang and Wang 2000; Sittipunt *et al.* 2001; Zhu *et al.* 2006; Ali and Wight 1991; Ali and Wight 1991; Corley *et al.* 1981; Paulay *et al.* 1982; Carvajal and Pollner 1983; Pilakoutas and Elnashai 1995; Thomsen and Wallace 1995; Kabeyasawa and Hiraishi 1998; Jiang 1999; Salonikios *et al.* 1999; Hidalgo *et al.* 2002; Ji 2002; Zhou 2004; Zhang 2007; Dazio *et al.* 2009; Orakcal *et al.* 2009; Tran 2010). In total, 146 reinforced concrete shear walls are included in the database, which is presented in Appendix A. The shear walls were subjected to cyclic loading, and load-displacement curves like those shown in Figure 3-3 were recorded. From such hysteresis curves, the “backbone curve”, shown as solid straight lines in Figure 3-3, was extracted for each test specimen. In Figure 3-3, and in the following, the lateral displacement is measured by the dimensionless quantity drift, $\delta = u/h_w$, where u =displacement and h_w =wall height as defined in Figure 3-4. In regards to the data used in this study, it is noted that the loading protocol may affect the backbone curve. In fact, the backbone curve for identical specimens will change depending on the number, amplitude and sequence of cycles (Federal Emergency

Management Agency 2009). It is important to be aware of this issue when finalizing damage models for use in practice. In this chapter, the data is employed as an example of developing multivariate damage models by logistic regressions, thus keeping the effect of loading protocol outside the scope. Hence, the models developed later do not convey the effect of loading protocol on the damage and their use in practice is restricted.

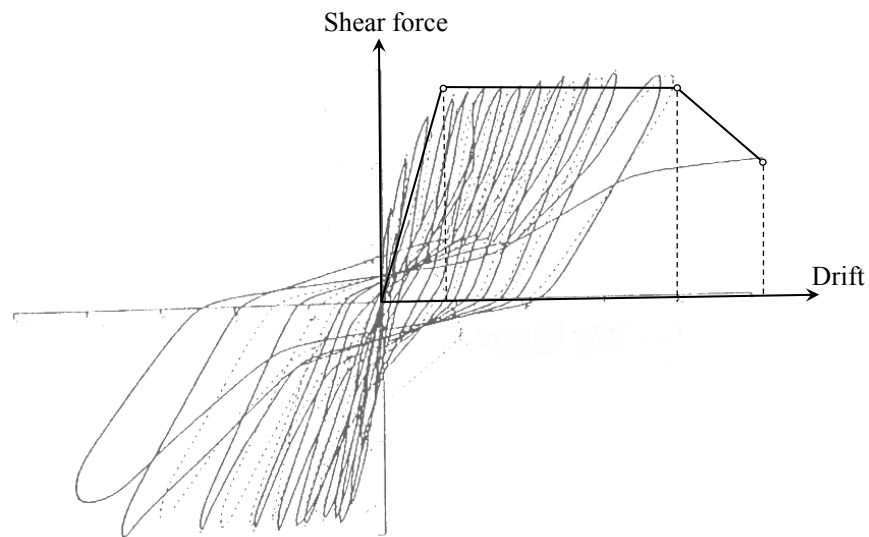


Figure 3-3. Backbone curve from cyclic testing (Pilakoutas and Elnashai 1995).

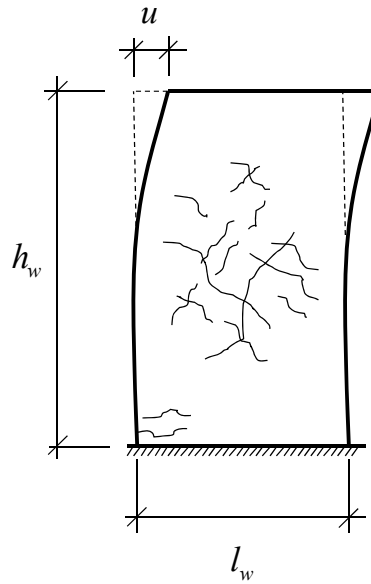


Figure 3-4. Reinforced concrete shear wall.

In lieu of more information about actual damage from the tests, it is hypothesized that the three characteristic points on the backbone curve identify the transition from one damage state to another.

Figure 3-5 illustrates this assumption by showing the drift-ranges where the wall is assumed to be in Damage State 1 (ds_1), Damage State 2 (ds_2), etc. The visual damage for the wall whose hysteretic curve is shown in Figure 3-3 is reported by Pilakoutas and Elnashai (1995) and illustrated in Figure 3-6. Pilakoutas and Elnashai (1995) also tested five more walls and they reported similar propagation of visual damage. As shown in Figure 3-6, the propagation of damage on the wall starts with development of minor cracks. This visual damage is mainly observed when the wall is in ds_1 . The repair action for this damage state is replacement and repair of finishes and in some cases epoxy injection of cracks. As wall enters ds_2 , the cracks will propagate over the length of wall and spalling of cover concrete will begin. Paching of the spalled concrete, epoxy injection of cracks and replacement of

finishes are recommended as repair actions for this damage state in the literature. In ds_3 , sever crushing of cover concrete occurs, which necessitates the replacement of cover concrete. Ultimately, the last damage state essentially corresponds to sever crushing of core concrete and sometimes is accompanied with the reinforcement buckling or fracture. The repair action for this damage state is the replacement of damaged steel and concrete or replacement of the wall. It is emphasized that the damage states are here identified in terms of drift-value ranges solely because the test data on shear wall is provided in this form. However, the methodology described in this paper can be applied to any set of data that shows the damage state for given regressor values, regardless of the definition of damage and therefore can be used also when different factors contribute to the damage state of a structure.

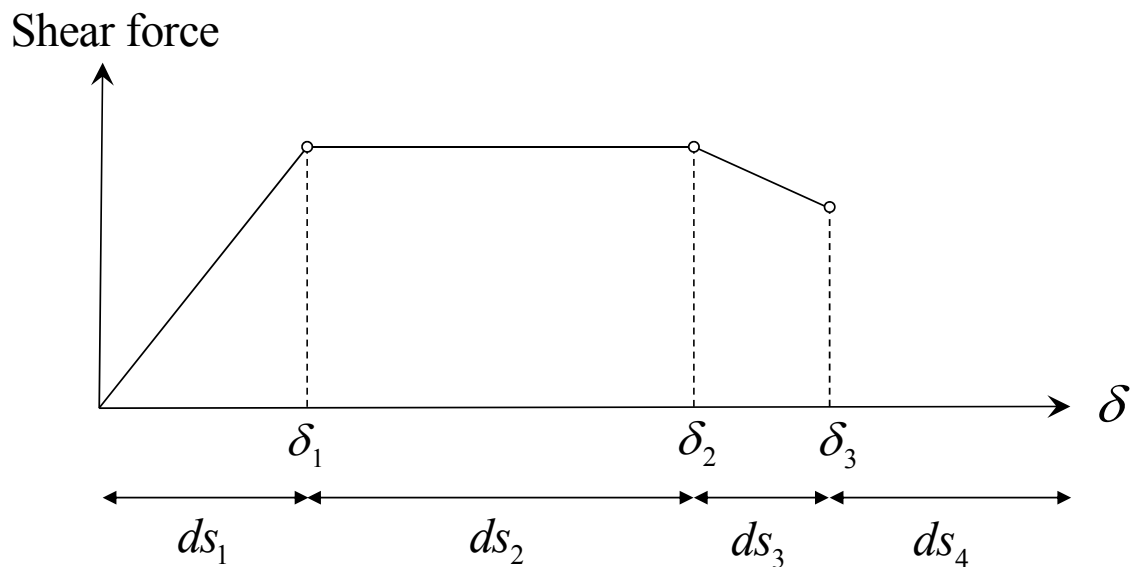


Figure 3-5. Damage states relative to backbone curve.

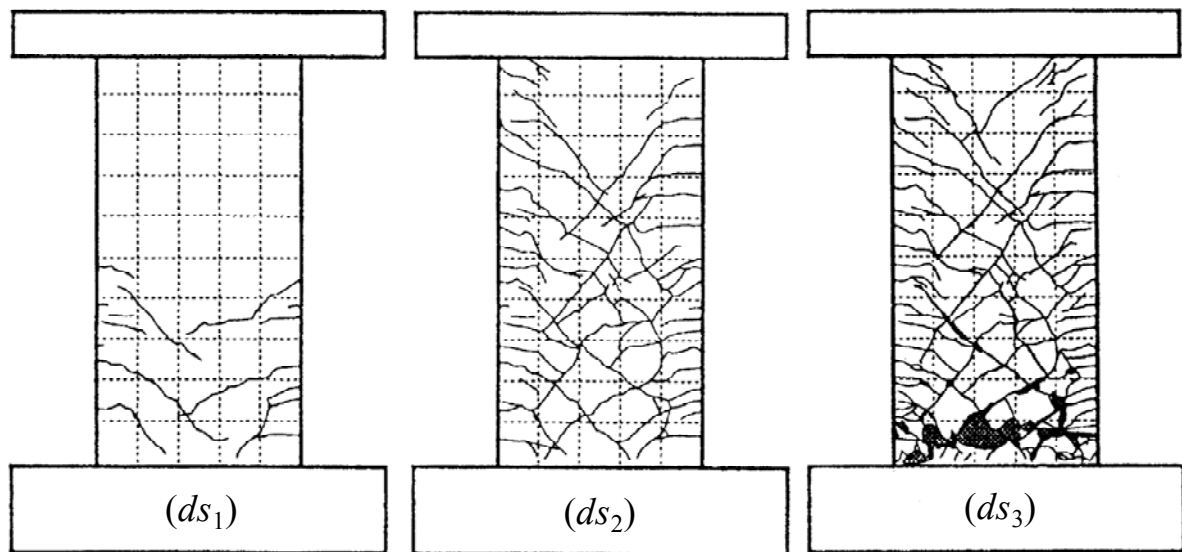


Figure 3-6. The visual damage observed during cyclic test of the wall whose hysteretic curve is shown in Figure 3-3 (Pilakoutas and Elnashai 1995).

As shown in Figure 3-5, the drift values at the transition points between damage states are referred to as δ_1 , δ_2 , and δ_3 . These drift values cannot serve as observations for logistic regression models because δ_1 , δ_2 , and δ_3 identify the *transition* between damage states. Rather, data of the form shown in Table 3-2 is sought. Figure 3-7 illustrates the approach adopted for making the data amenable to logistic regression. Instead of directly using the values for δ_1 , δ_2 , and δ_3 , drift-values within each damage state in

Figure 3-5 are utilized. In each damage state two drift-values are selected to represent the observed values of drift for that damage state. Those two drift-values represent the extreme points on the drift axis at which the damage state of interest is observed. To illustrate this, Table 3-4 shows the data for *one* shear wall (specifically the first row in the table in the Appendix) organized in a way that is amenable to logistic regression, using two drift values for each damage state. For completeness, an alternative strategy of selecting five drift-values in each damage state is also explored.

Figure 3-8 shows the selected five drift-values in each damage state. Results presented later in this chapter show that the results are not highly sensitive to the number of selected drift-values in each damage state.

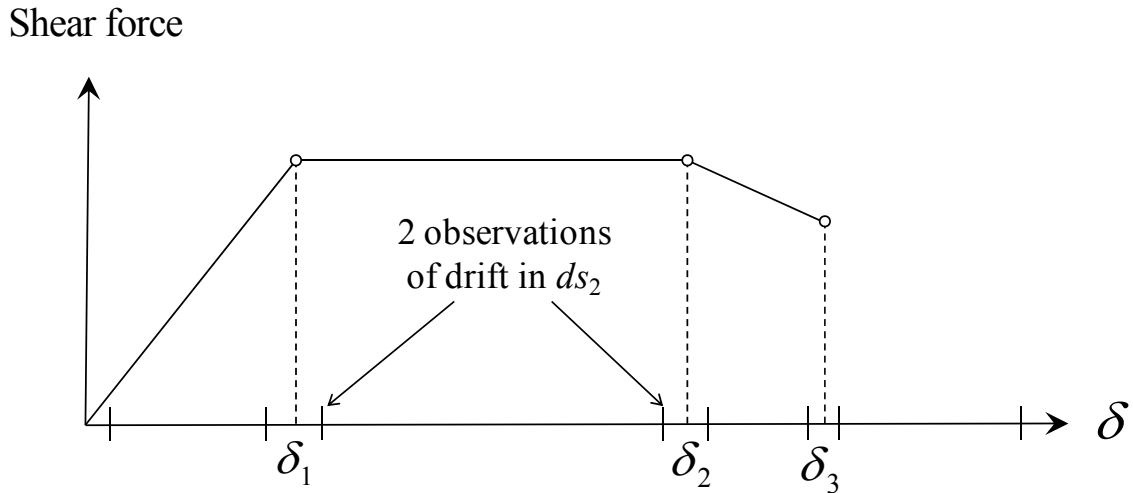


Figure 3-7. Two observed drift-values for each damage state.

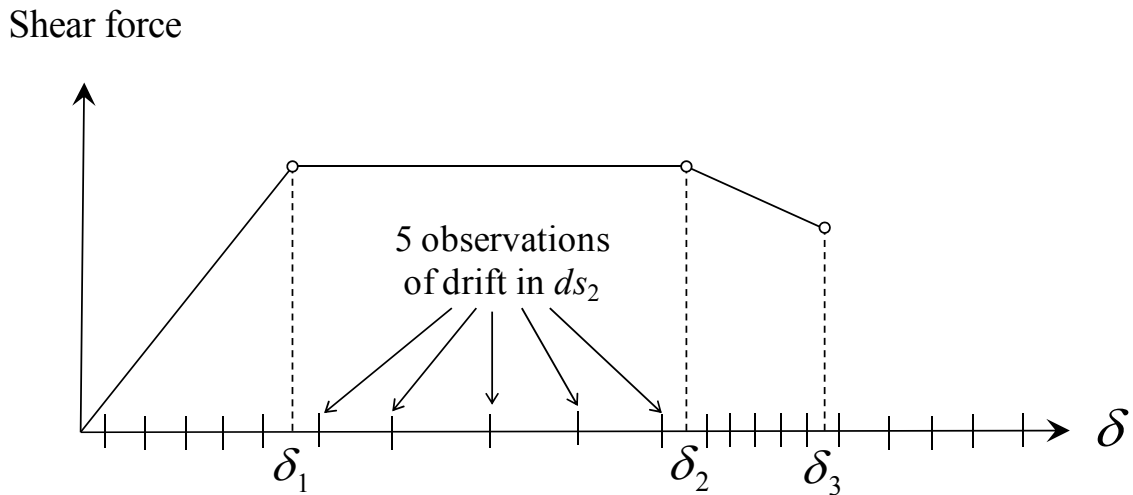


Figure 3-8. Five observed drift-values for each damage state.

Table 3-4. Damage state allocation for the observation in the first row of the table in the Appendix.

ds	$P/(A_g f'_c)$	h_w/l_w	f'_c	f_{yl}	f_{yib}	ρ_{tw}	ρ_{ib}	ρ_{hw}	ρ_{hb}	δ
1	0.073	2.00	47.1	399.91	471.62	0.27	3.17	0.26	1.55	0.012
1	0.073	2.00	47.1	399.91	471.62	0.27	3.17	0.26	1.55	0.60
2	0.073	2.00	47.1	399.91	471.62	0.27	3.17	0.26	1.55	0.63
2	0.073	2.00	47.1	399.91	471.62	0.27	3.17	0.26	1.55	2.16
3	0.073	2.00	47.1	399.91	471.62	0.27	3.17	0.26	1.55	2.18
3	0.073	2.00	47.1	399.91	471.62	0.27	3.17	0.26	1.55	2.86
4	0.073	2.00	47.1	399.91	471.62	0.27	3.17	0.26	1.55	2.88
4	0.073	2.00	47.1	399.91	471.62	0.27	3.17	0.26	1.55	3.55

3.8 APPRAISAL OF DRIFT AS DAMAGE INDICATOR

Before damage models are developed it is of interest to study the suitability of using drift as the only damage indicator. This is done because the application of the fragility function in Eq. (3-4) would only allow the inclusion of one *EDP*, namely the drift. To get a sense for the suitability of that approach in this situation, two results are studied. First, histograms of observed values for δ_1 , δ_2 , and δ_3 are plotted in Figure 3-9. The histograms expose a substantial variability in the drift-values at which the shear walls transition from a damage state to another. This suggests that the utilization of drift alone as a damage indicator is not a successful approach in this situation.

The second result that is studied to get a sense of drift as a damage indicator is a set of ordinary Bayesian linear regression models for δ_1 , δ_2 , and δ_3 . This is done to include

variation in material and geometry parameters in the prediction of drift-values at which walls transition from one damage state to another. The resulting models are

$$\delta_1 = \theta_{1,1} + \theta_{1,2} \cdot h_2(\mathbf{x}) + \theta_{1,3} \cdot h_3(\mathbf{x}) + \dots + \theta_{1,10} \cdot h_{10}(\mathbf{x}) + \varepsilon_1 \quad (3-23)$$

$$\delta_2 = \theta_{2,1} + \theta_{2,2} \cdot h_2(\mathbf{x}) + \theta_{2,3} \cdot h_3(\mathbf{x}) + \dots + \theta_{2,10} \cdot h_{10}(\mathbf{x}) + \varepsilon_2 \quad (3-24)$$

$$\delta_3 = \theta_{3,1} + \theta_{3,2} \cdot h_2(\mathbf{x}) + \theta_{3,3} \cdot h_3(\mathbf{x}) + \dots + \theta_{3,10} \cdot h_{10}(\mathbf{x}) + \varepsilon_3 \quad (3-25)$$

where h_i are explanatory functions listed in Table 3-5. The smooth lines in Figure 3-9 show the probability distribution for δ_1 , δ_2 , and δ_3 obtained by employing these models for a specific wall with properties $P/A_g f'_c=0.35$, $h_w/l_w=2.14$, $f'_c=40.2\text{MPa}$, $f_{yl}=305\text{MPa}$, $f_{y1b}=432\text{MPa}$, $\rho_{lw}=0.67\%$, $\rho_{lb}=4.5\%$, $\rho_{hw}=1\%$, and $\rho_{hb}=2.26\%$.

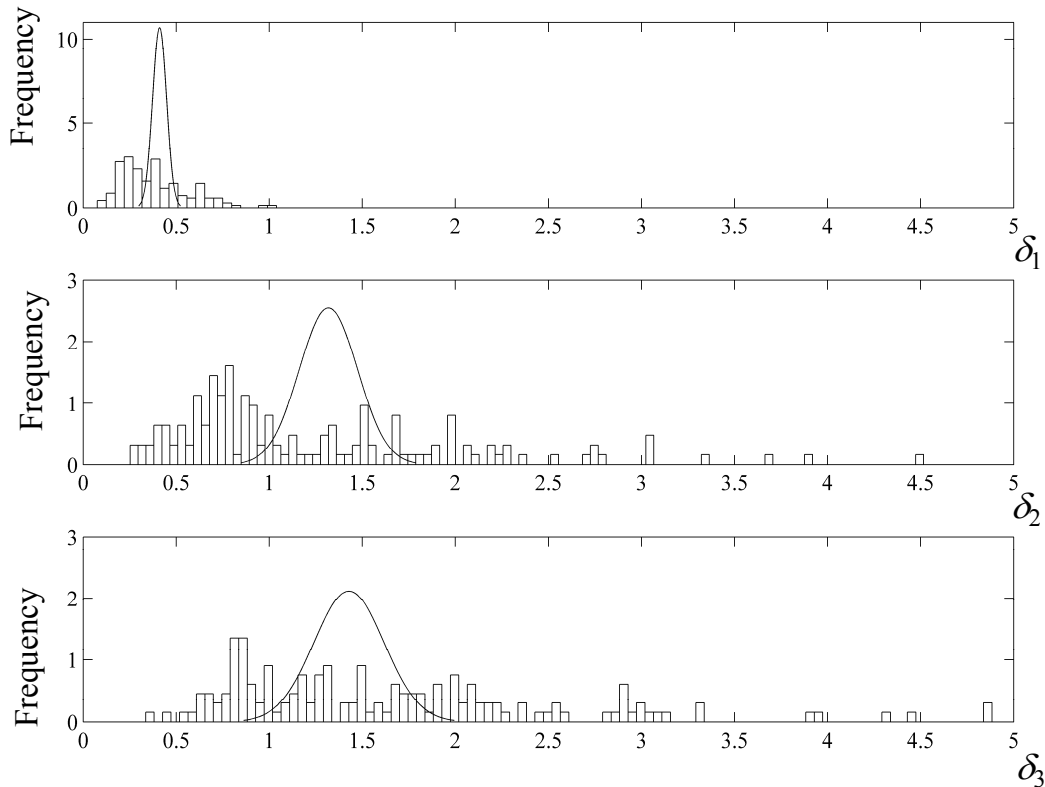


Figure 3-9. Frequency diagram and PDF for drift.

It is apparent in Figure 3-9 that even when geometry and material parameters are accounted for; there is substantial variability in the drift at which a shear wall transitions from one damage state to another. However, this variability is noticeably less than the variability in histograms, which emphasizes the importance of including material and geometry parameters in the damage models in addition to drift.

Table 3-5. List of explanatory functions

h_2	Axial load ratio	$P/A_g f'_c$	[-]
h_3	Aspect ratio (wall height over wall length)	h_w/l_w	[-]
h_4	Concrete compressive strength	f'_c	[MPa]
h_5	Yield strength of flexural reinforcement (web)	f_{yl}	[MPa]
h_6	Yield strength of flexural reinforcement	f_{yb}	[MPa]
h_7	Flexural reinforcement (web)	ρ_{lw}	[%]
h_8	Flexural reinforcement (boundary)	ρ_{lb}	[%]
h_9	Horizontal reinforcement (web)	ρ_{hw}	[%]
h_{10}	Horizontal reinforcement (boundary)	ρ_{hb}	[%]
h_{11}	Natural logarithm of drift	$\ln(\delta)$	[%]

Table 3-5 gives an overview of the explanatory functions that are used in this regression exercise. It is noted that the natural logarithm of δ is employed rather than δ itself, so that zero damage probability is predicted at zero drift. In the following, \mathbf{h} denotes an n -by-10 dimensional matrix whose rows contain the value of the 10 explanatory functions in Table 3-5 for each of the n observations. When s drift-values are used for each of the 4 damage states then $s \times 4$ drift values are used for each of the 146 shear walls, hence $n = s \times 4 \times 146$. The n -dimensional vector \mathbf{y} is also defined, which contains the damage state for each observation. \mathbf{h} and \mathbf{y} are input to the subroutine *mnrfit* in the computer program MATLAB®, which

implements the previously described methodology and produces means, variances, and covariance for the model parameters. The result is estimates for the model parameters in Eq. (3-15), yielding three models of the form in Eq. (3-13) for p_1 , p_2 , and p_3 . Specifically, the model parameters are computed by the command $\theta = mnrfit(\mathbf{h}, \mathbf{y}, 'model', 'ordinal')$, where θ are point estimates for the model parameters and the options 'model' and 'ordinal' are employed to obtain multinomial logistic regression models of the form of Eq. (3-13). For the considered shear wall data, which includes four damage states, the models read

$$\ln\left(\frac{p_1}{1-p_1}\right) = \theta_{ds_1} + \theta_2 \cdot h_2(\mathbf{x}) + \theta_3 \cdot h_3(\mathbf{x}) + \dots + \theta_{11} \cdot h_{11}(\mathbf{x}) \quad (3-26)$$

$$\ln\left(\frac{p_2}{1-p_2}\right) = \theta_{ds_2} + \theta_2 \cdot h_2(\mathbf{x}) + \theta_3 \cdot h_3(\mathbf{x}) + \dots + \theta_{11} \cdot h_{11}(\mathbf{x}) \quad (3-27)$$

$$\ln\left(\frac{p_3}{1-p_3}\right) = \theta_{ds_3} + \theta_2 \cdot h_2(\mathbf{x}) + \theta_3 \cdot h_3(\mathbf{x}) + \dots + \theta_{11} \cdot h_{11}(\mathbf{x}) \quad (3-28)$$

Table 3-6 and Table 3-7 show the statistics of the model parameters, given 2 and 5 drift-observations in each damage state, respectively. In those tables, it is observed that the estimated model parameters are close for 2 and 5 drift-observations. Figure 3-10 illustrates the results further by displaying the variation in damage probabilities with δ for 2 and 5 drift-values in each damage state, computed for a wall with $P/A_g f'_c = 0.4$, $h_w/l_w = 2$, $f'_c = 30\text{MPa}$, $f_{yl} = 450\text{MPa}$, $f_{ylb} = 500\text{MPa}$, $\rho_{lw} = 0.25\%$, $\rho_{lb} = 4\%$, $\rho_{hw} = 1.77\%$, and $\rho_{hb} = 1.5\%$. It is observed in Figure 3-10 that the results for 2 drift-observations in each damage state are quite close to the results for 5 observations. In other words, the results are not highly dependent on the choice of 2 or 5 drift-observations. Figure 3-10 also illustrates that the logistic regression models are akin to uniaxial fragility functions, but the logistic regression models take many input

parameters. To investigate the effect of the number of observations on the statistical uncertainty, Figure 3-11 shows the confidence bands. The confidence bands are computed using a first-order Taylor series expansion around the mean estimation of p (Gardoni *et al.* 2002). It is seen in that figure that the confidence bands for models developed with 5 drift-observations in each damage state are narrower than those developed with 2 drift-observations. It demonstrates that the statistical uncertainty reduces when the number of observations increases. It is also reiterated that the dispersion shown in the curves Figure 3-10 and Figure 3-11 is statistical uncertainty stemming from the data, rather than from estimating a dispersion parameter in a lognormal distribution in conventional fragility analysis.

Table 3-6. Statistics of the model parameters, given 2 drift-observations, θ_4 , θ_5 , and θ_6 have unit 1/MPa.

Par.	θ_{ds1}	θ_{ds2}	θ_{ds3}	θ_2	θ_3	θ_4	θ_5	θ_6	θ_7	θ_8	θ_9	θ_{10}	θ_{11}
Max. L. Est.	-6.28	-3.54	-1.57	-2.85	0.88	0.0021	0.0013	0.0011	-0.29	0.0078	1.58	-0.16	-2.72
St. dev.	0.33	0.27	0.25	0.64	0.08	0.004	0.0006	0.0005	0.4	0.04	0.37	0.07	0.12
Correlation coefficients													
θ_{ds2}	0.89												
θ_{ds3}	0.84	0.92											
θ_2	0.15	0.11	0.93										
θ_3	-0.66	-0.65	-0.63	-0.25									
θ_4	-0.05	-0.05	-0.05	-0.03	0.15								
θ_5	-0.41	-0.47	-0.49	0.05	-0.008	-0.41							
θ_6	0.074	0.12	0.15	-0.15	0.02	-0.11	-0.59						
θ_7	-0.15	-0.03	-0.04	-0.15	0.12	-0.19	-0.05	-0.11					
θ_8	-0.014	-0.03	-0.02	-0.14	-0.18	-0.2	0.31	-0.39	0.08				
θ_9	-0.23	-0.21	-0.2	0.09	0.05	0.15	0.11	0.2	-0.77	-0.3			
θ_{10}	0.10	0.09	0.09	-0.12	0.03	-0.02	-0.06	-0.26	0.35	0.07	-0.55		
θ_{11}	0.70	0.55	0.42	0.2	-0.49	-0.01	-0.12	-0.11	0.03	0.004	-0.2	0.11	

Table 3-7. Statistics of the model parameters, given 5 drift-observations, θ_4 , θ_5 , and θ_6 have unit 1/MPa.

Par.	θ_{ds1}	θ_{ds2}	θ_{ds3}	θ_2	θ_3	θ_4	θ_5	θ_6	θ_7	θ_8	θ_9	θ_{10}	θ_{11}
Max. L. Est.	-7.81	-4.44	-2.26	-3.82	1.18	0.003	0.0016	0.0015	-0.32	-0.004	2.09	-0.21	-3.52
St. dev.	0.24	0.19	0.17	0.43	0.06	0.003	0.0004	0.0003	0.26	0.03	0.24	0.05	0.09
Correlation coefficients													
θ_{ds2}	0.88												
θ_{ds3}	0.83	0.92											
θ_2	0.19	0.14	0.12										
θ_3	-0.69	-0.67	-0.65	-0.27									
θ_4	-0.05	-0.05	-0.05	-0.03	0.15								
θ_5	-0.39	-0.47	-0.49	0.04	0.015	-0.41							
θ_6	0.038	0.11	0.14	-0.16	0.04	-0.11	-0.58						
θ_7	-0.015	-0.03	-0.04	-0.16	0.11	-0.19	-0.038	-0.11					
θ_8	0.0009	-0.01	-0.007	-0.13	-0.19	-0.2	0.31	-0.39	0.09				
θ_9	-0.025	-0.23	-0.22	0.07	0.09	0.16	0.11	0.21	-0.77	-0.3			
θ_{10}	0.12	0.11	0.11	-0.11	0.002	-0.02	-0.07	-0.26	0.34	0.07	-0.55		
θ_{11}	0.76	0.59	0.46	0.24	-0.55	-0.02	-0.13	-0.13	0.03	0.023	-0.24	0.13	

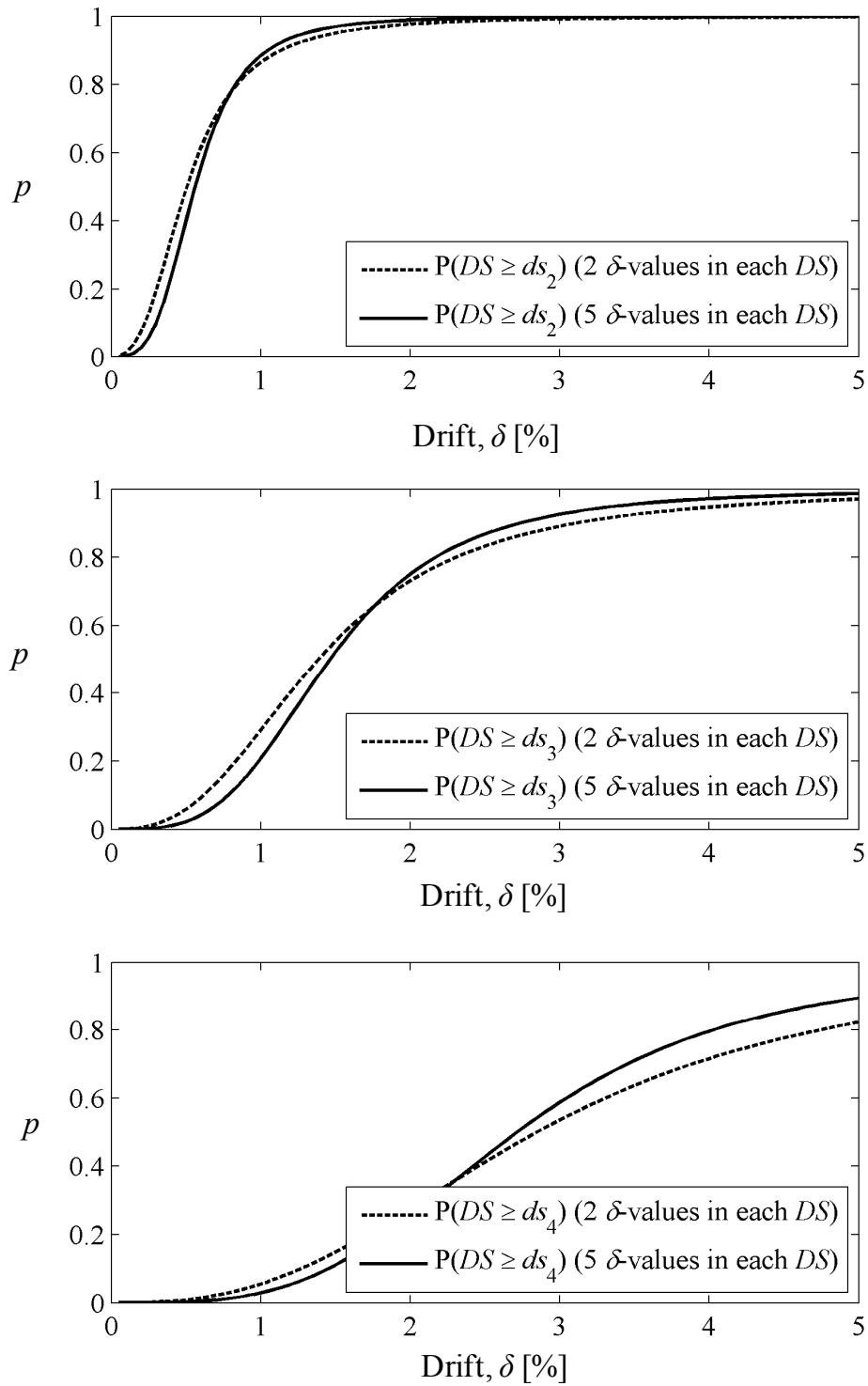


Figure 3-10. Variation of damage probabilities with δ for a specific shear wall.

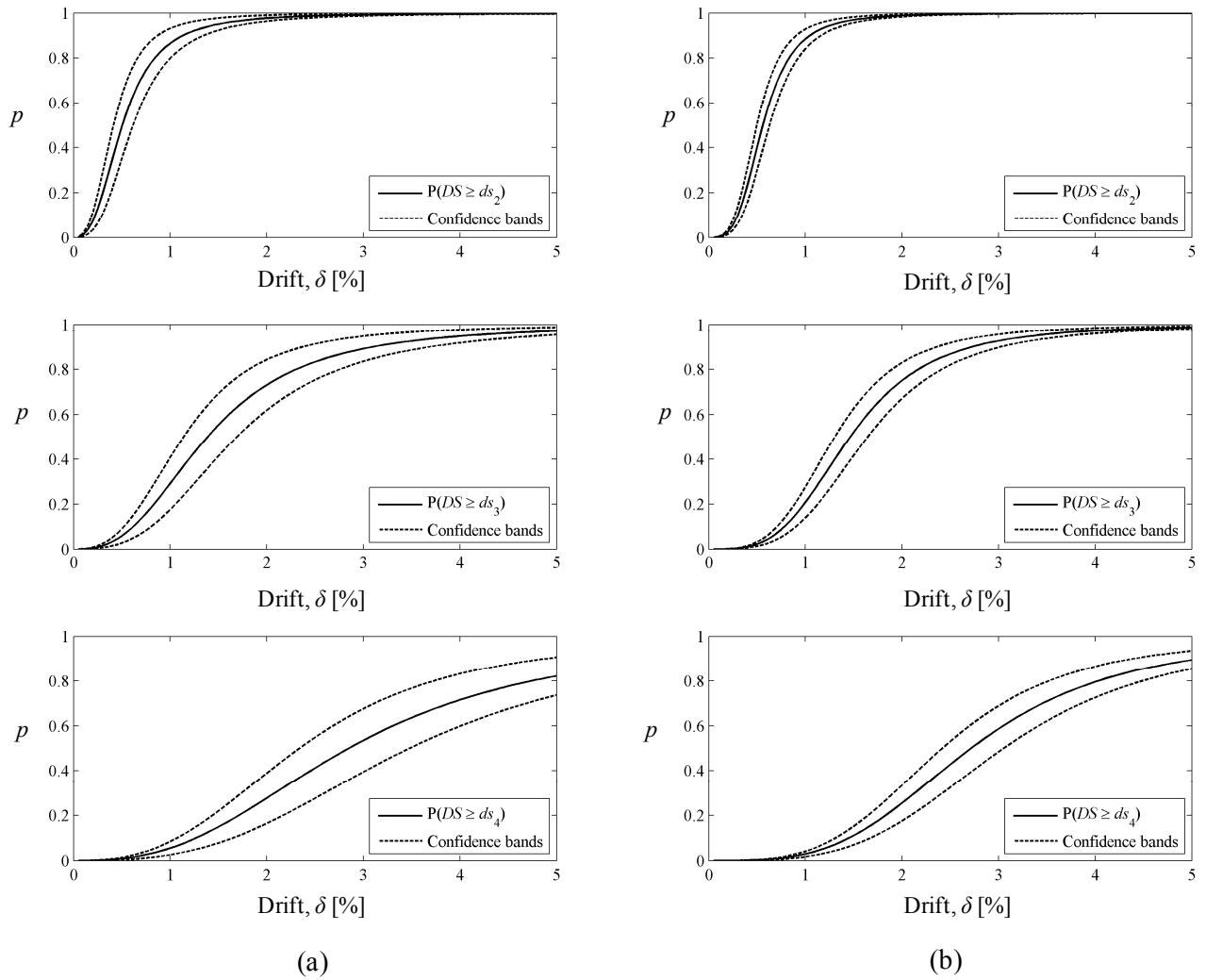


Figure 3-11. Confidence bands for damage probabilities: a) 2 δ -values in each damage state; b) 5 δ -values in each damage state.

3.9 MODEL SELECTION PROCEDURE

The models developed above contain all the explanatory functions that are available in the database. Because it is unlikely that all of them are equally influential on damage, it is of interest to simplify the models form by removing unimportant explanatory functions. In the following, the procedure proposed by Gardoni *et al.* (2002) is used to select more parsimonious models. In this procedure, the significance of each explanatory function is

measured by the coefficient of variation (COV), *i.e.*, the ratio of the standard deviation to the mean value, of the associated model parameter. That is, the explanatory function whose model parameter has the largest COV is least important compared with the other explanatory functions, and can potentially be removed from the model. However, at some point the removal of explanatory functions must stop to avoid deterioration of the overall model quality. Thus, an indicator that measures the overall model quality is needed. In this chapter, the residual deviance, D , proposed by McCullagh and Nelder (1989) is employed for this purpose:

$$D = 2 \cdot \sum_{i=1}^n \sum_{j=1}^k y_{ij} \cdot \ln \left(\frac{y_{ij}}{p_{ij}} \right) \quad (3-29)$$

where n , k , y_{ij} , and p_{ij} have the same definition as in Eq. (3-16). D is computed before and after the deletion of an explanatory function to determine if the removal caused significant model deterioration. If D does not increase by an unacceptable amount, *i.e.*, greater than one percent, the model reduction is accepted. The following steps summarize the model selection procedure:

- 1- Compute the model parameters and their COV's, as well as the residual deviance, D_1 , by the MATLAB command `[θ , D_1 , stat]=mnrfi(h, y, 'model', 'ordinal')`. The variable *stat* contains a host of model statistics; the MATLAB command `[stat.t]` extracts the "t-statistics" of the model parameters, collected in a vector. The command `[stat.t].^(-1)` returns estimates of COV of the model parameters.

- 2- Identify the model parameter, θ_i , with the largest absolute COV. The associated explanatory function, h_i , is least informative and an attempt can be made to remove it from the model.
- 3- For the reduced model, compute the residual deviance, D_2 , by the above MATLAB command.
- 4- Compute the change in the residual deviance before and after the deletion of h_i by $(D_2-D_1)/D_1$. If the residual deviance has not changed significantly, accept the reduced model and turn to step 1, 2, and 3 to reassess the reduced model for possible further model reduction. Otherwise, the reduction is not desirable and the model form before the reduction is as parsimonious as possible.

The above-listed procedure is elaborated to achieve an optimal balance between the model parsimoniousness and the model accuracy. Figure 3-12 shows schematically the model selection algorithm.

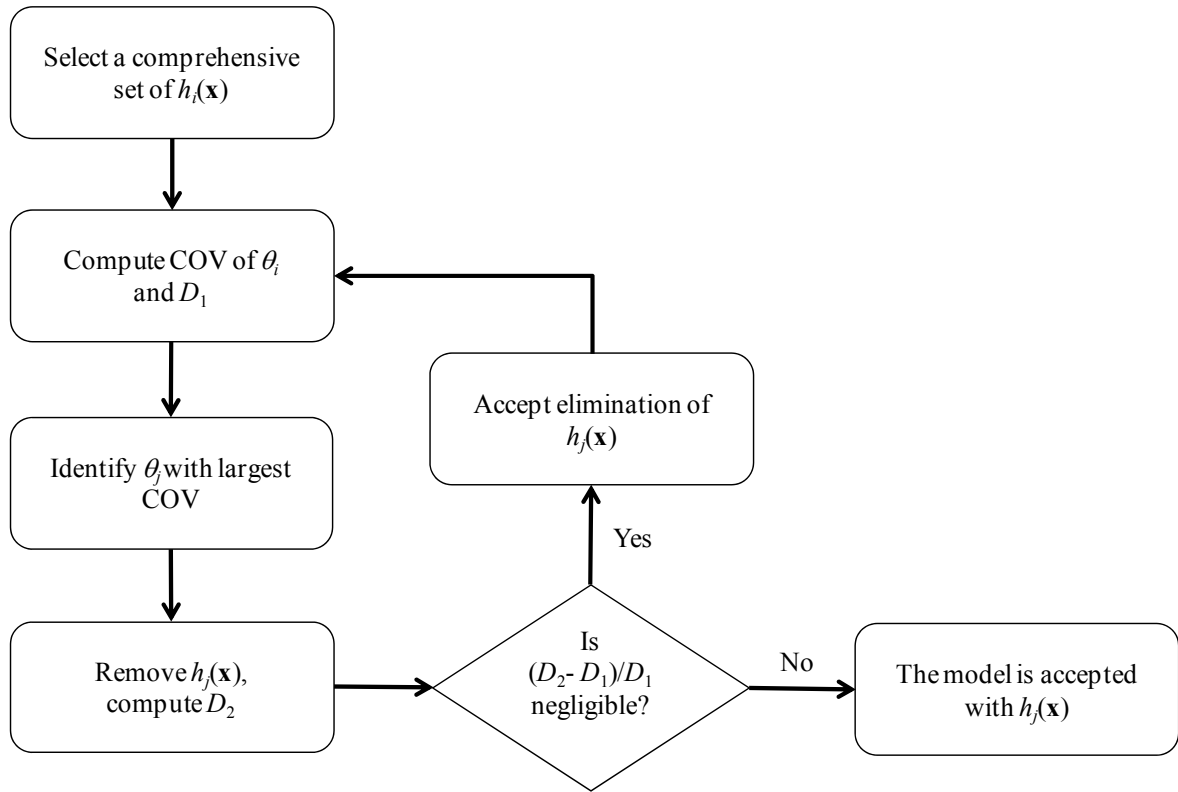


Figure 3-12. Model selection algorithm.

Figure 3-13 summarizes the deletion process for the case of 5 drift-observations in each damage state. In Figure 3-13 the COV for each θ is shown by solid circles for each attempt to delete an explanatory variable. At the first step, when the model contains all ten explanatory functions listed in Table 3-5, the residual deviance, D , is 4578.45 and θ_8 has the largest COV at 1.1379. As a result, ρ_{lb} is removed from the model. This deletion is denoted by a cross-mark in Figure 3-13. Next, the reduced model with nine explanatory functions is assessed. The residual deviance for the reduced model is 4578.47, which is a negligible increase from the previous value. In the next steps, f'_c , ρ_{lw} , ρ_{hb} , and f_{ylb} were removed from the model, leading to increases in D equal to 0.022%, 0.024%, 0.47%, 0.48%, and 1.61%, respectively. Figure 3-14 shows the change in the residual deviance before and after the

deletion of each explanatory function depicted in Figure 3-14. After these five steps, the parameter with the largest COV is θ_2 . The deletion of $P/A_g f_c$ from the model causes a more substantial increase in the residual deviance of the model as shown in Figure 3-14. This is an indication that further reduction deteriorates the quality of the model. Stopping at this step, the five explanatory functions shown in Table 3-8 remain, each associated with the shown second-moment statistics. Table 3-8 shows that θ_{11} has the least absolute COV among the remaining model parameters; it is therefore concluded that $\ln(\delta)$ is the most important explanatory function in the model. Table 3-8 also shows that h_w/l_w is the second most important explanatory function. The practical range for each explanatory function is also provided later. The examples provided in the next section demonstrates that how different variables of wall significantly affects the damage probabilities.

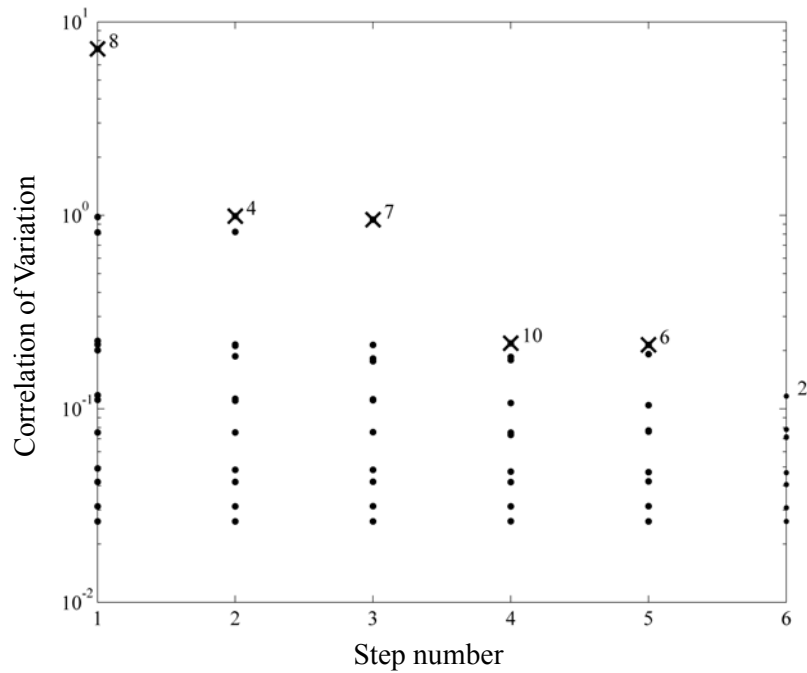


Figure 3-13. Stepwise deletion process to obtain a parsimonious model.

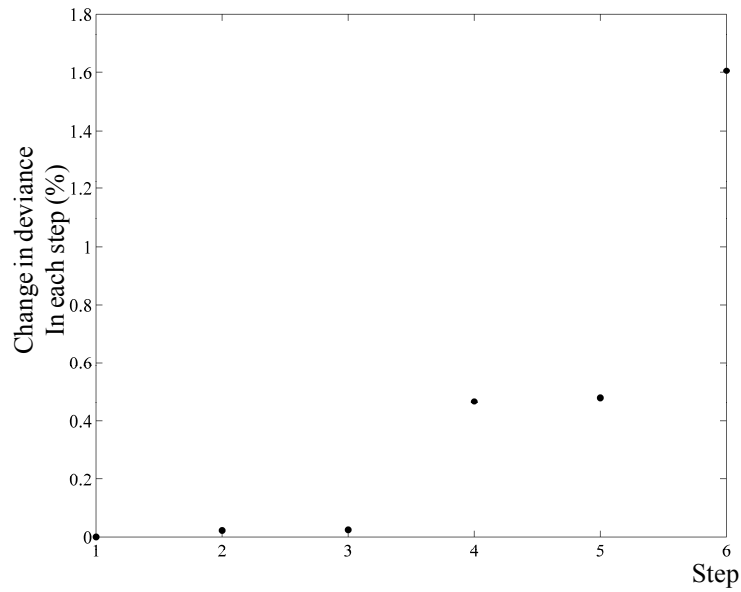


Figure 3-14. Change in the residual deviance of the multinomial logistic regression models in each iteration of deletion process.

Table 3-8. Model parameters for the final model.

Model parameter	Explanatory function	Mean of θ_i	COV of θ_i in %
θ_{ds1}	-	-7.78	3.1
θ_{ds2}	-	-4.47	4.1
θ_{ds3}	-	-2.32	7.2
θ_2	$P/A_g f'_c$	-3.41	12
θ_3	h_w/l_w	1.19	4.7
θ_5	f_{yl}	0.0028	7.9
θ_9	ρ_{hw}	1.65	7.1
θ_{11}	$\ln(\delta)$	-3.44	2.6

3.10 MODEL APPLICATION

To demonstrate that the multinomial logistic regression models can be employed to produce the same results as a fragility function, Figure 3-15 contrasts the fragility functions produced with the models developed above and univariate models. The univariate models are developed in accordance with the procedure presented in the Appendix H of Applied Technology Council (2012). The procedure prescribes the computation of μ_j and σ_j in Eq. (3-4) for three curves. μ_j for $j=1,2,3$ are the median value of observed δ_1 , δ_2 , and δ_3 in the database, respectively. σ_j is computed considering two contributors in uncertainty in fragility models. The first contributor is the standard deviation, σ_{jr} , of observed $\ln(\delta_1)$, $\ln(\delta_2)$, and $\ln(\delta_3)$. The second contributor, σ_{ju} , is the uncertainty that the tests represent actual conditions of installation and loading. According to the prescribed procedure, σ_{ju} is identical for different damage states and equal to 0.1. Ultimately, σ_j is calculated as $\sqrt{\sigma_{jr}^2 + \sigma_{ju}^2}$. The effect of all other variables in the database is ignored because the univariate model cannot take more than one input variable. This is in contrast with the multivariate models where the value of all variables in the database is considered in the model development. Depending on the wall properties the curves extracted from multivariate models shift closer or farther to the curves produced by the univariate models in Figure 3-15. That is, the increase in the values of h_w/l_w , f_{yl} , and ρ_{hw} shifts the curves to right while the increase in $P/A_g f'_c$ shifts the curves to left. This implies that the drift values at which the wall enters to the next damage state are higher in walls with higher value of h_w/l_w , f_{yl} , and ρ_{hw} . Conversely, those drift values are lower for the walls subjected to higher $P/A_g f'_c$. This result confirms the analytical study conducted by Kazaz *et al.* (2012), which suggests that yield and ultimate drift ratio of walls decrease for

walls with higher $P/A_g f'_c$. The curves developed by the multivariate models in Figure 3-15 are plotted for a wall with $P/A_g f'_c=0.4$, $h_w/l_w=2$, $f_{yl}=450\text{MPa}$, and $\rho_{hw}=1.77\%$. As shown in that figure, for such wall there is a significant difference between the results from multivariate and univariate models for the aforementioned wall. However, as stated earlier, the difference between curves depends on the parameters such as $P/A_g f'_c$, h_w/l_w , f_{yl} , and ρ_{hw} . To further investigate the effect of these parameters on damage probabilities, the damage probabilities are plotted versus different parameters in Figure 3-16. In that figure, the fragility surface for $P(DS \geq ds_2)$, $P(DS \geq ds_3)$, and $P(DS \geq ds_4)$ are shown. Each fragility surface shows damage probabilities plotted against drift and aspect ratio for the shear wall defined above. In Figure 3-16, three fragility curves are also plotted against h_w/l_w , f_{yl} , and ρ_{hw} , showing the variation of damage probabilities at $\delta=2\%$. In these plots, the abscissa axes are limited to values that are in the “practical range,” *i.e.*, the range of regressor values in the database used to develop this model. Specifically, these ranges are $0.35 < h_w/l_w < 7$, $0 < f_{yl} < 1079$, $0\% < \rho_{hw} < 1.77\%$. The other explanatory functions are kept constant and equal to the value for the wall in Figure 3-15. Figure 3-16 shows that the probability of damage is not only influenced by δ , but that damage probability also diminishes with increasing value of h_w/l_w . This is reasonable because walls with high aspect ratios are primarily associated with flexural deformation and can tolerate more drift before sustaining damage. In the univariate plots it is also observed that the effect of f_{yl} and ρ_{hw} on $P(DS \geq ds_2)$ are negligible. Kazaz *et al.* (2012) also found that the increase in the value of ρ_{hw} does not have significant influence on the yield drift ratio, which agrees with the result of current study.

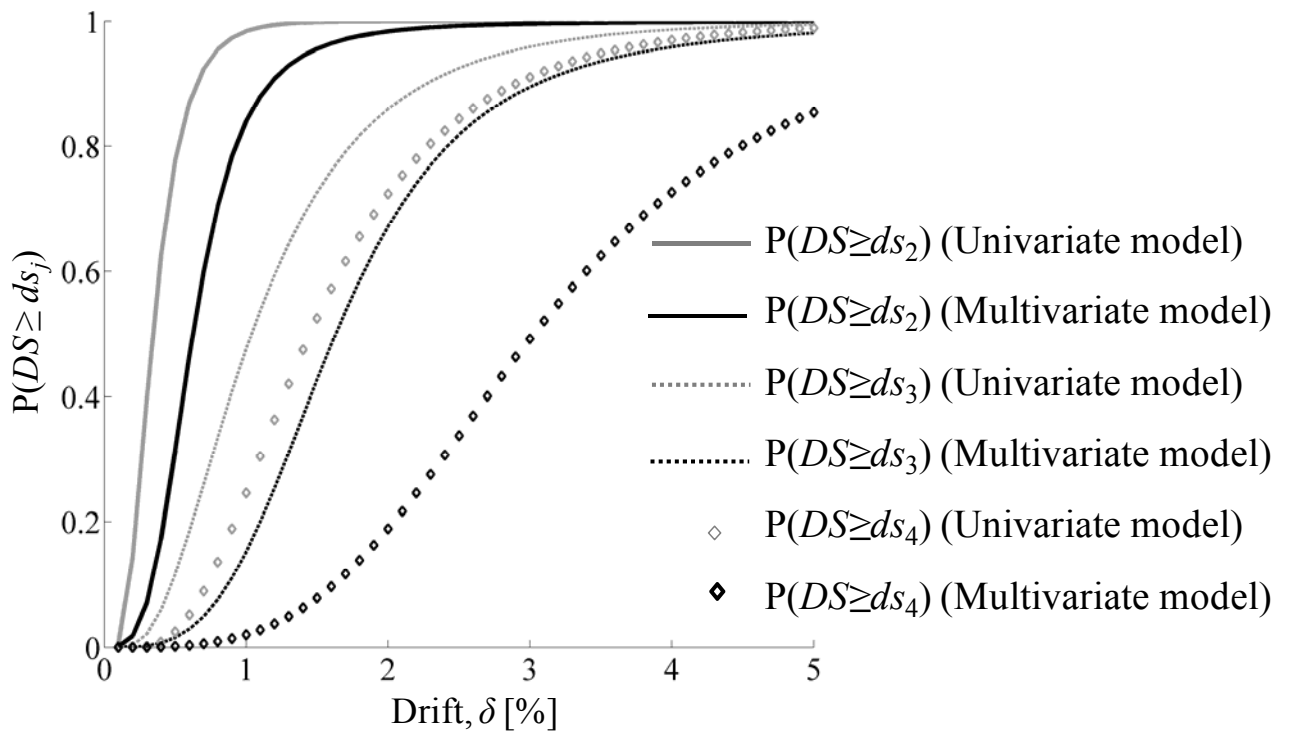


Figure 3-15. Variation of damage probabilities with δ for a specific shear wall.

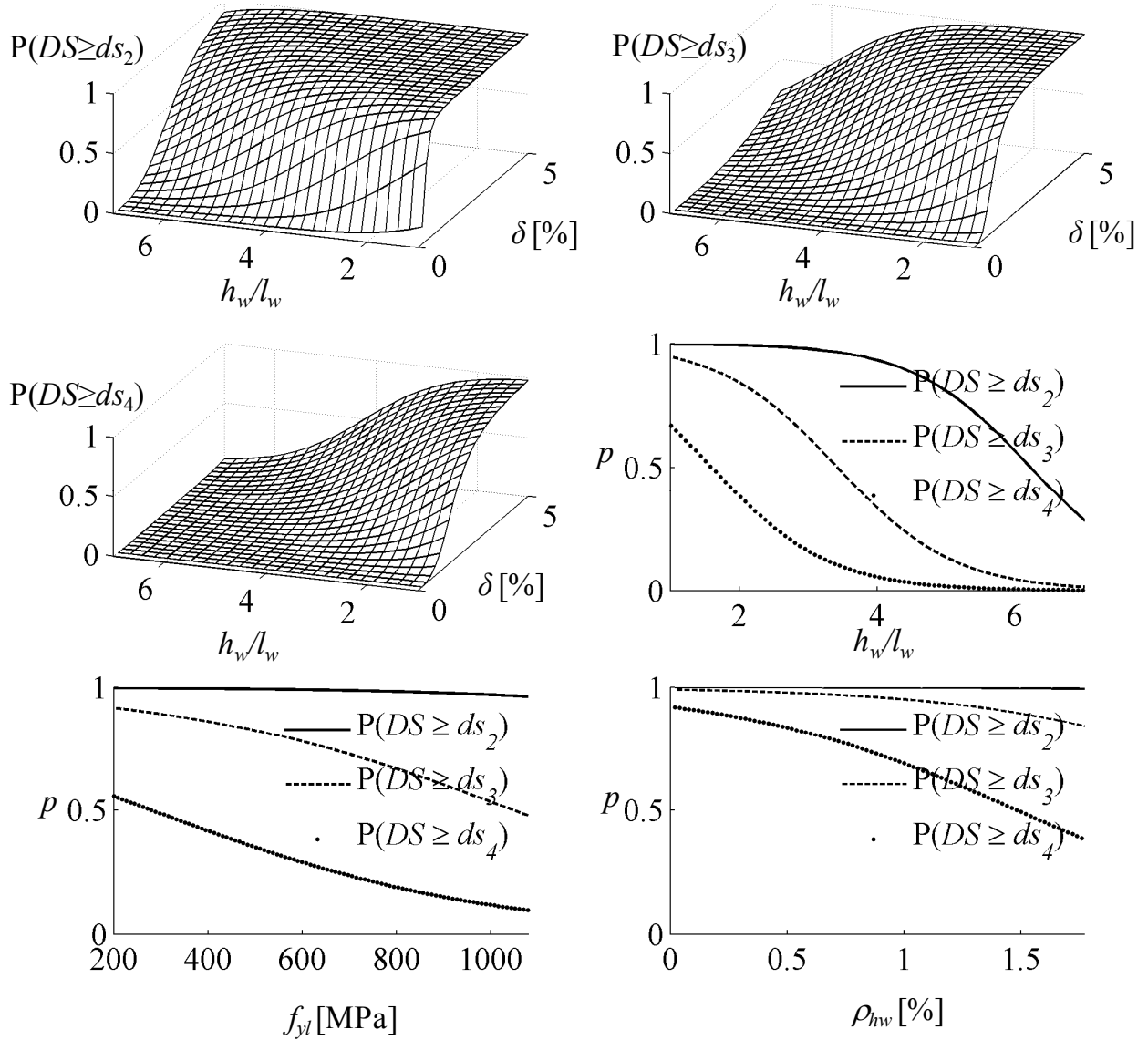


Figure 3-16. Variation of fragility probabilities with δ , h_w/l_w , f_{yl} , and ρ_{hw} for a specific shear wall.

3.11 CONCLUSIONS

This chapter addresses damage modeling in performance-based earthquake engineering. The role of fragility functions in modern PBEE is first examined and it is observed that the majority of existing approaches link the probability of damage to a single demand parameter.

As an extension of the state-of-the-art, this chapter advocates the development of

multivariate fragility models. Logistic regression is found to be ideal for this purpose, and the resulting multinomial and multivariate models relate the probability of damage to any number of material properties, geometry parameters, and structural responses. This approach remedies several limitations inherent in the use of univariate fragility functions. Importantly, the new models are compatible with existing PBEE approaches, such as the ATC-58 framework for PBEE. As a demonstration of the logistic regression approach, multinomial and multivariate damage probability models are developed in this chapter for reinforced concrete shear walls. A model selection procedure is also outlined, by which only the most influential parameters are retained in the final models. The resulting models show that the imposed drift and the aspect ratio are among the parameters that have the greatest influence on damage in reinforced concrete shear walls.

Chapter 4: SIMULATION OF VISUAL DAMAGE TO BUILDING

COMPONENTS

The objective in this chapter is to simulate the damage to building components due to earthquakes. To achieve this objective, this chapter presents new software implementations, which include a new building “component” concept. Importantly, this work directly addresses the vision described in the introduction of this thesis, aiming for simulation of detailed visual damage. This facilitates the prediction of repair actions, and in turn better repair cost estimates.

Several specific objectives are addressed in this study: 1) Formulation of a consistent model format for predicting the detailed visual damage to components; 2) Rigorous computation of the quantity that should be repaired for each component; 3) Development and implementation of a library of component-specific damage and repair action models; 4) Assessment of total cost, considering repair actions, repair quantities, economy of scale, or potential demolition of the building.

The work extends the existing computer program Rt (Mahsuli and Haukaas 2013) and the ultimate objective is risk-based optimization of building designs. As mentioned in the introduction to this thesis, the extended software is called Rts, and its long-term vision is presented in Chapter 1. Rts is object-oriented and has several classes that organize and orchestrate the analysis. In this thesis, new classes for simulation of damage are implemented.

4.1 A NEW BUILDING COMPONENT CONCEPT

Rts is developed with the object-oriented programming language C++ (Deitel and Deitel 2013). This means that objects are instantiated at run-time from classes that are created by the developer. The concept of object-oriented programming is presented in many books, including that by Eckel (2000). In object-oriented programming, each class has “data members,” such as numbers and arrays that store the class data, and “member functions,” where the algorithms for conducting the tasks are implemented. Member functions are often referred to simply as “methods.” The private data members and methods can only be called inside their class. In contrast, the public data members and methods can be called not only inside their class, but also by other classes. In Rts, a new class is designed to simulate the performance of building components. These classes are inherited from a base class called *RComponent*, introduced in this thesis. Similar to Rt, the name of classes in Rts starts with the letter R.

The *RComponent* class has methods that provide information for assessing the performance of building components. This information ranges from construction cost and environmental impacts of component manufacturing, use, and demolishing (Guerra 2010), to required repair actions and quantities due to earthquakes. This is in contrast with the traditional finite element class whose methods solely focus on the mechanical aspects of the structural components, *i.e.*, stiffness and forces. Rather, the *RComponent* class in this thesis is intended to simulate the monetary impact of design, manufacturing, construction, and damage due to hazards, such as earthquake, flood, wind, *etc.* The total cost will ultimately include all events that may occur in the lifespan of a building, from construction to demolition.

To further explain the difference between the traditional finite element and the building component class, Figure 4-1 contrasts these two classes in Rts. In this figure, each of the classes is shown with a box that has the name of the class at the top and the methods of the class listed below followed by parentheses. The box on the left-hand side indicates the RElement class. This class essentially represents the traditional finite element, which provides information about stiffness, mass matrix, load vectors, *etc.* These methods are called during finite element analyses to compute the mechanical response of the building components.

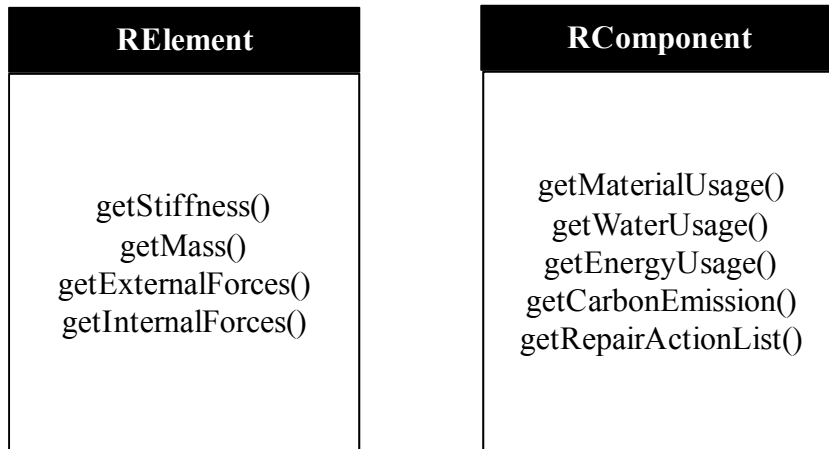


Figure 4-1. Traditional finite element versus building component class.

In Figure 4-1, the RComponent is on the right-hand side. The methods of RComponent will provide a wide range of information with which the direct and indirect cost of design is assessed. For example, getMaterialUsage() is designed to provide information about the material used for construction, *e.g.*, amount of concrete and reinforcement steel for RC components. The material usage is an input for assessing workforce, and hence the total cost of construction. The RComponent will also provide information about the environmental

impacts (Guerra 2010), *i.e.*, water usage, energy usage, carbon emission, at four phases: Extraction and manufacturing, on-site construction, operation, maintenance and end-of-life.

The last information provided by the RComponent class is the earthquake impact, *i.e.*, repair actions and the quantity that should be repaired with each repair action. This is provided by the method `getRepairActionList()`, which is in focus in this chapter. As discussed later, the algorithm in the `getRepairActionList()` entails the simulation of detailed visual damage. Therefore, a number of hidden component-specific methods that simulate visual damage are also implemented. In the following, the idea of a library of components is discussed, followed by detailed damage models. The details of the communication within each class, and the communication between the components and the orchestrating structural analysis is described in Appendix B.

4.2 LIBRARY OF COMPONENTS

The building component class is intended to evolve into a library of structural and non-structural components. In the literature, several component libraries already exist. The National Institute of Standards and Technology Interagency Report (NISTIR) 6389 set up a library of building components called Unifomat II element classification system (NIST 1999). This report provides a format for classifying building components and associated construction work. The NIST classification is intended for cost estimation and does not provide information for performance of components.

The ATC-58 project (Applied Technology Council 2012) established a library of components, focusing on fragility specifications for different building components. The ATC-58 library provides information in two parts for each building component. The first part provides the basic information about the component as illustrated in Figure 4-2. This

information includes the NISTIR classification number, the unit of repair quantity, the structural response used for damage prediction, the description of damage, and pictures of visual damage at each damage level.

Fragility specification			
RC wall panel (flexurally controlled)			
Developer and date:	Comartin (example for Guidelines), November 2008		
Component category:	B1044.000		
Basic composition:	Reinforced concrete and paint both sides		
Normative quantity (unit):	sf of wall area		
Demand parameter:	Interstory drift		
No. of damage states (other than DS0-undamaged):	3		
Type of damage states:	Sequential		
Sequential damage states			
	DS1	DS2	DS3
Description:	Flexural cracks < 3/16" Shear (diagonal) cracks < 1/16" No significant spalling No fracture or buckling of r/f Not structurally significant	Flexural cracks > 1/4" Shear (diagonal) cracks > 1/8" Moderate spalling/ loose cover No fracture or buckling of r/f Insignificant residual drift/shortening Repairable in place	Max. crack widths >3/8" Significant spalling/ loose cover Fracture or buckling some r/f Significant residual drift/shortening Repair in place impractical
Illustrations:			

Figure 4-2. Fragility specification for RC walls: basic identifier information (Applied Technology Council 2012).

The second part of the ATC-58 specification, exemplified in Figure 4-3, includes parameters of log-normal fragility functions. It also includes the description of repair actions

for each damage level, information about the repair cost and time, casualty rate, *etc.* The example in Figure 4-3 shows the fragility specification for RC walls.

Median demand (θ):	1.5%	3%	5%
Dispersion (β) ¹ :	0.2	0.3	0.4
Probability:			
Correlation:			
Consequence functions			
Repair description:	Patch cracks each side Paint each side	Remove loose concrete Patch spalls with NS grout Patch cracks each side Paint each side	Shore Demo existing wall Replace Patch and paint
Repair costs:	Max. consequence up to lower quantity Min. consequence over upper quantity Dispersion (β):	\$4.00 per up to 800 sf \$2.00 per sf over 4000 sf 0.2	\$10.00 per sf up to 800 sf \$5.00 per sf over to 4000 sf 0.3
Repair time:	Max. consequence up to lower quantity Min. consequence over upper quantity Dispersion (β):	\$50.00 per sf up to 200 sf \$30.00 per sf over 2000 sf 0.3	0.02hr per sf up to 800 sf 0.01hr per sf over 4000 sf 0.2
Casualty-affected planar area (sf) per normative unit:	0.04hr per sf up to 800 sf 0.02hr per sf over to 4000 sf 0.3	0.4hr per sf up to 200 sf 0.2hr per sf over 2000 sf 0.3	n/a
Casualty rate in affected planar area:	n/a	n/a	n/a
Post event tagging flag:	n/a	n/a	n/a
Total damage quantity (red tag trigger)	green	red	red
	n/a	40% of all walls	10% of all walls

Figure 4-3. Fragility specification for RC walls: parameters of log-normal fragility function, repair cost and time (Applied Technology Council 2012).

The library of components in Rts complements the ATC-58 library in several ways. First, in the Rts library each visual damage scenario is predicted using a separate model. For instance, for RC components the concrete cracking, concrete crushing, and reinforcement buckling are simulated employing different models. This is done because the damage mechanism for each visual damage scenario is different, and thus different structural

responses and models should be employed. Second, in ATC-58 the repair quantity and the location of the damaged zone on the component are not determined. That is, it is not determined in Figure 4-2 which part of the wall sustains concrete cracking in DS_1 or how much surface of wall is spalled in DS_2 . This information is important because a robust assessment of repair quantities and costs depends on it. In contrast, as shown in the subsequent section, in the Rts framework the repair quantities are assessed more precisely. In fact, in the damage simulation in Rts the location of damaged zones is simulated and the repair quantities are assessed. Also, information about manufacturing, construction, and environmental impacts is missing in the ATC-58 library, although it can be argued that this is essential for truly optimal design.

4.3 MODEL DEVELOPMENT

The objective of damage modelling in this chapter is to simulate visual damage “in detail” for each component. Here, the term “in detail” means that the visual damage at different “segments” of the component is predicted. This type of simulation is important because it facilitates the prediction of repair actions and the assessment of the repair quantities.

The first step in the development of this type of damage models is to define the possible visual damage scenarios that may occur on the component. Subsequently, for each visual damage scenario, a required repair action is identified. As an example, Figure 4-4 displays different scenarios of visual damage that can occur for RC components.

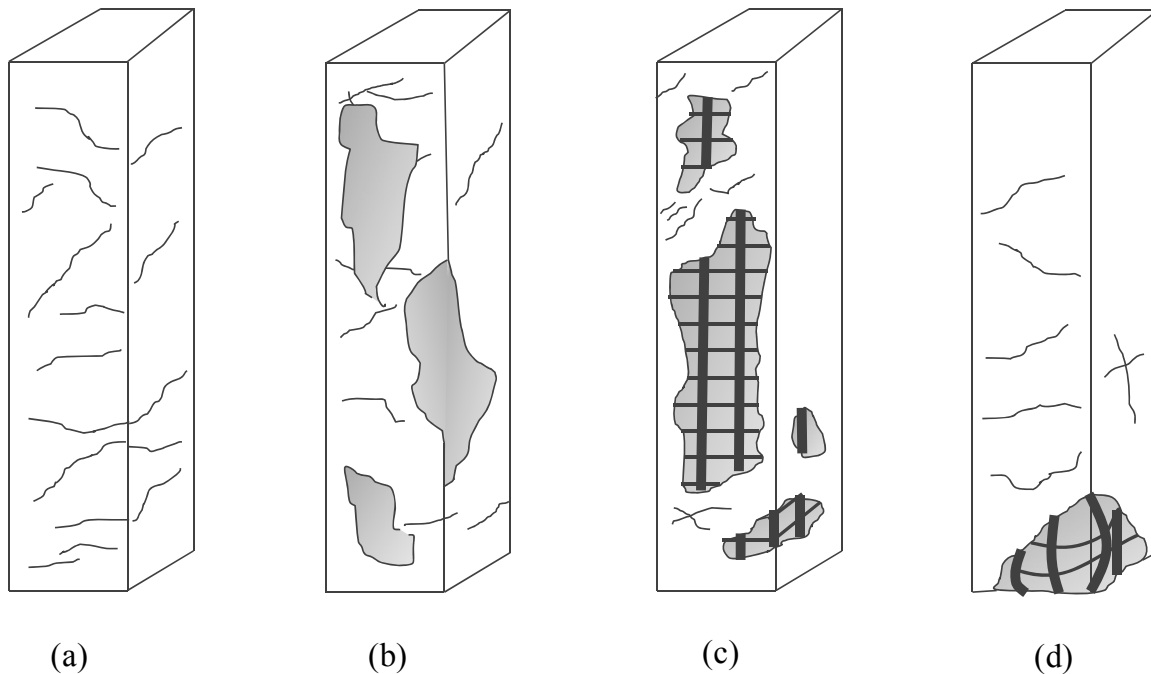


Figure 4-4. Visual damage scenarios for RC components: (a) Concrete cracking; (b) Cover concrete spalling; (c) Cover concrete falling; (d) Reinforcement bar buckling/fracture (Berry *et al.* 2008; Pagni and Lowes 2006; Brown and Lowes 2007).

The scenario shown in Figure 4-4 (a) is concrete cracking. The necessity of taking repair action depends on the width of the crack. Discussions with contractors and structural engineers show that the width of crack at which the owners decide to repair the component is highly variable (Pagni and Lowes 2006). A crack width of 0.6 mm is suggested by the same authors as well as Berry *et al.* (2008) as the value beyond which repair action is required. Table 4-1 lists the required repair action for each visual damage scenario.

Table 4-1. Visual damage scenarios versus repair actions for RC components.

Visual damage scenario	Repair action
Concrete cracking	Epoxy injection
Concrete cover spalling	Patching of concrete cover
Concrete cover falling	Concrete cover replacement
Reinforcement bar buckling/fracture	Section replacement

The second scenario of visual damage is concrete cover spalling as shown in Figure 4-4 (b). The concrete cover spalling is an important visual damage for performance assessment because it initiates more costly, time-consuming, and disruptive repair actions (Lehman *et al.* 2001). In defining this scenario of visual damage, it is important to characterize the extent of spalling that requires replacement of concrete cover, rather than patching of the cover concrete. Patching of concrete cover essentially entails removing any loosened concrete that has not spalled, cleaning the surface, and replacing the concrete with a mortar (Applied Technology Council 1998). Similarly, the concrete cover replacement necessitates removal of cover concrete and placement of new concrete. However, in contrast with patching, a substantial volume of new concrete should be placed around longitudinal reinforcement, which often entails shoring of the structure. This is done to ensure adequate bond between new and old concrete as well as new concrete and reinforcement bars (Pagni and Lowes 2006). In addition, if more than 150 mm of concrete thickness is removed, epoxy adhesive or epoxy-anchored dowels are required to ensure bond between new and old concrete (Applied Technology Council 1998). In this thesis, the exposure of longitudinal reinforcement bar is considered as the visual damage that necessitates replacement of

concrete cover. This visual damage is also suggested by Applied Technology Council (1998), Pagni and Lowes (2006), Brown and Lowes (2007), and Berry *et al.* (2008). The spalling of concrete cover that exposes the longitudinal reinforcement is shown in Figure 4-4 (c) and named falling of cover concrete. In the literature, this visual damage scenario is frequently called “severe” damage to the concrete cover and core.

The last visual damage scenario is bar buckling and fracture and shown in Figure 4-4 (d). The prediction of this visual damage is critical because bar buckling and fracture is normally followed by significant loss of lateral-load strength of the component. This visual damage requires replacement of section that contains buckled bar. This repair action entails shoring the structure, removing the damaged concrete using jack-hammer or chipping, removing the damaged reinforcement bars, placing new reinforced bars, placing epoxy-anchored dowels if needed, and placing new concrete (Applied Technology Council 1998). Applied Technology Council (1998) suggests different methods for connecting new and existing bars including mechanical connections such as sleeve, splice, and threaded coupler.

Once the visual damage scenarios and repair actions are defined, damage models should be developed to simulate the visual damage. Each damage model is associated with a visual damage scenario. Also, the surface of component is divided into several segments. The developed models simulate the visual damage at each segment separately. The simulated visual damage will be shown in the Rts screen during the analysis.

4.3.1 RC Column Component

The segments for the reinforced concrete column component are shown in Figure 4-5. The number of segments that cover the surface of the column depends on the height of the column. That is, the number of segments on each side of the column equals to the column

height in meter rounded down to the nearest integer number. Therefore, each segment covers approximately one meter of the column height. Figure 4-5 displays a segment-discretized column whose height is greater than four meters and less than five meters. Considering four sides of the column, there are total of sixteen segments on the column. As the analysis runs, a unique visual damage displays on each segment of the component. The basic assumption here is the whole segment sustains a unique visual damage scenario. For example, once the model predicts concrete spalling, the whole segment sustains spalled concrete cover.

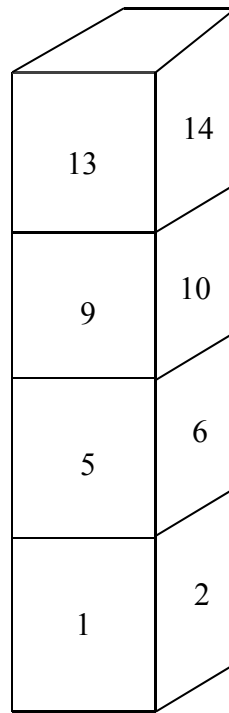


Figure 4-5. Segments of RC column component for which visual damage is simulated; segments are numbered from bottom to top and counter clockwise.

The models for visual damage and repair actions of RC components are examined in Chapter 2. Only a few models can be used for the purpose of this study, *i.e.*, simulation of visual damage at the component segments. Having this objective in mind, the models that simulate damage at the material level are best for damage simulations.

Experimental studies indicate that the minimal visual damage for RC components, *i.e.*, concrete cracking and concrete cover spalling, is primarily predicted using maximum deformations, rather than cumulative cyclic deformation demand (Kunnath *et al.* 1997) . On the contrary, the severe visual damage scenarios, *i.e.*, concrete cover falling and reinforcement bar buckling, are affected by not only the maximum deformations but also the cyclic deformation demands (Berry *et al.* 2008).

The concrete cracking is characterized with the maximum residual crack width, *i.e.*, the crack width visible once the earthquake loading ceases. However, in the literature consistently maximum crack width has been in focus (Brown and Lowes 2007). Thus, a model for maximum crack width is implemented here. The crack width is widely related to the maximum tensile strain in reinforcement in the literature (Oh and Kang 1987; Gergely and Lutz 1968; Applied Technology Council 1996; American Concrete Institute 1999; Oh and Kim 2007). In Rts, the model proposed by Oh and Kang (1987) is implemented, the model reads

$$w_{cr,max} = a_0 \cdot d \cdot (\epsilon_{s,max} - 0.0002) \cdot \frac{h_2}{h_1} \quad (4-1)$$

where a_0 is defined as follows,

$$a_0 = 159 \left(\frac{t_c}{h_1} \right)^{4.5} + 2.83 \cdot \left(\frac{A_1}{A_s} \right)^{1/3} \quad (4-2)$$

d =bar diameter, $\epsilon_{s,max}$ =maximum tensile strain in extreme reinforcement bar, h_2 =distance from neutral axis to the extreme concrete fibre in tension side, h_1 =distance from neutral axis to the centroid of reinforcement bar in tension, t_c =concrete cover thickness, A_1 =average

effective area of concrete around each reinforcement bar. The model in Eq. (4-1) is used for crack width on the flexural members subjected to the static load. Oh and Kim (2007) proposed a method for computing the maximum residual crack width under repeated loading. However, the model in Eq. (4-1) is used here because the example column here is subjected to the static load. Oh and Kang (1987) compared the results of their model with 747 test data published in the literature. The comparison showed the maximum crack width computed with their model has better correlation with test data than the well-known Gergely and Lutz model (Gergely and Lutz 1968).

As suggested by the Applied Technology Council (1996), Lehman *et al.* (2004), and Berry *et al.* (2008), the concrete cover spalling can be predicted using the maximum compressive strain in concrete cover, $\epsilon_{c,max}$. That is, the concrete cover spalls once the compressive strain in cover exceeds a certain value. Applied Technology Council (1996) suggests the value of 0.004 for compressive strain at which concrete cover spalls. However, Lehman *et al.* (2004) conducted experimental studies and found that the strain value at which concrete cover spalls is scatter. From their experiments, they concluded that the strain value at the onset of concrete cover spalling has mean value of 0.0066 and coefficient of variation of 0.33. In Rts, the following conditional equation is used to simulate concrete cover spalling

$$\epsilon_{c,max} \geq \epsilon_{spalling} \quad (4-3)$$

where $\epsilon_{spalling}$ is a random variable, which is log-normally distributed with the mean 0.004 and coefficient of variation 0.33.

The concrete cover falling is simulated using the maximum deformation and hysteretic cyclic deformation demands. In the literature, there is no distinct model to simulate

falling of concrete cover. As discussed in Chapter 2, the most commonly model used for reinforced concrete components is the model proposed by Park and Ang (1985). However, that model is defined at the component level and does not distinguish between different visual damage scenarios. The model implemented in Rts has the same format of the Park and Ang model; however, it is at the material level and has the following form

$$D_c = \theta_1 \cdot \frac{\varepsilon_c - \varepsilon_{c,y}}{\varepsilon_{c,u} - \varepsilon_{c,y}} + \theta_2 \cdot \frac{\int dE}{\sigma_{c,y} \cdot \varepsilon_{c,u}} \quad (4-4)$$

where θ_1 , θ_2 =the model parameters that should be calibrated against test data, ε_c =maximum compressive strain in concrete cover, $\varepsilon_{c,y}$ =yielding strain, $\varepsilon_{c,u}$ = ultimate strain, $\int dE$ =hysteretic energy absorbed in concrete cover material, $\sigma_{c,y}$ =yielding stress for the concrete. The value of D_c greater than 1 indicates the falling of cover concrete.

Previous works have shown that the cyclic history has more significant effect on the reinforcement buckling and fracture than the concrete cover spalling (Kunnath *et al.* 1997). However, limited test data are available to develop a history-based damage model (Berry *et al.* 2008). In addition to the cyclic history, Moyer and Kowalsky (2003) realized that the maximum tensile strain in reinforcement bar affects the bar buckling. Whereas, Lehman *et al.* (2004) found that it is unclear whether the maximum compressive strain is more influential on bar buckling or the maximum tensile strain. The model implement in Rts for bar buckling is of similar form of the model in Eq. (4-4) and is written as

$$D_s = \theta_1 \cdot \frac{\varepsilon_s - \varepsilon_{s,y}}{\varepsilon_{s,u} - \varepsilon_{s,y}} + \theta_2 \cdot \frac{\int dE}{\sigma_{s,y} \cdot \varepsilon_{s,u}} \quad (4-5)$$

where ε_s =maximum absolute strain in reinforcement bar and all other entries in Eq. (4-5) have definitions analogous to those of Eq. (4-4) except the entries in Eq. (4-5) are associated with the reinforcement bars. Also, the value of D_s greater than 1 indicates the bar buckling and fracture.

The models in Eq. (4-1) and Eq. (4-3) to Eq. (4-5) are assessed at the centre of each segment of the RC column component. This is conducted in the public methods of the `RRCColumnComponent`. Specifically, the maximum crack width in each segment is computed in the method `getCrackWidthVector()`, which returns a vector whose elements are the maximum crack width in each segment. The occurrence of concrete cover spalling, falling and reinforcement bar buckling are determined in the methods `getSpalledCoverVector()`, `getFallenCoverVector()`, and `getBucklingVector()`, respectively. Each method returns result in a vector whose dimension is the number of segments and elements are Booleans. The true value of Booleans means that the corresponding segment sustains the visual damage. Therefore, the true value in the i^{th} element of the vector returned by the `getSpalledCoverVector()` means the concrete cover has spalled on the segment number i .

The visual damage methods are called by the method `getRepairActionList()`. Depending on the visual damage of each segment, the repair action is determined as shown in Table 4-1. This method sums the repair quantity for each repair action listed in Table 4-1. As stated before, the epoxy injection is required on a segment whose maximum crack width exceeds 0.6 mm and whose concrete cover is not spalled. The repair quantity for the epoxy injection, concrete cover patching, and concrete cover replacement are computed as the total area of the segments, which requires that repair action. The repair quantity of the section

replacement is computed as the volume of the reinforced concrete that should be replaced. If the reinforcement bar buckles in a segment, the reinforced concrete section covered by the segment should be replaced regardless of the damage on the other segments surrounding the section.

4.3.2 RC Shear Wall Component

The other component examined in this chapter is RC shear wall. Similar to the column component, the visual damage for RC shear wall component is simulated at separate segments. The segments of the wall component form a net called “segment mesh” herein. The segments height in the segment mesh is the wall height divided by 0.3 meter rounded down to the nearest integer. The segments width is also the wall width divided by 0.3 meter and rounded down to the nearest integer. Thus, the segments have approximate dimension of 0.3-by-0.3 meter. The assumption here is that each segment sustains unique visual damage and a single repair action is conducted on each segment of that dimension. The repair actions listed for RC column component can be conducted on RC shear wall (Oesterle *et al.* 1979; Lefas and Kotsovos 1990).

The shear wall component is modelled by the linear Quad4 elements. This is the only plane element available in Rts at the time of writing this thesis. The damage models for RC shear wall are based on the maximum strain values because this is the structural response that can be captured at the segments of the component and represents the deformations.

As demonstrated by Vecchio (2000), the initial cracking is primarily predicted using the maximum principal strain. Here, the maximum crack width is predicted using the maximum principal strain, $\varepsilon_{pr,max}$, and the model,

$$w_{cr,max} = \theta_1 \cdot \epsilon_{pr,max} \quad (4-6)$$

The cover concrete spalling and falling are predicted using the maximum compressive axial strain, $\epsilon_{yy,min}$, because crushing of concrete is attributed to the compressive strains in the literature. The conditional equations for spalling and falling of concrete cover are as follows

$$|\epsilon_{yy,min}| \geq \epsilon_p \quad (4-7)$$

, and

$$|\epsilon_{yy,min}| \geq \epsilon_f \quad (4-8)$$

where ϵ_p and ϵ_f are random variables that represent compressive strain value at the onset of concrete cover spalling and falling, respectively.

The bar buckling is predicted using the maximum tensile axial strain as suggested by Berry *et al.* (2008) and Moyer and Kowalsky (2003) and maximum compressive axial strain. The conditional equation for bar buckling reads

$$\max(|\epsilon_{yy,min}|, |\epsilon_{yy,max}|) \geq \epsilon_{buckling} \quad (4-9)$$

where $\epsilon_{buckling}$ is a random variable that represents strain value at the onset of bar buckling.

The models in Eqs. (4-6) to Eq. (4-9) are evaluated at the centre of each segment. It is done with mapping centre of each segment to an element in the finite element mesh. The number of element and the local coordination of the centre of the segment on the plane element are stored in the matrix `segmentElementMatchingMatrix`. During the analysis, the

strains are read from the mapped element for each segment. Figure 4-6 shows the segment mesh and finite element mesh for an RC shear wall component.

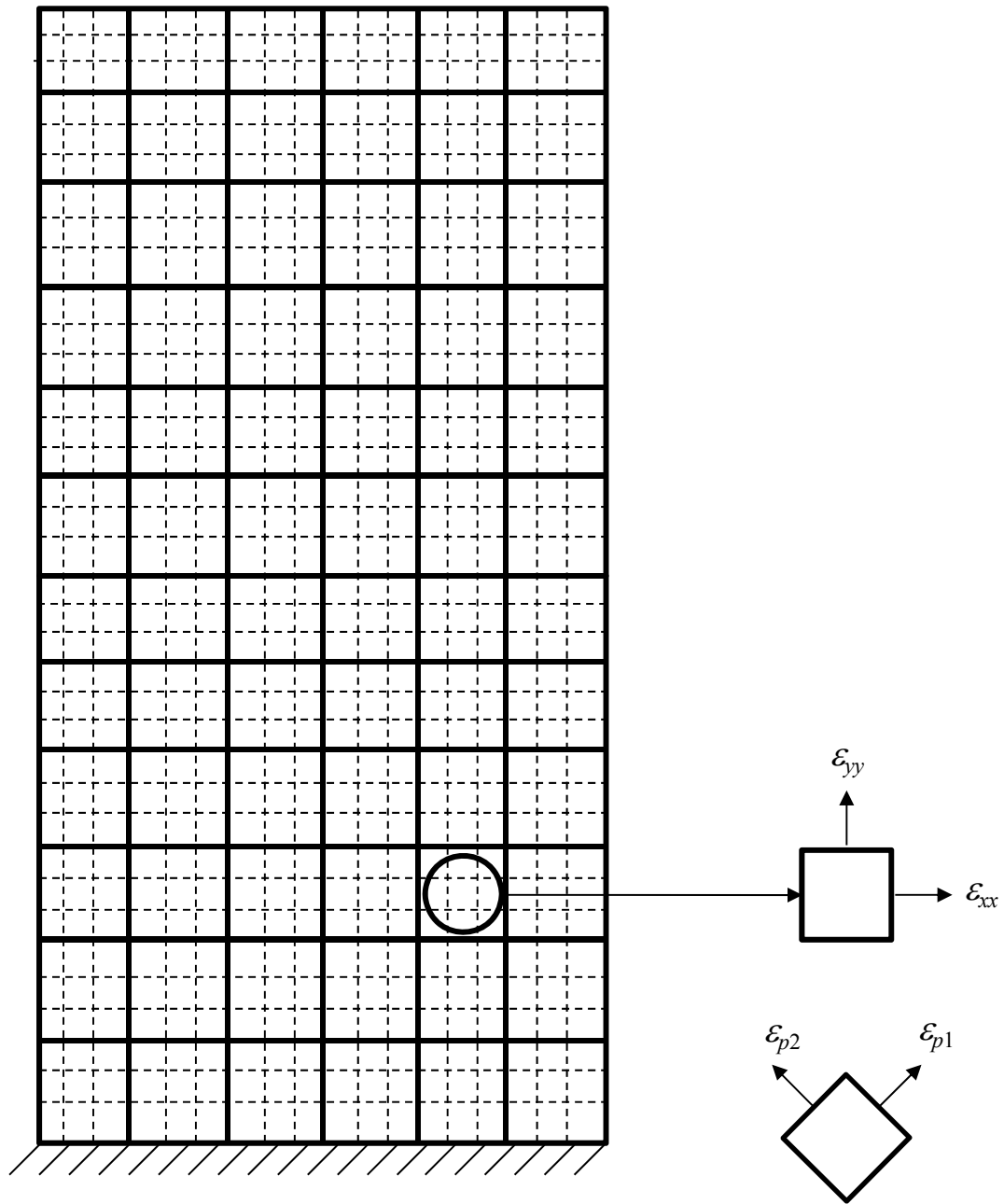


Figure 4-6. RC shear wall component; the segment mesh is shown by solid lines; the finite element mesh is shown by the dashed lines.

The maximum crack width in each segment is computed in the method `getCrackWidthMatrix()`, which returns a matrix whose elements are the maximum crack width in each segment. The occurrence of concrete cover spalling, falling and reinforcement bar buckling are determined in the methods `getSpalledCoverMatrix()`, `getFallenCoverMatrix()`, and `getBucklingMatrix()`, respectively. Each method returns result in a matrix whose dimension is the dimension of segment mesh and elements are Booleans. The true value of Booleans means that the corresponding segment sustains the visual damage. For example, the true value in the i^{th} row and j^{th} column of the matrix returned by the `getSpalledCoverMatrix ()` indicates the concrete cover has spalled on the segment located in the i^{th} row and j^{th} column of the segment mesh.

The visual damage methods of RC shear wall component are called by the method `getRepairActionList()`. Similar to RC column component, depending on the visual damage of each segment, the repair action is determined as shown in Table 4-1. This method sums the repair quantity for each repair action listed in Table 4-1. The epoxy injection is considered for a wall component if the crack width exceeds 0.6 mm on any segment and the total crack length on the wall exceeds half of the wall width. The total crack length on the wall is computed using the model developed by Talachian (2010). Note that as the wall is modelled by the plane elements, both sides of the wall sustain the same visual damage. Thus, the quantity of the epoxy injection, patching concrete cover, and concrete cover replacement for each segment is twice the area of segments shown in Figure 4-6.

4.4 COORDINATION OF REPAIR

The coordination of repair in Rts is motivated by the need for assessing the cost of earthquake damage in light of the influence of several factors. These factors are listed as follows:

- The repair actions needed for each component;
- The quantity that should be repaired using each repair action and this quantity hereafter is called repair quantity;
- The cost of repair per unit repair quantity;
- The economy of scale, which is the cost advantage that arises from higher repair quantities;
- The decision for the demolition and reconstruction of the building after an earthquake.

The prediction of the above mentioned parameters is rife with uncertainty. Therefore, the utilization of probabilistic methods and models is a fundamental premise.

In Rts, the repair coordination starts at the component level. That is, the first two factors, *i.e.*, the repair actions and the repair quantities, are computed for each component rigorously. This is conducted in the method `getRepairActionList()` in the `RComponent` class. This method provides information about required repair actions and repair quantities in two vectors. The first vector contains the name of repair actions for the component. The size of this vector equals to the number of possible repair actions for the component, and hence, differs for different component types. The second vector is called repair quantity vector and as its name suggests, it contains the repair quantity for each repair action.

The coordination of repair for buildings is further conducted in the class `RRepairManagerModel`. This class computes the cost of earthquake damage to buildings. This class is a model, which takes input from component classes and return output to the downstream model(s). Figure 4-7 shows the sequence of the calls for the simulation of damage and cost in Rts. To assess the cost of earthquake to building, the following tasks are conducted successively during the evaluation of the `RRepairManagerModel` class:

Task 1: The method `evaluateModel()` in the `RRepairManagerModel` calls the `getRepairActionList()` in all the components. This call is shown in Figure 4-7 with an arrow labeled call number 1.

Task 2: The `getRepairActionList()` makes call number 2 to all the methods of the component that simulate the visual damage or provides information about the geometry and computes the repair quantity vector.

Task 3: Calls number 4, 5, 6, and 7 are made from the visual damage methods to the private data members of the class or public methods of material class, which are used to simulate visual damage. In Figure 4-7 the visual damage methods for the `RRCCColumnComponent` and `RRCShearWallComponent` are shown. The simulation of visual damage to these components are further discussed in the section model development. The private methods and data members are shown in italic format.

Task 4: The `evaluateModel()` adds up the repair quantity from different component objects and creates a list of repair actions and repair quantities.

Task 5: The `evaluateModel()` makes call number 8 and sends the repair action to the method `getRepairActionCostPerUnitQuantity` to compute the cost of repair for each repair action.

Task 6: The evaluateModel() makes call number 9 and sends the repair quantity to the method getEconomyOfScale(). This method computes the factor with which the cost per unit quantity decreases.

Task 7: The evaluateModel() computes the repair cost, which equals to the sum of the products of the repair quantity and repair cost per unit quantity and the economy of scale.

Task 8: The evaluateModel() makes call number 10 and sends the ratio of the repair cost to construction cost to the method shouldDemolish(). The method shouldDemolish() returns a Boolean, which shows whether the building should be demolished or repaired.

Task 9: The evaluateModel() outputs the repair cost as the response of the RRepairManagerModel() if shouldDemolish() returns false; otherwise, it outputs the cost of demolition and construction.

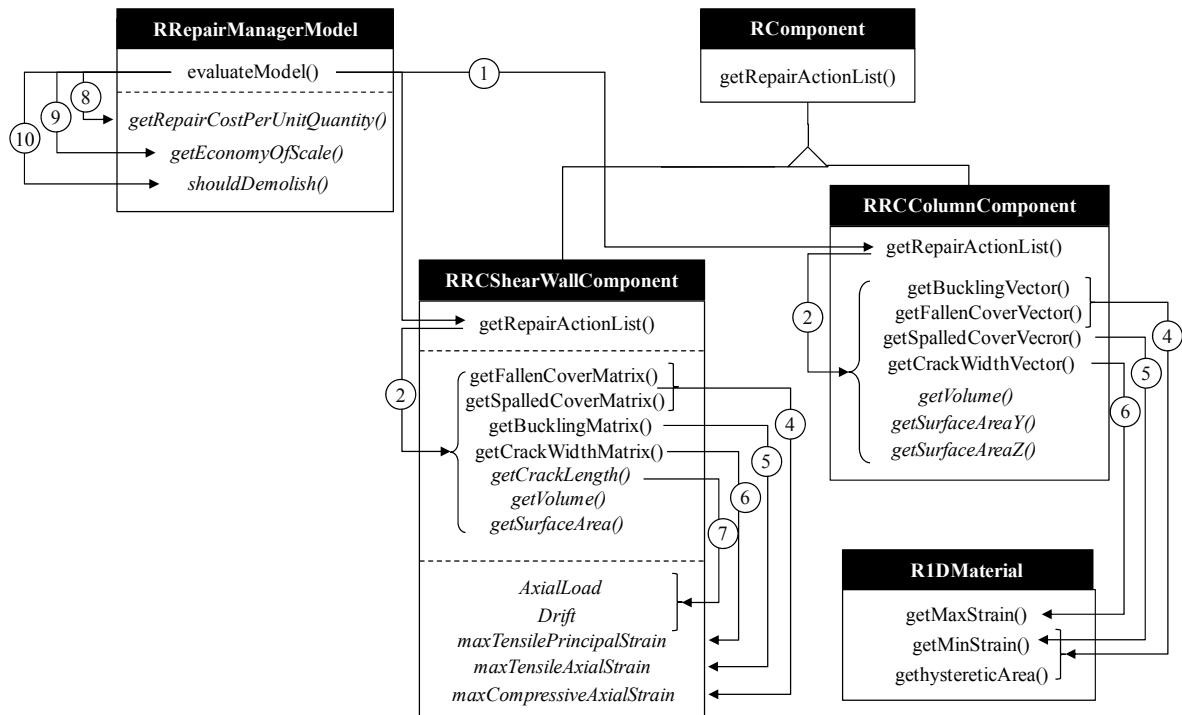


Figure 4-7. Simulation of damage and assessment of earthquake cost in Rts.

The consideration of “demolition decision” in the cost assessment is one of the novelties in the coordination of the repair in Rts. The demolition decision refers to the decision made by the owners or stakeholders after an earthquake to demolish and rebuilt the damaged building. Traditionally, in earthquake engineering (Stone and Taylor 1993; Park *et al.* 1985; Earthquake Engineering Research Institute 1994; Bracci *et al.* 1989) the decision on the demolition of building is made solely considering the structural damage. However, reports from past earthquakes (Collins 2011; Bayer 2012; Key 2011) show that the facts such as whether the building is insured or not, the city regulations, the cost of repair, *etc.* may affect the demolition decision. The quantification of the effect of those factors requires research that occurs at the interface of earth science, building science, engineering, and public policy (Wen and Ellingwood 2005). The development of demolition model requires a thorough investigation of earthquake reconnaissance data for buildings and is outside the scope of this thesis.

4.5 DEMONSTRATION EXAMPLES

Four examples are provided to demonstrate the simulation of damage to building components in Rts. In the first two examples, the visual damage to RC column is examined. In the third example an RC shear wall component is subjected to a lateral load and the visual damage is simulated. The last example demonstrates the visual damage and repair quantities for a building. The examples are explanatory and have potential for improvements with regards to comprehensive models to simulate the detailed visual damage. In particular, the damage models employed in this section are calibrated neither against test data nor the previous studies. Also, the classes for conducting inelastic dynamic analysis are not developed in Rts at the time of writing this thesis, and thus the examples are conducted using static analysis.

The results of the following examples are intended to demonstrate the detailed simulation of the visual damage and the framework, which enables robust prediction of repair actions and loss.

4.5.1 Example 1: Push-over Analysis of Cantilevered RC Column

In this example a cantilevered column is subjected to static lateral force and the visual damage at each segment of the column is simulated at different drift ratio.

The height of RC column in this example is four meters. Figure 4-8 shows the fibre-discretized cross-section of RC column. As shown in that figure, the cover concrete is discretized in two layers of concrete fibres and each layer includes twenty fibres. Also, the reinforcement bar is discretized with ten fibres. Also, the core concrete is discretized with 16-by-16 fibres. The material model for steel and concrete is a bilinear model.

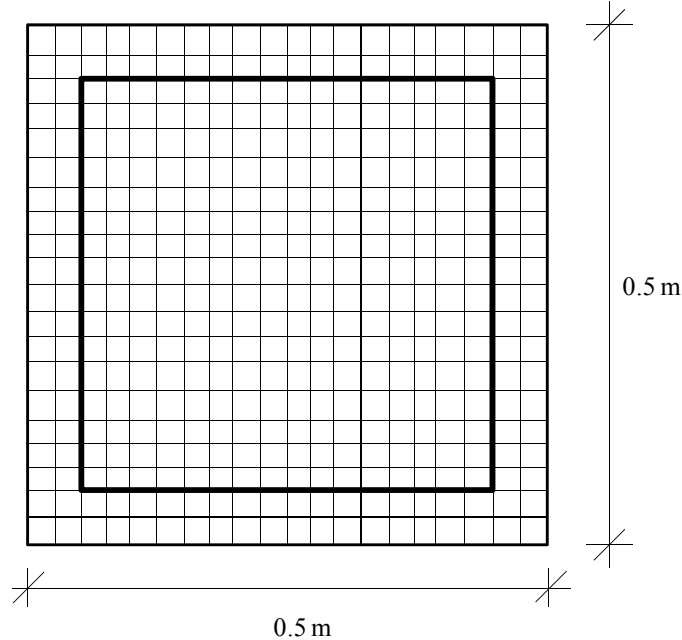


Figure 4-8. Fibre-discretized cross-section for RC column component.

The mean of maximum tensile strain in reinforcement fibres is used for crack width computation in Eq. (4-1). The average of maximum compressive strain in the outer layer of fibres in concrete cover is used to predict spalling of concrete cover. Whereas, the average of maximum compressive strain and the average of the hysteretic energy absorbed by the inner fibres are used in Eq. (4-4) to predict falling of concrete cover. The average of the maximum strain and the average of the hysteretic energy absorbed by the reinforcement fibres are used in Eq. (4-5) to predict bar buckling. The mean of parameters in Eq. (4-4) and Eq. (4-5) are presented in Table 4-2. Note that θ_2 has relatively smaller value than θ_1 , which means that the hysteretic energy term in Eq. (4-4) and Eq. (4-5) make smaller contribution to the damage. This is consistent with the study that Park and Ang (1985) conducted on the contribution of hysteretic energy on their damage model.

Table 4-2. Mean value of parameters in Eq. (4-4) and Eq. (4-5).

Parameter	Mean
$\varepsilon_{c,y}$	0.0015
$\varepsilon_{c,u}$	0.00615
$\sigma_{c,y}$	40 [MPa]
$\varepsilon_{s,y}$	0.002
$\varepsilon_{s,u}$	0.0075
$\sigma_{s,y}$	400 [MPa]
θ_1	0.9
θ_2	0.15

The column is modelled with one displacement-based element and four sections. Figure 4-9 shows a snapshot from Rts during push-over analysis. The push-over curve is plotted in the right-hand side window and the visual damage for the column component is displayed in the left-hand side window. This figure shows the column at 3.8% drift ratio. The gray color shows the segments of the component that the cover concrete has spalled. The black color represents the region of the component where the cover is fallen and reinforcements are exposed.

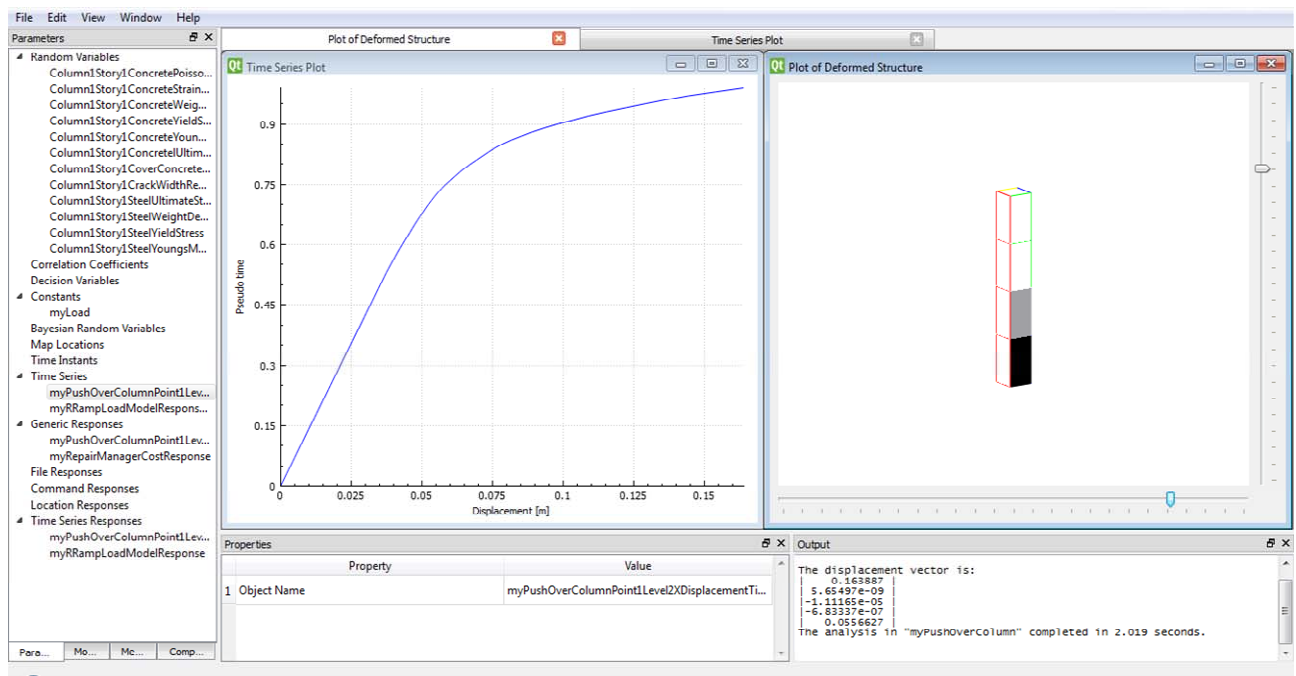


Figure 4-9. Snapshot of Rts: Push-over curve and visual damage for RC column component.

Figure 4-10 shows the complete push-over curve and the visual damage on the component. The visual damage for the compression side starts with the concrete cover spalling followed by falling of cover concrete and ends with reinforcement bar buckling. While the visual damage for the tension side starts with the concrete cracking and ends with reinforcement bar buckling.

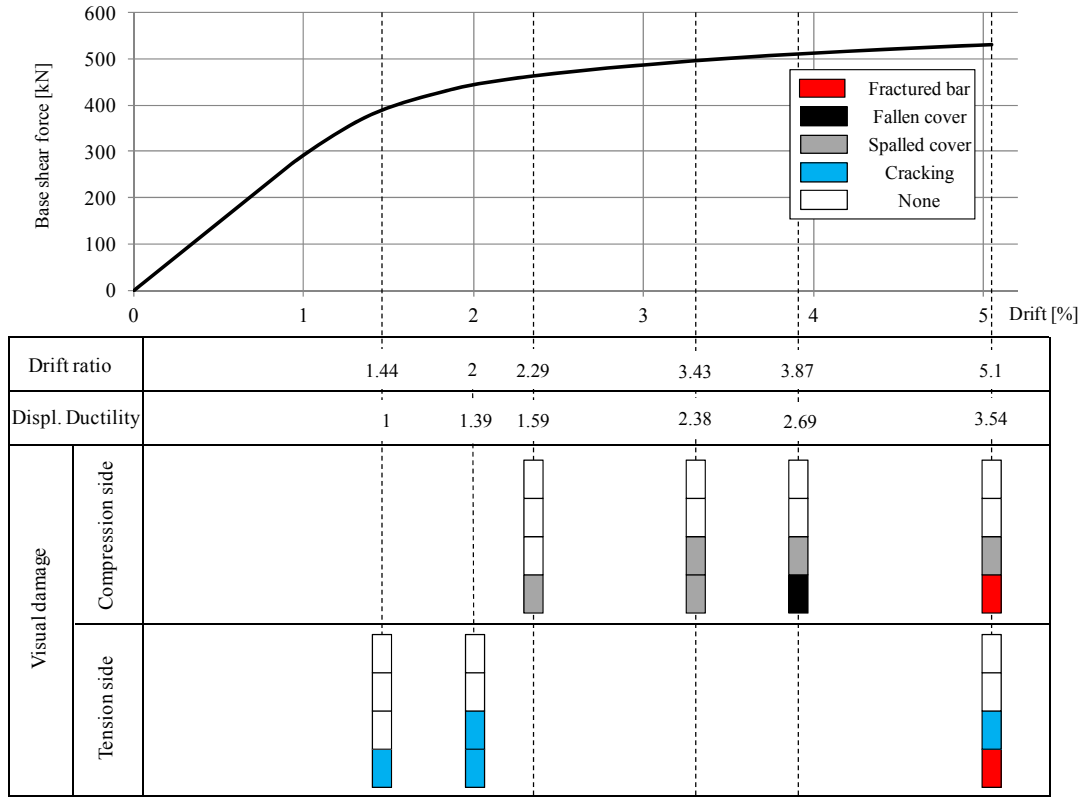


Figure 4-10. Push-over curve and visual damage on the four segments of the RC column component: compression and tension sides.

In Figure 4-10, it is recognized that the propagation of damage is directly correlated with the drift ratio. This is consistent with fragility models that predict the damage probability using the drift ratio as the only structural response. In that figure, it is also shown that the damage propagation is also correlated with the displacement ductility. It shows that although the damage models in this chapter are at the material-level, the results are consistent with the models whose input is at the component level, *i.e.*, displacement ductility (Berry and Eberhard 2004). Also, in Figure 4-10, it is seen that the severe damage, *i.e.*, concrete cover falling and reinforcement buckling, occurs at the component toe. This makes sense because the maximum moment occurs at the base, and thus the plastic hinge forms there.

4.5.2 Example 2: Cantilevered RC Column Subjected to Cyclic Loading

In this example, the RC column in the previous example is subjected to a cyclic loading. The snapshot from Rts is shown in Figure 4-11. In Rts, the cyclic load is created in a model called RSineLoadModel. The response of that model is shown in the left-hand side window Figure 4-11 and the corresponding visual damage is displayed in the right-hand side window.

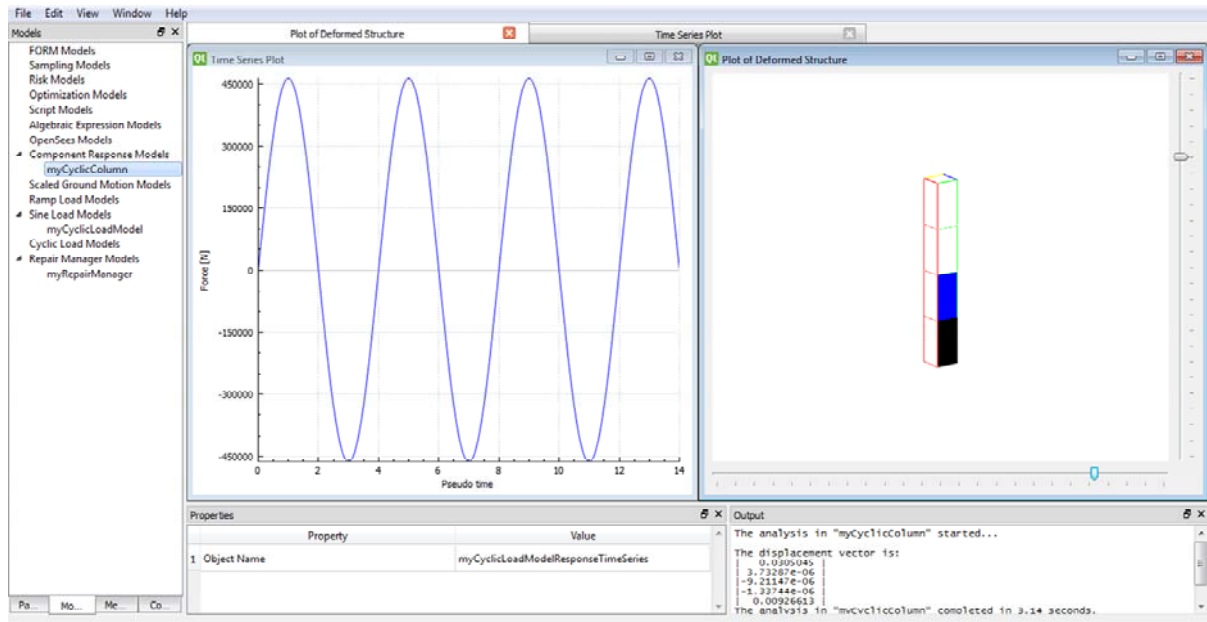


Figure 4-11. Rts snapshot: Cyclic loading versus visual damage in each segment.

Figure 4-12 shows the cyclic loading and visual damage in detail. In that figure, the visual damage is shown for the two sides of the column. The east side of the column is in compression in positive loading cycles while the west side is in tension. As shown in that figure, the concrete cracking and spalling of concrete cover occur at the first half cycle. It is because these visual damage scenarios are predicted by the maximum strains, rather than cyclic dissipated energy as formulated in Eqs. (4-1) and (4-3). In contrast, the cumulative cyclic energy computed in each loading cycle causes the falling of concrete cover and buckling of reinforcement after three and half cycles and eighth cycles, respectively. This is

consistent with previous studies (Kunnath *et al.* 1997) that states cyclic history has stronger influence on severe damage, *i.e.*, bar buckling and fracture, than minimal damage, *i.e.*, initial spalling.

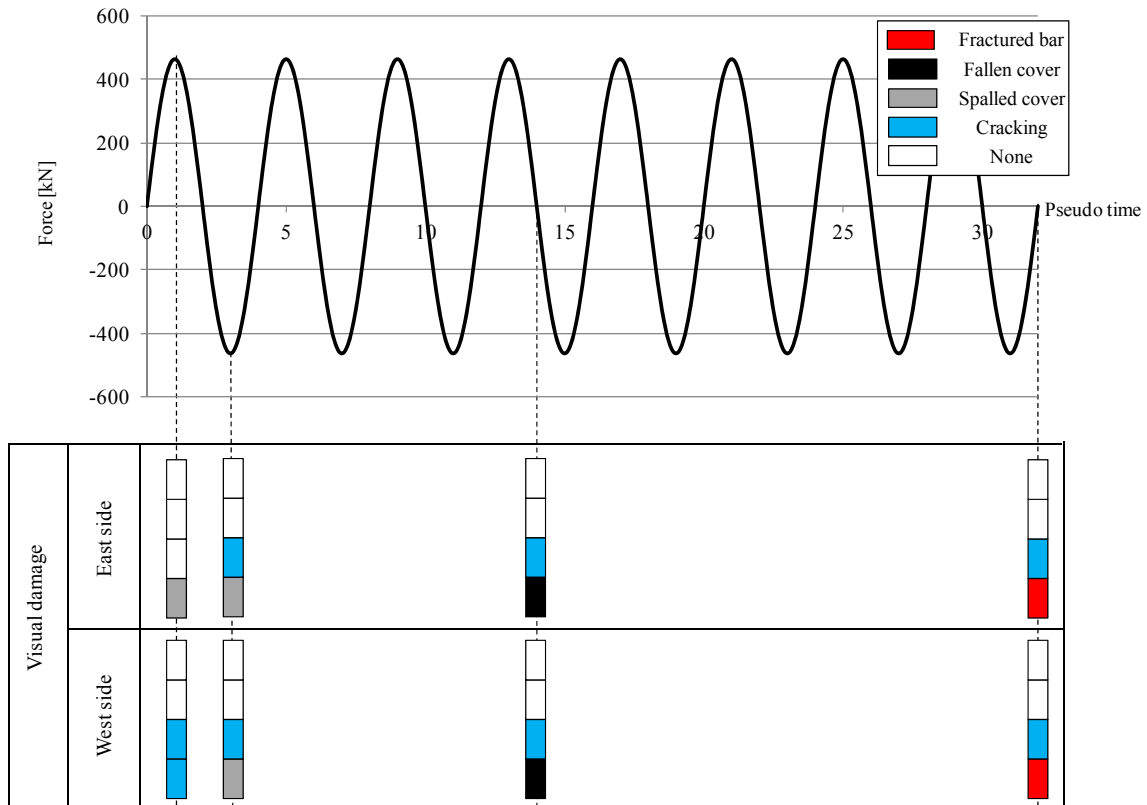


Figure 4-12. Cyclic loading and visual damage on the four segments of the RC column component: East and west sides.

The maximum structural response is constant in all cycles because the material model was bilinear and does not include stiffness degradation. Although the maximum structural response in the column in Figure 4-12 remains constant the visual damage changes with the cycle numbers. This shows that the maximum structural response may not be always a proper indicator for damage. This is also one example that shows a damage scenario, which cannot be captured by univariate models that solely make prediction on the value of maximum

response, *e.g.*, maximum inter-story drift. A method for developing multivariate damage models is discussed in the previous Chapter.

4.5.3 Example 3: Cantilevered RC Shear Wall Subjected to Lateral Load

In this example the visual damage to an RC shear wall subjected to the lateral load is simulated. The models for simulation of visual damage are presented in the section Model Development. Table 4-3 presents the mean value of parameters and key strain variables in Eqs. (4-6) to (4-9).

Table 4-3. Mean value of parameters and key strain variables in Eqs. (4-6) to (4-9).

Parameter/Variable	Mean
θ_1	100
ε_p	0.003
ε_f	0.005
$\varepsilon_{buckling}$	0.0073

As shown in Figure 4-13, the example wall is four meter high and three meter wide and its thickness is 0.2 meter. Figure 4-13, the segment mesh, which is 12-by-6.

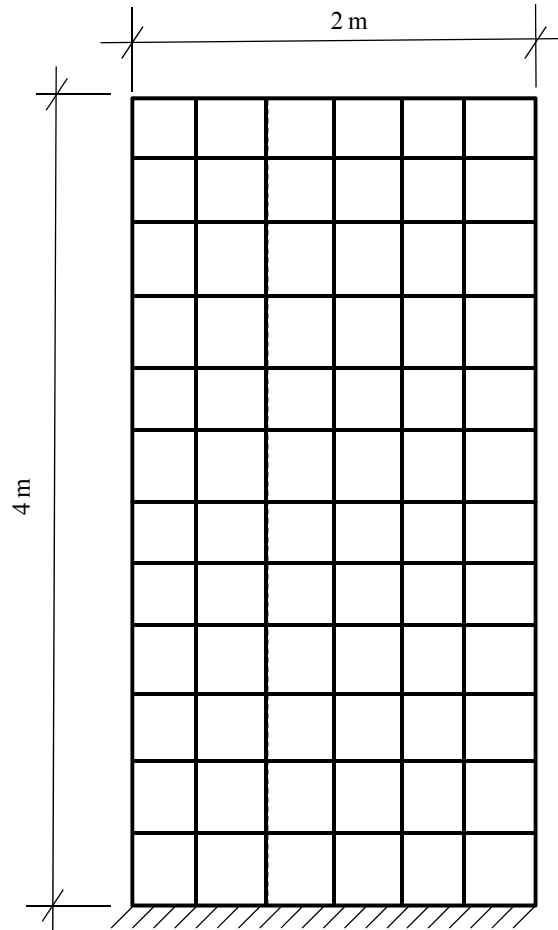


Figure 4-13. The wall component dimensions and segments.

Figure 4-14 is excerpted from Rts screenshot and shows the visual damage at different segments of the wall at three drift ratios, 1%, 1.5%, and 2%. The visual damage at the bottom corners of the wall is more severe. This is because the stress and thus strains are higher at those zones. Also, the concrete crushing occurs at the corner of the wall in compression while concrete cracking mostly occurs at the tension side. In Figure 4-14, it is also seen that the segments at the middle of the wall experience less damage because the change in strains are more limited at those regions.

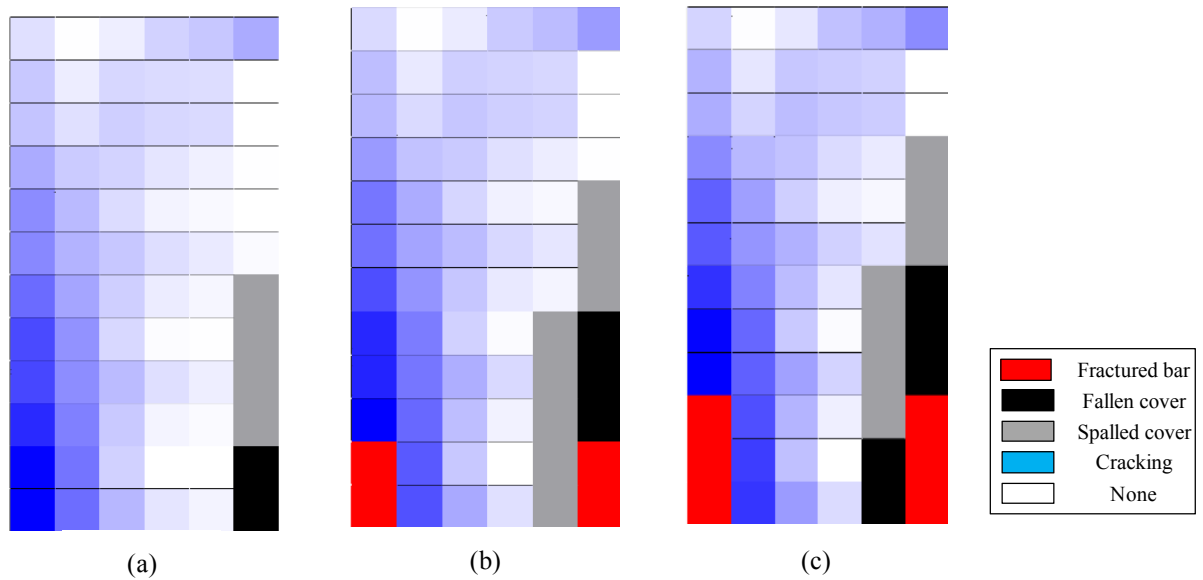


Figure 4-14. Visual damage to RC shear wall component: a) $\delta=1\%$; b) $\delta=1.5\%$; c) $\delta=2\%$.

4.5.4 Example 4: One Story Building Subjected to Lateral Load

In this example, visual damage is simulated on a one story building. Figure 4-15 shows the plan view of the building, which includes four columns and a core shear wall located at the centre. The elevation view of building at axes 2 and 3 are shown in Figure 4-16. The components have the same dimensions as in the previous examples. The columns and core shear wall are connected with a slab whose thickness is 0.2 meter.

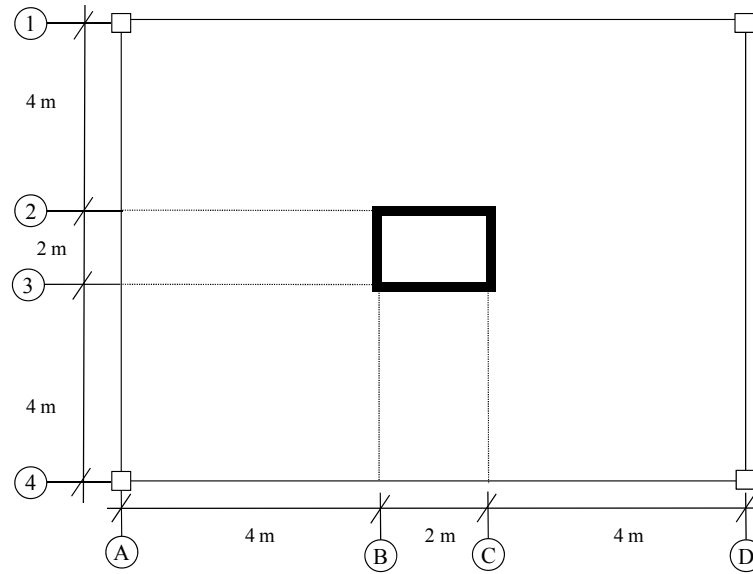


Figure 4-15. Plan view of building.

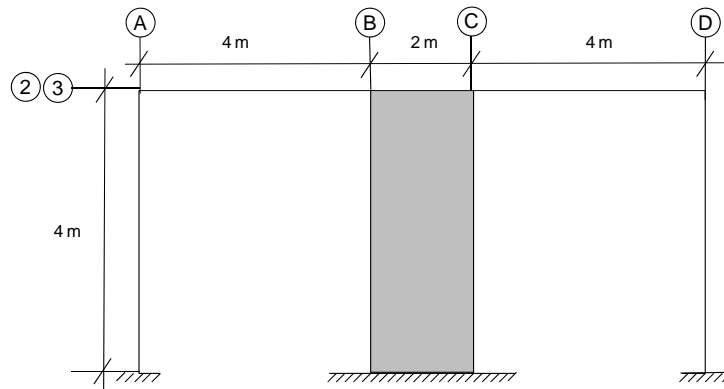


Figure 4-16. Elevation view of building.

The building is subjected to the point lateral loads at the top of four columns. Figure 4-17 is excerpted from Rts screen at inter-story drift ratios 1%, 1.5%, and 2% and shows the visual damage on columns and shear walls.

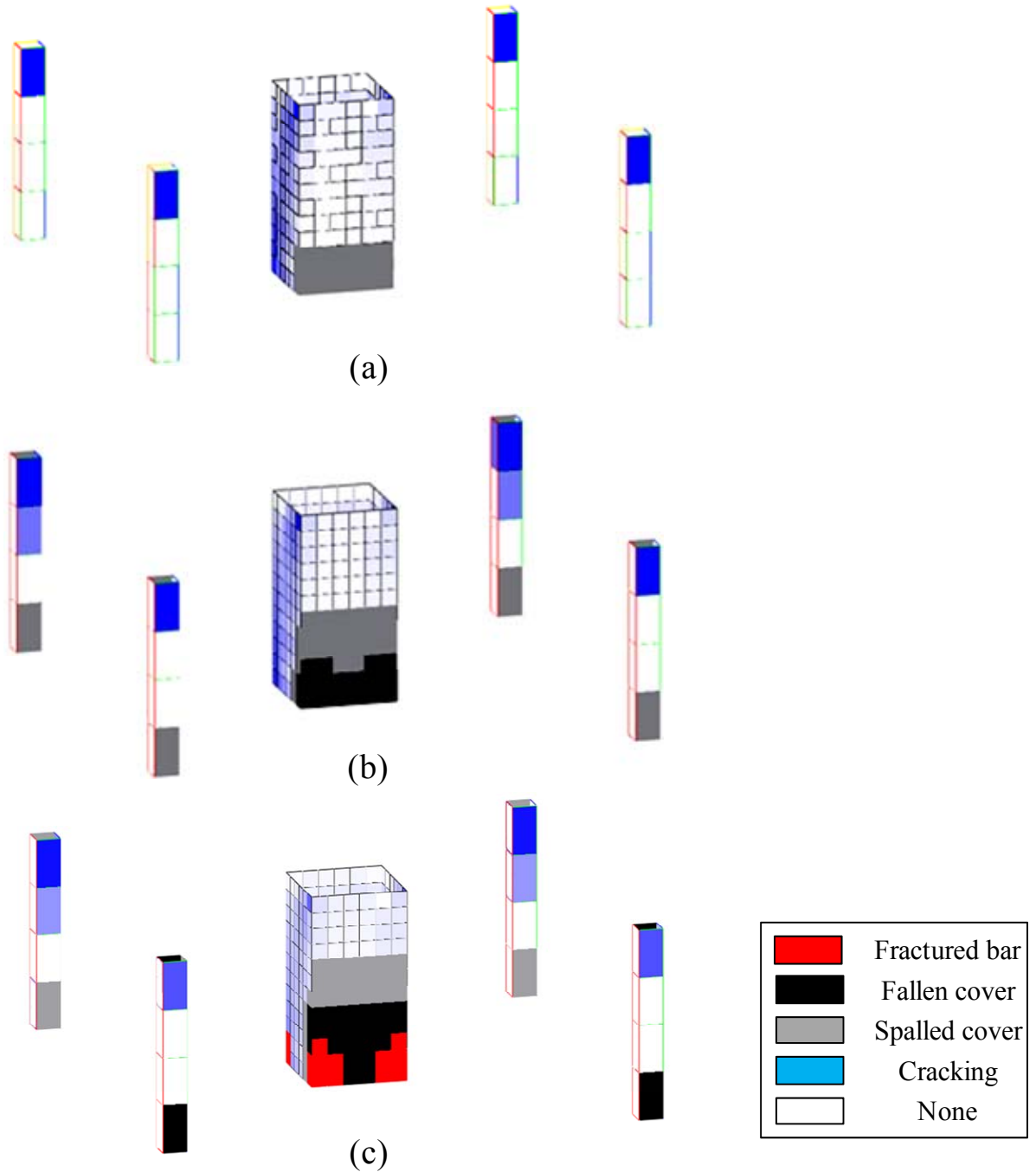


Figure 4-17. Visual damage on columns and shear walls at three inter-story drift ratios: a) $\delta=1\%$; b) $\delta=1.5\%$; c) $\delta=2\%$.

In Figure 4-17, it is seen that the visual damage on the core shear wall is more severe than column. This makes sense because lateral loads are primarily carried by the core shear

wall while the columns essentially carry the gravity loads. It is also seen that the visual damage scenarios at the bottom segment of columns are concrete crushing, *i.e.*, spalling and falling of concrete cover, because they are in compression. In contrast, the visual damage at the top segment of the columns is concrete cracking as they are in tension.

The total quantity that should be repaired with different repair actions is computed in the repair manager model and listed in Table 4-4.

Table 4-4. Repair actions and repair quantities at different drift ratios.

Repair action [unit]	Repair quantities		
	$\delta=1\%$	$\delta=1.5\%$	$\delta=2\%$
Epoxy injection [m ²]	2	5.33	9.22
Patching concrete cover [m ²]	5.33	10.67	9.17
Concrete cover replacement [m ²]	0	4.44	7.78
Section replacement [m ³]	0	0	0.622

In Table 4-4, the repair quantities for epoxy injection, patching concrete cover, and concrete cover replacement are assessed as the surface area of the component that requires repair. The repair quantity for the section replacement is computed as the volume of the section that should be replaced. The epoxy injection is applied for walls if the crack length exceeds half of the wall width. It is noted that the type of the component should also be considered for the cost assessment. This is because the cost assessment is affected by several factors. Those factors include the elevation of the damaged zone, the method for shoring of

the structure, and the quantity that should be repaired within a single component with a certain repair action. The cost assessment is the subject of future studies.

4.6 CONCLUSIONS

A software framework for assessing the performance of building components is proposed. The ultimate objective in the proposed framework is to improve the assessment of the design cost of building components, and provide a tool for optimal risk-based design. The framework entails design of a new building component class, which is intended to provide information on the direct and indirect monetary cost of design of building components. This information will include the construction cost, environmental impacts of manufacturing, use, and demolishing, and the repair actions and quantities due to earthquake damage. This information can be used in the models in the Rts computer program to assess the design costs. Particularly, the detailed visual damage to building components can be simulated during and after earthquake. The simulation of detailed visual damage facilitates robust prediction of the repair actions and rigorous assessment of the quantities that should be repaired. The component classes for RC column and shear wall can then be developed. These components are used in four examples that demonstrate the simulation of visual damage. The new component class is intended to develop a library of structural and non-structural components, where component-specific models for simulation of environmental impact, seismic damage, and repair actions are developed and implemented.

Chapter 5: CONCLUSIONS AND FUTURE WORK

The long-term vision, objectives, motivations and contributions in this thesis are summarized in the Introduction. This chapter provides the conclusive remarks on the research paradigm from a broader viewpoint. Several research needs and tasks to advance this paradigm are also suggested.

5.1 OVERVIEW OF THE RESEARCH APPROACH

This thesis examines the damage modelling for PBEE from a new perspective. Two distinct approaches for seismic damage modelling in the literature are examined. The first approach models damage by a number between 0, *i.e.*, undamaged and 1, *i.e.*, damaged. The damage indices developed in the 1980's and 1990's represent a commendable effort for assessment of seismic damage by this approach. The second approach considers the uncertainty in the damage prediction by predicting the probability of incurring damage. The fragility models that predict the damage probability conditioned upon the value of a single structural response. The present study advances the existing approaches in two aspects. First, it suggests a new method for developing multivariate fragility models. The multivariate fragility models enable the modeller to quantify the damage probability under influence of multiple variables, *e.g.*, structural responses, structural characteristics, and material properties. Second, it suggests the simulation of detailed seismic damage. The simulation of detailed damage entails the prediction of visual damage in detail at the segments of the building components. The advancements in this study offer the following advantages:

- 1) The multivariate fragility models do not cross, and thus, they do not predict negative damage probabilities.
- 2) The multivariate fragility models can be developed using a broader range of test data, which represent the damage to a component type that differs in geometry, material properties
- 3) The multivariate fragility models quantify the variability of damage probability with design variables
- 4) The multivariate fragility models can be used in all PBEE frameworks that require the probability that structural components are in one of several damage states
- 5) The detailed simulation of visual damage leads to rational and robust prediction of required repair actions, with which the repair decisions, costs and time are estimated.
- 6) The detailed simulation of visual damage helps the rigorous estimation of quantities that need to be repaired.
- 7) The simulation of visual damage facilitates the communication between structural engineers and contractors who make repair decisions based on the visible damage after an earthquake.
- 8) In the visual damage modelling, certain damage models are employed to simulate different scenarios of damage. This is because each visual damage scenario may occur by different mechanisms. It also leads to development of refined models, which is necessary for steadily improvements of models.
- 9) The reliability-based analysis for PBEE presented in Chapter 1 can be conducted by the visual damage simulations.

5.2 FUTURE RESEARCH DIRECTIONS

In the course of this study, a number of research topics and tasks are identified for further advancements. In the following, these research topics and tasks are presented in two categories: multivariate fragility models and simulation of visual damage.

First, in regards to multivariate fragility models presented in Chapter 3, the following tasks are identified:

- In this thesis the multivariate fragility models is developed for RC shear walls. It is suggested that further research efforts focus on developing a library of multivariate fragility models for building components.
- In Chapter 3, in lieu of information on the visual damage, the backbone curve has been used to identify the damage states for RC shear wall. Future work should utilize test data that provide information about the visual damage to damage states.
- The loading protocol has significant effect on the cyclic envelop and damage (Federal Emergency Management Agency 2009). However, as mentioned in Chapter 3, the focus of this thesis is on the modelling technique. The number of cycles in the loading protocol, the amplitude of each cycle, and the sequence of the loading cycles significantly affect the hysteretic curve. These variables can be used as explanatory functions in the multivariate fragility models in future work.
- In Chapter 3, the maximum likelihood method is employed to predict the model parameters. Future work can implement a Bayesian method to estimate the distribution of model parameters for logistic regression.

- In Chapter 3, the multinomial logistic regression for ordinal data is used because the damage states for shear wall happen subsequently. Future work may employ logistic regression models for nominal data for components whose damage states do not occur in order.

Second, the following suggestions are made for further development of the simulations of damage and prediction of repair actions and costs:

- It is suggested that a library of building components be developed by data-gathering efforts. The data can be gathered by using questionnaires to solicit information from contractors in regards to possible visual damage scenarios, repair actions, construction and repair cost. The further research is needed to simulate each visual damage scenario.
- Further work should develop and implement models for the environmental impacts, *e.g.*, carbon emission, associated with manufacturing, use, and demolishing of the component in its life-cycle.
- Further work should implement models for assessing costs associated with construction, demolition, repair, *etc.*
- The damage models in Chapter 4 simulate the local damage to components. Further research is suggested to develop and implement a model to predict global damage, *i.e.*, building collapse, reduction in overall stiffness of the structure, strength degradation, *etc.*
- Further research is suggested to develop and implement a model for demolition decision. This model should be developed considering effect of several factors on the stakeholder's decision for demolishing. These factors may include building age, building occupancy

class, insurance contract, whether the current structural design of building complies with the advanced seismic codes, city regulations, repair cost, cost of demolition and reconstruction, availability of resources, *i.e.*, labor, material, *etc.* global structural damage, extent of earthquake damage to the buildings in the vicinity of current building, possibility of business abruption, time of repair.

- Further research is suggested to create the finite elements for building components from building information models. This promotes the structural software interoperability.
- Further research is suggested to develop a model for repair time. The model can use the required repair actions and the methods for developing a Gantt chart.
- Further research is suggested to improve the visual damage simulations for RC components. Combining a variety of analytical models for reinforced concrete load-deformation response, *e.g.*, modified compression field theory (Vecchio and Collins 1986) and distributed stress field model (Vecchio 2000) and advanced finite elements will improve the damage simulations such as simulation of crack width for RC shear wall. Also, the implementation of the advanced material models for unconfined and confined concrete, *e.g.*, the material model proposed by Mander *et al.* (1988), will improve the simulation of RC Column.
- Future work should implement a “smoothing” method for the assessments of the repair cost. It is because the gradient-based reliability methods such as first order reliability method require models that are continuously differentiable, *i.e.*, smooth, with respect to the random variables.

- Further research is suggested to compute the sensitivity of visual damage and repair cost with respect to the random variables and decision variables.

BIBLIOGRAPHY

- Abrams, D. P. (2002). "Consequence-based engineering approaches for reducing loss in mid-America." *University of Notre Dame*.
- Adebar, P., Ibrahim, A. M. M., and Bryson, M. (2007). "Test of high-rise core wall: Effective stiffness for seismic analysis." *ACI Struct.J.*, 104(5), 549-559.
- Adebar, P., and Van Leeuwen, J. (1999). "Side-face reinforcement for flexural and diagonal cracking in large concrete beams." *ACI Struct.J.*, 96(5), 693-704.
- Agresti, A. (1996). *An introduction to categorical data analysis*. John Wiley & Sons Inc., New York.
- Ali, A., and Wight, J. (1991). "RC structural walls with staggered door openings." *J.Struct.Eng.*, 117(5), 1514-1531.
- Alire, D. (2003). "Seismic evaluation of existing unconfined RC joints". M.Sc. Thesis. University of Washington, Seattle.
- American Concrete Institute. (1999). "Building code requirements for structural concrete." *Rep. No. ACI-318*, Farmington Hills, Mich.
- Ang, A. H., and Tang, W. H. (2007). *Probability concepts in engineering: emphasis on applications in civil and environmental engineering*. John Wiley & Sons Inc., New York.
- Applied Technology Council. (2012). "Development of next generation performance-based seismic design procedures for new and existing buildings." *Rep. No. ATC-58*, Redwood City, CA.
- Applied Technology Council. (1998). "Repair of earthquake damaged concrete and masonry wall building." *Rep. No. FEMA-308*, Redwood City, CA.

- Applied Technology Council. (1996). "Improved Seismic Design Criteria for California Bridges: Provisional Recommendations" *Rep. No. ATC-32*, Redwood City, CA.
- Applied Technology Council. (1989). "Procedures for postearthquake safety evaluation of buildings." *Rep. No. ATC-20*, Applied Technology Council, Redwood City, CA.
- Applied Technology Council. (1985). "Earthquake damage evaluation data for California." *Rep. No. ATC-13*, Applied Technology Council, Redwood City, CA.
- ATC-58 Project Task Report. (2004). "Engineering demand parameters for structural framing systems." *Rep. No. Phase 2, Task 2.2*, Applied Technology Council, Redwood City, CA.
- Bai, J., Hueste, M., and Gardoni, P. (2009). "Probabilistic assessment of structural damage due to earthquakes for buildings in Mid-America." *J.Struct.Eng.*, 135(10), 1155-1163.
- Bai, J., Gardoni, P., and Hueste, M. B. D. (2011). "Story-specific demand models and seismic fragility estimates for multi-story buildings." *Struct.Saf.*, 33(1), 96-107.
- Balaguru, P., and Shah, S. (1982). "A method of predicting crack widths and deflections for fatigue loading." *ACI Special Publication*, 75 153-176.
- Bayer, K. (2012). "Quake city landmark will soon be rubble." *The New Zealand Herald*.
- Beck, J. L., Porter, K. A., Shaikhutdinov, R., Au, S., Mizukoshi, K., Miyamura, M., Ishida, H., Moroi, T., Tsukada, Y., and Masuda, M. (2002). "Impact of seismic risk on lifetime property values." *Rep. No. Final Report, CUREE-Kajima Joint Research Program Phase IV*, Consortium of Universities for Earthquake Engineering Research, Richmond, CA.
- Beck, J., Kiremidjian, A., Wilkie, S., Mason, A., Salmon, T., Goltz, J., Olson, R., Workman, J., Irfanoglu, A., and Porter, K. (1999). "Decision support tools for earthquake recovery of businesses." *Rep. No. Final Report for CUREE-Kajima Phase III*, Consortium of Universities for Earthquake Engineering Research, Richmond, CA.
- Beckingsale, C. W. (1980). "Post elastic behavior of reinforced concrete beam-column joints". Ph.D. dissertation. University of Canterbury, New Zealand.

- Berry, M., and Eberhard, M. O. (2004). *Performance models for flexural damage in reinforced concrete columns*. Pacific Earthquake Engineering Research Center, College of Engineering, University of California.
- Berry, M., Parrish, M., and Eberhard, M. (2004). "PEER Structural Performance Database User's Manual (Version 1.0)." *University of California, Berkeley*.
- Berry, M. P., Lehman, D. E., and Lowes, L. N. (2008). "Lumped-plasticity models for performance simulation of bridge columns." *ACI Struct.J.*, 105(3), 270-279.
- Bett, J. B., Klingner, R. E., and Jirsa, J. O. (1988). "Lateral load response of strengthened and repaired reinforced concrete columns." *ACI Struct.J.*, 85(5), 499-508.
- Birss, G. R. (1978). "The elastic behaviour of earthquake resistant reinforced concrete interior beam-column joints". M.Sc. thesis. University of Canterbury, New Zealand.
- Bozorgnia, Y., and Bertero, V. V. (2003). "Damage spectra: Characteristics and applications to seismic risk reduction." *J.Struct.Eng.*, 129(10), 1330-1340.
- Bracci, J. M., Reinhorn, A. M., Mander, J. B., and Kunnath, S. K. (1989). "Deterministic model for seismic damage evaluation of RC structures." *Rep. No. 89-0033*, National Center for Earthquake Engineering Research, State University of New York, Buffalo NY.
- Broms, B. B. (1965). "Crack width and crack spacing in reinforced concrete members." *ACI Journal Proceedings*, 62(10), 1237-1256.
- Brown, P. C. (2008). "Probabilistic earthquake damage prediction for reinforced concrete building components". M.S. thesis. University of Washington, Seattle.
- Brown, P. C., and Lowes, L. N. (2007). "Fragility functions for modern reinforced-concrete beam-column joints." *Earthquake Spectra*, 23(2), 263-289.
- Carvajal, O., and Pollner, E. (1983). "Muros de Concreto Reforzados con Armadura Minima." *Boletin Tecnico, Universidad Central De Venezuela, Facultad De Ingenieria*, Ano 21 (72-73)(Enero-Diciembre), 5-36.

- Chan, L. S., Chen, Y., Chen, Q., Chen, L., Liu, J., Dong, W., and Shah, H. (1998). "Assessment of global seismic loss based on macroeconomic indicators." *Nat.Hazards*, 17(3), 269-283.
- Chang, S. E., and Shinozuka, M. (2004). "Measuring improvements in the disaster resilience of communities." *Earthquake Spectra*, 20(3), 739-755.
- Chi, M., and Kirstein, A. F. (1958). "Flexural cracks in reinforced concrete beams." *ACI Journal Proceedings*, 54(4), 865-878.
- Chung, Y. S., Meyer, C., and Shinozuka, M. (1990). "Automatic seismic design of reinforced concrete building frames." *ACI Struct.J.*, 87(3), 326-340.
- Clark, A. P. (1956). "Cracking in reinforced concrete flexural members." *ACI Journal Proceedings*, ACI, 851-862.
- Collins, S. (2011). "Insurance too little for many firms to rebuild ." *The New Zealand Herald*.
- Comerio, M. C. (2013). "Housing recovery in Chile: A qualitative mid-program review." *Rep. No. 2013/01*, Pacific Earthquake Engineering Research Center, University of California, Berkeley.
- Comerio, M. C. (2006). "Estimating downtime in loss modeling." *Earthquake Spectra*, 22(2), 349-365.
- Consortium of Universities for Research in Earthquake Engineering. (2010). "General guidelines for the assessment and repair of earthquake damage in residential woodframe buildings." *Rep. No. EDA-06*, Consortium of Universities for Research in Earthquake Engineering, Richmond, CA.
- Corley, W., Fiorato, A., and Oesterle, R. (1981). "Structural walls." *ACI Special Publication*, 77-131.

- Cornell, C. A., Jalayer, F., Hamburger, R. O., and Foutch, D. A. (2002). "Probabilistic basis for 2000 SAC federal emergency management agency steel moment frame guidelines." *J.Struct.Eng.*, 128(4), 526-533.
- Cornell, C., and Krawinkler, H. (2000). "Progress and challenges in seismic performance assessment." *PEER Center News*.
- Daniell, J. E., Wenzel, F., and Khazai, B. (2010). "The cost of historic earthquakes today – economic analysis since 1900 through the use of CATDAT." *Australian Earthquake Engineering Society 2010 Conference*, Perth, Western Australia.
- Dazio, A., Beyer, K., and Bachmann, H. (2009). "Quasi-static cyclic tests and plastic hinge analysis of RC structural walls." *Eng.Struct.*, 31(7), 1556-1571.
- De, L., D., and Ang, A. H. -. (1994). "Damage model for reinforced concrete buildings. Further study with the 1985 Mexico City earthquake." *Part 3 (of 3)*, A.A. Balkema, Innsbruck, Austria, 2081-2081.
- Deitel, P. J., and Deitel, H. M. (2013). *C++ How to Program (Early Objects Version)*. Prentice Hall.
- Der Kiureghian, A. (2005). "Non-ergodicity and PEER's framework formula." *Earthquake Engineering and Structural Dynamics*, 34(13), 1643-1652.
- Dowrick, D. J. (1991). "Damage costs for houses and farms as a function of intensity in the 1987 Edgecumbe earthquake." *Earthquake Engineering and Structural Dynamics*, 20(5), 455-469.
- Durrani, A. J. (1982). "Experimental and analytical study of internal beam to column connections subjected to reversed cyclic loading". PhD dissertation. Michigan University.
- Earthquake Engineering Research Institute. (1994). "Expected seismic performance of buildings." Applied Technology Council, Oakland, CA: EERI.

- Earthquake Engineering Research Institute. "Damaged Concrete Buildings Database." <http://db.concretecoalition.org/> (March, 2013).
- Eckel, B. (2000). *Thinking in C++*. Prentice Hall, Upper Saddle River, New Jersey.
- Eguchi, R. T., Goltz, J. D., Taylor, C. E., Chang, S. E., Flores, P. J., Johnson, L. A., Seligson, H. A., and Blais, N. C. (1998). "Direct economic losses in the Northridge earthquake: a three-year post-event perspective." *Earthquake Spectra*, 14(2), 245-264.
- Endoh, Y., Kamura, T., Otani, S., and Aoyama, H. (1991). "Behavior of R/C beamcolumn connections using light-weight concrete." *Trans.Jpn.Concr.Inst*, 13 319-326.
- Fajfar, P. (1992). "Equivalent ductility factors, taking into account low-cycle fatigue." *Earthquake Eng.Struct.Dyn.*, 21(10), 837-848.
- Federal Emergency Management Agency. (2009). "Effect of strength and stiffness degradation on seismic response." *Rep. No. FEMA P440A*, Redwood City, CA.
- Federal Emergency Management Agency. (2007). "Interim testing protocol for determining the seismic performance characteristics of structural and nonstructural components." *Rep. No. FEMA 461*, Redwood City, CA.
- Federal Emergency Management Agency. (2006). "Next-generation performance-based seismic design guidelines." *Rep. No. FEMA 445*, Washington, D.C.
- Federal Emergency Management Agency. (2000). "Prestandard and commentary for the seismic rehabilitation of buildings." *Rep. No. FEMA 356*, Washington, D.C.
- Federal Emergency Management Agency. (1999). "The Repair of Earthquake Damaged Concrete and Masonry Wall Buildings." *Rep. No. FEMA 308*, Federal Emergency Management Agency, Washington, DC, Redwood City, CA.
- Federal Emergency Management Agency. (1997). "NEHRP guidelines for the seismic rehabilitation of buildings." *Rep. No. FEMA 273*, Washington, D.C.

- Frangou, M., Pilakoutas, K., and Dritsos, S. (1995). "Structural repair/strengthening of RC columns." *Constr.Build.Mater.*, 9(5), 259-266.
- Gardoni, P., Mosalam, K. M., and Der Kiureghian, A. (2003). "Probabilistic seismic demand models and fragility estimates for RC bridges." *J.Earth.Eng.*, 07 79-106.
- Gardoni, P., Der Kiureghian, A., and Mosalam, K. M. (2002). "Probabilistic capacity models and fragility estimates for reinforced concrete columns based on experimental observations." *J.Eng.Mech.*, 128(10), 1024-1038.
- Gergely, P., and Lutz, L. A. (1968). "Maximum crack width in reinforced concrete flexural members." *ACI Special Publication*, 20 87-117.
- Ghobarah, A. (2001). "Performance-based design in earthquake engineering: state of development." *Eng.Struct.*, 23(8), 878-884.
- Graf, W. P., and Lee, Y. (2009). "Code-oriented damage assessment for buildings." *Earthquake Spectra*, 25(1), 17-37.
- Guerra, E. (2010). "A probabilistic for estimating environmental impacts over the life cycle of buildings". M.A.Sc. The University of British Columbia, Vancouver, BC, Canada.
- Guidance. (2012). "Guidance: Repairing and rebuilding houses affected by the Canterbury earthquakes." Ministry of Business, Innovation and Employment, Canterbury, New Zealand.
- Gunturi, S. K. V., and Shah, H. C. (1992). "Building specific damage estimation." *10 vols*, Publ by A.A. Balkema, Madrid, Spain, 6001-6001.
- Hanson, R. D., and Comartin, C. (2000). "The repair of earthquake damaged buildings." *World Conference on Earthquake Engineering, 12 WCEE*, New Zealand.
- Hasselmann, T., K., and Wiggins, J.,H. (1982). "Earthquake damage to high-rise buildings as a function of interstory drift." *3rd International Earthquake Microzonation Conference*, Seattle, WA, 883-894.

- Haukaas, T. (2008). "Unified reliability and design optimization for earthquake engineering." *Prob.Eng.Mech.*, 23(4), 471-481.
- Haukaas, T., Allahdadian, S., and Mahsuli, M. (2013). "Risk measures for minimization of earthquake costs." *11th International Conference on Structural Safety and Reliability, ICOSSAR 2013, June 16, 2013 - June 20, 2013*, Taylor & Francis - Balkema, New York, NY, United states, 2619-2626.
- Haukaas, T., and Javaherianyazdi, A. (2013). "New damage models for performance-based earthquake engineering." *4th International Conference on Computational Methods in Structural Dynamics and Earthquake Engineering COMPDYN 2013, June 12 - June 14*, Kos Island, Greece.
- Haukaas, T., and Der Kiureghian, A. (2007). "Methods and object-oriented software for FE reliability and sensitivity analysis with application to a bridge structure." *J.Comput.Civ.Eng.*, 21(3), 151-163.
- Hayashi, K., Teraoka, M., Mollick, A., and Kanoh, Y. (1994). "Bond properties of main reinforcing bars and restoring force characteristics in RC interior beam-column sub-assembly using high strength materials." *Proc. 2nd US-Japan-New-Zealand-Canada multilateral meeting on structural performance of high strength concrete in seismic regions*.
- Hidalgo, P. A., Ledezma, C. A., and Jordan, R. M. (2002). "Seismic behavior of squat reinforced concrete shear walls." *Earthquake Spectra*, 18(2), 287-308.
- Hognestad, E. (1962). "High strength bars as concrete reinforcement, Part 2: Control of flexural cracking." *Portland Cement Association, Research and Development Laboratories*, 4(1), 46-63.
- Hosmer, D., and Lemeshow, S. (2000). *Applied logistic regression*. John Wiley & Sons Inc., New York.
- Hwang, H., and Jaw, J. (1990). "Probabilistic Damage Analysis of Structures." *J.Struct.Eng.*, 116(7), 1992-2007.

- Hwang, H. H. M., and Huo, J. (1994). "Generation of hazard-consistent fragility curves." *Soil Dyn. Earthquake Eng.*, 13(5), 345-354.
- Jaiswal, K., and Wald, D. J. (2013). "Estimating economic losses from earthquakes using an empirical approach." *Earthquake Spectra*, 29(1), 309-324.
- Jalayer, F., Franchin, P., and Pinto, P. E. (2007). "A scalar damage measure for seismic reliability analysis of RC frames." *Earthquake Engineering and Structural Dynamics*, 36(13), 2059-2079.
- Ji, S. (2002). "Dynamic analysis of the elastic-plastic response of high-rise reinforced concrete frame-wall structures subjected to ground motion". PhD dissertation. Tongji University, China.
- Jiang, H. (1999). "Research on seismic behavior of shear walls dissipating energy along vertical direction with application". PhD dissertation. Tongji University, China.
- Joh, O., Goto, Y., and Shibata, T. (1991a). "Behavior of reinforced concrete beam-column joints with eccentricity." *ACI Special Publication*, 123 317-358.
- Joh, O., Goto, Y., and Shibata, T. (1991b). "Influence of transverse joint and beam reinforcement and relocation of plastic hinge region on beam column joint stiffness deterioration." *ACI Special Publication*, 123 187-224.
- Kaar, P. H., and Mattock, A. H. (1963). "High strength bars as concrete reinforcement, part 4: control of cracking." *Portland Cement Association, Research and Development Laboratories*, 5(1), 15-38.
- Kaar, P. H., and Hognestad, E. (1965). "High strength bars as concrete reinforcement, part 7: control of cracking in T-beam flanges." *Portland Cement Association, Research and Development Laboratories*, 7(1), 42-53.
- Kabeyasawa, T., and Hiraishi, H. (1998). "Tests and analyses of high-strength reinforced concrete shear walls in Japan." *ACI Special Publication*, 176 281-310.

- Kam, W. Y., and Pampanin, S. (2011). "The seismic performance of RC buildings in the 22 February 2011 Christchurch earthquake." *Structural Concrete*, 12(4), 223-233.
- Kappos, A. J., Lekidis, V., Panagopoulos, G., Sous, I., Theodulidis, N., Karakostas, C., Anastasiadis, T., Salonikios, T., and Margaritis, B. (2007). "Analytical estimation of economic loss for buildings in the area struck by the 1999 Athens earthquake and comparison with statistical repair costs." *Earthquake Spectra*, 23(2), 333-355.
- Karim, K. R., and Yamazaki, F. (2001). "Effect of earthquake ground motions on fragility curves of highway bridge piers based on numerical simulation." *Earthquake Eng.Struct.Dyn.*, 30(12), 1839-1856.
- Karim, K. R., and Yamazaki, F. (2003). "A simplified method of constructing fragility curves for highway bridges." *Earthquake Engineering and Structural Dynamics*, 32(10), 1603-1626.
- Kazaz, I., Gulkan, P., and Yakut, A. (2012). "Deformation limits for structural walls with confined boundaries." *Earthquake Spectra*, 28(3), 1019-1046.
- J. Key. (2011). "Thousands of Christchurch homes face demolition." stuff.co.nz 2011).
- Kinali, K., and Ellingwood, B. R. (2007). "Seismic fragility assessment of steel frames for consequence-based engineering: A case study for Memphis, TN." *Eng.Struct.*, 29(6), 1115-1127.
- Kircher, C. A., Nassar, A. A., Kustu, O., and Holmes, W. T. (1997). "Development of building damage functions for earthquake loss estimation." *Earthquake Spectra*, 13(4), 663-682.
- Kiremidjian, A. S. (1985). "Subjective probabilities for earthquake damage and loss." *Struct.Saf.*, 2(4), 309-317.
- Koduru, S. D., and Haukaas, T. (2010). "Probabilistic seismic loss assessment of a vancouver high-rise building." *J.Struct.Eng.*, 136(3), 235-245.

- Koutsourelakis, P. S. (2010). "Assessing structural vulnerability against earthquakes using multi-dimensional fragility surfaces: A Bayesian framework." *Prob.Eng.Mech.*, 25(1), 49-60.
- Krätzig, W., and Meskouris, K. (1997). "Seismic damage evaluation treated as a low-cycle fatigue process." *Proceedings, Seismic Design Methodologies for the Next Generation of Codes, Bled, Slovenia*, 139-149.
- Krawinkler, H., and Miranda, E. (2004). "Performance-based earthquake engineering, Chapter 9." *Earthquake engineering : From engineering seismology to performance-based engineering*, CRC Press, Boca Raton, Florida.
- Krawinkler, H. (1987). "Performance assessment of steel components." *Earthquake Spectra*, 3(1), 27-41.
- Krawinkler, H., and Zohrei, M. (1983). "Cumulative damage in steel structures subjected to earthquake ground motions." *Comput.Struct.*, 16(1-4), 531-541.
- Kunnath, S. K., El-Bahy, A., Taylor, A. W., and Stone, W. C. (1997). "Cumulative seismic damage of reinforced concrete bridge piers." *Technical Report NCEER*, US National Center for Earthquake Engineering Research.
- Kunnath, S., Reinhorn, A., and Park, Y. (1990). "Analytical Modeling of Inelastic Seismic Response of R/C Structures." *J.Struct.Eng.*, 116(4), 996-1017.
- Kuroiwa, J., and Kogan, J. (1980). "Repair and strengthening of buildings damaged by earthquakes." *Proceedings of the 7th World Conference on Earthquake Engineering*. Turk Natl Comm on Earthquake Eng, Ankara, Istanbul, Turk, 569-576.
- Lang, K. (2002). *Seismic vulnerability of existing buildings*. vdf Hochschulverlag AG, .
- Lee, K. H., and Rosowsky, D. V. (2006). "Fragility analysis of woodframe buildings considering combined snow and earthquake loading." *Struct.Saf.*, 28(3), 289-303.

- Lefas, I. D., and Kotsovos, M. D. (1990). "Strength and deformation characteristics of reinforced concrete walls under load reversals." *ACI Struct.J.*, 87(6), 716-726.
- Lefas, I. D., Kotsovos, M. D., and Ambraseys, N. N. (1990). "Behavior of reinforced concrete structural walls. Strength, deformation characteristics, and failure mechanism." *ACI Struct.J.*, 87(1), 23-31.
- Lehman, D., Moehle, J., Mahin, S., Calderone, A., and Henry, L. (2004). "Experimental evaluation of the seismic performance of reinforced concrete bridge columns." *J.Struct.Eng.*, 130(6), 869-879.
- Lehman, D. E., Gookin, S. E., Nacamull, A. M., and Moehle, J. P. (2001). "Repair of earthquake-damaged bridge columns." *ACI Struct.J.*, 98(2), 233-242.
- Li, G., Zhang, Y., and Li, H. (2013). "Seismic damage analysis of reinforced concrete frame using the force analogy method." *J.Eng.Mech.*, 139(12), 1780-1789.
- Lovegrove, J., and El Din, S. (1982). "Deflection and cracking of reinforced concrete under repeated loading and fatigue." *ACI Special Publication*, 75 133-152.
- Mackie, K., Wong, J., and Stojadinovic, B. (2007). "Comparison of post-earthquake highway bridge repair costs." Proceedings of the ASCE Structures Congress, 16-19.
- Mahin, S. A., and Bertero, V. V. (1981). "An evaluation of inelastic seismic design spectra." *Journal of the Structural Division*, 107(9), 1777-1795.
- Mahin, S. A. (1998). "Lessons from damage to steel buildings during the Northridge earthquake." *Eng.Struct.*, 20(4-6), 261-270.
- Mahsuli, M., and Haukaas, T. (2013). "Computer program for multimodel reliability and optimization analysis." *J.Comput.Civ.Eng.*, 27(1), 87-98.
- Mander, J., Priestley, M., and Park, R. (1988). "Theoretical stress-strain model for confined concrete." *J.Struct.Eng.*, 114(8), 1804-1826.

- Mathey, R. G., and Watstein, D. (1960). "Effect of tensile properties of reinforcement on the flexural characteristics of beams." *ACI Journal Proceedings*, 56(6), 1253-1274.
- McCullagh, P., and Nelder, J. A. (1989). *Generalized linear models*. Chapman and Hall, London.
- McKenna, F., Scott, M. H., and Fenves, G. L. (2010). "Nonlinear finite-element analysis software architecture using object composition." *J.Comput.Civ.Eng.*, 24(1), 95-107.
- Mehanny, S. S. F., and Deierlein, G. G. (2001). "Seismic damage and collapse assessment of composite moment frames." *J.Struct.Eng.*, 127(9), 1045-1053.
- Meinheit, D. F., and Jirsa, J. O. (1977). "Shear strength of reinforced concrete beam-column joints." *CESRL Report - University of Texas at Austin, Department of Civil Engineering, Structures Research Laboratory*.
- Milburn, J. R. (1982). "Behavior of reinforced concrete beam-column joints designed to NZS 3101". M.Sc. thesis. University of Canterbury, New Zealand.
- Miles, S. B., and Chang, S. E. (2006). "Modeling community recovery from earthquakes." *Earthquake Spectra*, 22(2), 439-458.
- Mitrani-Reiser, J. (2007). "An ounce of prevention: probabilistic loss estimation for performance-based earthquake engineering" Ph.D. thesis. California Institute of Technology, California, US.
- Moehle, J., and Deierlein, G. G. (2004). "A framework methodology for performance-based earthquake engineering." *Proceedings of the 13th World conference on earthquake engineering*, 3812-3814.
- Moyer, M. J., and Kowalsky, M. J. (2003). "Influence of tension strain on buckling of reinforcement in concrete columns." *ACI Struct.J.*, 100(1), 75-85.

- NIST. (1999). "UNIFORMAT II elemental classification for building specifications, cost estimating, and cost analysis." *Rep. No. NISTIR 6389*, National Institute of Standards and Technology, Gaithersberg, Maryland.
- Oesterle, R., Aristizabal-Ochoa, J., Fiorato, A., Russell, H., and Corley, W. (1979). "Earthquake resistant structural walls - tests of isolated walls - Phase II." *Rep. No. Technical Report*, National Science Foundation, Washington DC.
- Oesterle, R., Fiorato, A., Johal, L., Carpenter, J., Russell, H., and Corley, W. (1976). "Earthquake Resistant Structural Walls - Tests of Isolated Walls - Phase II." *Rep. No. Technical Report*, National Science Foundation, Washington DC.
- Oh, B. H., and Kang, Y. (1987). "New formula for maximum crack width and crack spacing in reinforced concrete flexural members." *ACI Struct.J.*, 84(2), 103-112.
- Oh, B. H., and Kim, S. H. (2007). "Advanced crack width analysis of reinforced concrete beams under repeated loads." *J.Struct.Eng.*, 133(3), 411-420.
- Orakcal, K., Massone, L. M., and Wallace, J. W. (2009). "Shear strength of lightly reinforced wall piers and spandrels." *ACI Struct.J.*, 106(4), 455-465.
- Padgett, J. E., and DesRoches, R. (2008). "Methodology for the development of analytical fragility curves for retrofitted bridges." *Earthquake Engineering and Structural Dynamics*, 37(8), 1157-1174.
- Pagni, C. A., and Lowes, L. N. (2006). "Fragility functions for older reinforced concrete beam-column joints." *Earthquake Spectra*, 22(1), 215-238.
- Pang, X. (1991). "Constitutive laws of reinforced concrete in shear". PhD dissertation, Dept. of Civil and Environmental Engineering, University of Houston.
- Park, R., and Ruitong, D. (1988). "A Comparison of the behaviour of reinforced concrete beam-column joints designed for ductility and limited ductility." *Nat. Soc. Earthquake Eng. Bull*, 21 255-278.

- Park, Y., Ang, A., and Wen, Y. (1985). "Seismic Damage Analysis of Reinforced Concrete Buildings." *J.Struct.Eng.*, 111(4), 740-757.
- Park, Y., and Ang, A. H. -. (1985). "Mechanistic seismic damage model for reinforced concrete." *J.Struct.Eng.*, 111(4), 722-739.
- Park, Y., Ang, A. H. -. , and Wen, Y. K. (1987). "Damage-limiting aseismic design of buildings," *Earthquake Spectra*, 3(1), 1-26.
- Paulay, T., Priestley, M. J. N., and Syngge, A. J. (1982). "Ductility in earthquake resisting squat shearwalls." *Journal of the American Concrete Institute*, 79(4), 257-269.
- Paultre, P., and Mitchell, D. (1991). "Assessment of some Canadian seismic code requirements for concrete frame structures." *Canadian Journal of Civil Engineering*, 18(3), 343-357.
- Pessiki, S. P., Conley, C., Gergely, P., and White, R. N. (1990). "Seismic behavior of lightly-RC column and beam-column joint details." *Rep. No. NCEER-90-0014*, MCEER Publications, Buffalo, NY.
- Petryna, Y. S., and Kratzig, W. B. (2005). "Compliance-based structural damage measure and its sensitivity to uncertainties." *Uncertainties in Structural Mechanics and Analysis-Computational Methods*, Elsevier Ltd, 1113-1133.
- Pilakoutas, K. (1991). "Earthquake resistant design of reinforced concrete walls". PhD dissertation. Imperial College of Science Technology and Medicine.
- Pilakoutas, K., and Elnashai, A. (1995). "Cyclic behavior of reinforced concrete cantilever walls, Part I: Experimental results." *ACI Mater.J.*, 92(3), 271-281.
- Porter, K. A., Kiremidjian, A. S., and LeGrue, J. S. (2001). "Assembly-based vulnerability of buildings and its use in performance evaluation." *Earthquake Spectra*, 17(2), 291-312.
- Porter, K. (2009). "Cracking an open safe: HAZUS vulnerability functions in terms of structure-independent spectral acceleration." *Earthquake Spectra*, 25(2), 361-378.

- Porter, K. A., Beck, J. L., Shaikhutdinov, R. V., Au, S. K., Mizukoshi, K., Miyamura, M., Ishida, H., Moroi, T., Tsukada, Y., and Masuda, M. (2004). "Effect of seismic risk on lifetime property value." *Earthquake Spectra*, 20(4), 1211-1237.
- Powell, G. H., and Allahabadi, R. (1988). "Seismic damage prediction by deterministic methods: concepts and procedures." *Earthquake Eng.Struct.Dyn.*, 16(5), 719-734.
- Ramamoorthy, S. K., Gardoni, P., and Bracci, J. M. (2008). "Seismic fragility and confidence bounds for gravity load designed reinforced concrete frames of varying height." *J.Struct.Eng.*, 134(4), 639-650.
- Ramamoorthy, S. K., Gardoni, P., and Bracci, J. M. (2006). "Probabilistic demand models and fragility curves for reinforced concrete frames." *J.Struct.Eng.*, 132(10), 1563-1572.
- Ramirez, C. M., Liel, A. B., Mitrani-Reiser, J., Haselton, C. B., Spear, A. D., Steiner, J., Deierlein, G. G., and Miranda, E. (2012). "Expected earthquake damage and repair costs in reinforced concrete frame buildings." *Earthquake Engineering and Structural Dynamics*, 41(11), 1455-1475.
- Reitherman, R. (1985). "Review of earthquake damage estimation methods." *Earthquake Spectra*, 1(4), 805-847.
- Réveillère, A. (2012). "MATRIX project: New multi-hazard and multi-risk assessment methods for Europe." *Rep. No. D.4.1: Fragility functions-impact of repeated events with various intensities on the fragility functions for a given building typology at local scale.*
- Riisch, H., and Rehm, G. (1963). "Versuche mit Betonformstählen." *Deutscher Ausschuss Fur Stahlbeton, Bulletins*, (140 Part 1, 160, Part 2, 165 Part 3)
- Rodriguez, M., and Park, R. (1991). "Repair and strengthening of reinforced concrete buildings for seismic resistance." *Earthquake Spectra*, 7(3), 439-439.
- Rosowsky, D., and Ellingwood, B. (2002). "Performance-Based Engineering of Wood Frame Housing: Fragility Analysis Methodology." *J.Struct.Eng.*, 128(1), 32-38.

- Ryan, T. P. (2008). *Modern regression methods*. John Wiley & Sons Inc., New York.
- Ryu, H., Luco, N., Uma, S., and Liel, A. (2011). "Developing fragilities for mainshock-damaged structures through incremental dynamic analysis." *Ninth Pacific Conference on Earthquake Engineering, Auckland, New Zealand*.
- Saadatmanesh, H., Ehsani, M. R., and Jin, L. (1997). "Repair of earthquake-damaged RC columns with FRP wraps." *ACI Struct.J.*, 94(2), 206-215.
- Salonikios, T. N., Kappos, A. J., Tegos, I. A., and Penelis, G. G. (1999). "Cyclic load behavior of low-slenderness reinforced concrete walls: Design basis and test results." *ACI Struct.J.*, 96(4), 649-660.
- Sasani, M., and Der Kiureghian, A. (2001). "Seismic fragility of RC structural walls: displacement approach." *Journal of Structural Engineering New York, N.Y.*, 127(2), 219-228.
- Seligson, H. A., and Eguchi, R. T. (2005). "The true cost of earthquake disasters: an updated tabulation of losses for the 1994 Northridge earthquake." *International Symposium on Earthquake Engineering Commemorating the Tenth Anniversary of the 1995 Kobe Earthquake, Kobe, Japan*, .
- Shinozuka, M., Feng, M. Q., Lee, J., and Naganuma, T. (2000). "Statistical analysis of fragility curves." *J.Eng.Mech.*, 126(12), 1224-1231.
- Simoen, E., Moaveni, B., Conte, J., and Lombaert, G. (2013). "Uncertainty quantification in the assessment of progressive damage in a 7-story full-scale building slice." *J.Eng.Mech.*, 139(12), 1818-1830.
- Singhal, A., and Kiremidjian, A. S. (1996). "Method for probabilistic evaluation of seismic structural damage." *Journal of Structural Engineering New York, N.Y.*, 122(12), 1459-1467.

- Sittipunt, C., Wood, S. L., Lukkunaprasit, P., and Pattararattanakul, P. (2001). "Cyclic behavior of reinforced concrete structural walls with diagonal web reinforcement." *ACI Struct.J.*, 98(4), 554-562.
- Stone, J. C. (1996). *A course in probability and statistics*. Duxbury, Belmont, California.
- Stone, W. C., and Taylor, A. W. (1993). *Seismic Performance of Circular Bridge Columns Designed in Accordance with AASHTO/CALTRANS Standards*. U.S. Department of Commerce, National Institute of Standards and Technology, Gaithersburg, MD.
- Stone, W. C., and Taylor, A. W. (1994). "ISDP: integrated approach to seismic design of reinforced concrete structures." *Journal of Structural Engineering New York, N.Y.*, 120(12), 3548-3565.
- Taghavi, S., and Miranda, E. (2003). "Response assessment of non structural building components." *Rep. No. 2003/05*, Pacific Earthquake Engineering Research Centre, UC Berkeley, CA.
- Takahashi, J., Shibata, A., and Shiga, T. (1988). "Crack indices of reinforced concrete shear walls for seismic damage evaluation." *Proceedings of Ninth World Conference on Earthquake Engineering, vol. IV4*, 2-9.
- Talachian, S. (2010). "Probabilistic models for damage and repair cost for reinforced concrete structural members". M.A.Sc. thesis. The University of British Columbia, Vancouver, BC, Canada.
- Teraoka, M., Kanoh, Y., Tanaka, K., and Hayashi, K. (1990). "Strength and ductility behavior of RC interior beam-column joint using high strength concrete." *Proc. Jpn. Concr. Inst.*, 12 633-638.
- "The Official Website of the City of New York " <http://www1.nyc.gov/> .
- Thomsen IV, J. H., and Wallace, J. W. (2004). "Displacement-based design of slender reinforced concrete structural walls - Experimental verification." *J.Struct.Eng.*, 130(4), 618-630.

- Thomsen, J., and Wallace, J. (1995). "Displacement-based design of reinforced concrete structural walls: An experimental investigation of walls with rectangular and T-shaped cross-sections." *Rep. No. CU/CEE-95-06*, Clarkson University.
- Tran, T. A. (2010). "Lateral load behavior and modeling of low-rise RC walls for performance-based design". PhD Seminar. University of California, Los Angeles.
- Vallenas, J., Bertero, V., and Popov, E. (1979). "Hysteretic behavior of reinforced concrete structural walls." *Rep. No. UCB/EERC-79/20*, University of California, Berkeley.
- Vecchio, F. (2000). "Disturbed stress field model for reinforced concrete: formulation." *J.Struct.Eng.*, 126(9), 1070-1077.
- Vecchio, F. J., and Collins, M. P. (1986). "Modified compression field theory for reinforced concrete elements subject to shear." *Journal of the American Concrete Institute*, 83(2), 219-231.
- Ventura, C. E., Finn, W. D. L., Onur, T., Blanquera, A., and Rezai, M. (2005). "Regional seismic risk in British Columbia - Classification of buildings and development of damage probability functions." *Canadian Journal of Civil Engineering*, 32(2), 372-387.
- Vranes, K., and Pielke, R. (2009). "Normalized earthquake damage and fatalities in the united states: 1900-2005." *Nat.Hazards Rev.*, 10(3), 84-101.
- Walker, S. (2001). "Seismic Performance of Existing RC Beam-Column Joints". M.Sc. thesis. University of Washington.
- Wang, T. (1975). "Hysteretic Behavior of Reinforced Concrete Framed Walls". PhD Dissertation. University of California, Berkeley.
- Wen, Y., Ellingwood, B., Bracci, J. M., and Center, M. E. (2004). *Vulnerability function framework for consequence-based engineering*. Mid-America Earthquake Center.
- Wen, Y. K., and Ellingwood, B. R. (2005). "The role of fragility assessment in consequence-based engineering." *Earthquake Spectra*, 21(3), 861-877.

- Williams, M. S., and Sexsmith, R. G. (1995). "Seismic damage indices for concrete structures. A state-of-the-art review." *Earthquake Spectra*, 11(2), 319-319.
- Yang, T. Y., Moehle, J., Stojadinovic, B., and Der Kiureghian, A. (2009). "Seismic performance evaluation of facilities: Methodology and implementation." *J.Struct.Eng.*, 135(10), 1146-1154.
- Zaid, S. (2001). "Behavior of reinforced concrete beam-column connections under earthquake loading". Ph.D. dissertation. University of Tokyo, Japan.
- Zhang, H. (2007). "Study on the performance-based seismic design method for shear wall structures". PhD dissertation. Tongji University, China.
- Zhang, Y., and Wang, Z. (2000). "Seismic behavior of reinforced concrete shear walls subjected to high axial loading." *ACI Struct.J.*, 97(5), 739-750.
- Zhou, G. (2004). "Research on the hysteric behavior of high-rise reinforced concrete shear walls". Master's Thesis. Tongji University, China.
- Zhu, L., Elwood, K. J., Haukaas, T., and Gardoni, P. (2006). "Application of a probabilistic drift capacity model for shear-critical columns " *ACI Special Publication*, 236 81-102.

Appendix A REINFORCED CONCRETE SHEAR WALL DATABASE

This appendix presents the database of test data for the reinforced concrete shear wall. The database is utilized for developing models in Chapter 3.

Table A-1. Database of test data for RC shear wall.

Test No.	$P/(A_g f_c)$	h_w/l_w	f'_c [Mpa]	f_{yl} [MPa]	f_{ylb} [Mpa]	ρ_{lw} [%]	ρ_{lb} [%]	ρ_{hw} [%]	ρ_{hb} [%]	δ_y [%]	δ_u [%]	δ_c [%]
1	0.073	2	47.1	399.9	471.62	0.27	3.17	0.26	1.55	0.62	2.17	2.87
2	0.071	2	48.4	448.17	477.13	0.61	7.14	0.61	1.55	0.74	3.03	3.03
3	0.071	1.5	48.75	399.91	471.62	0.32	3.17	0.32	1.55	0.49	3.06	3.94
4	0	1	22.2	610	585	0.56	1.7	0.56	1.95	0.16	0.67	0.83
5	0	1	21.6	610	585	0.28	1.3	0.28	1.73	0.22	0.40	0.88
6	0.07	1	23.9	610	585	0.28	1.3	0.28	1.73	0.24	0.54	1.29
7	0	1	23.2	610	585	0.28	1.3	0.28	1.73	0.26	0.42	0.83
8	0	1	24.9	610	585	0.28	1.7	0.28	1.73	0.33	0.75	1.33
9	0	1.5	26.1	610	585	0.56	1.7	0.56	1.21	0.45	0.7	1.53
10	0	1.5	26.2	610	585	0.28	1.3	0.28	1.07	0.44	1.11	2
11	0.07	1.5	24.1	610	585	0.28	1.3	0.28	1.07	0.28	0.89	1.44
12	0	1.5	24.6	610	585	0.28	1.3	0.28	1.67	0.44	1	1.5
13	0	1.5	22	610	585	0.28	1.3	0.28	1.67	0.40	0.81	1.39
14	0	1.5	27.5	610	585	0.28	1.3	0.56	1.88	0.67	1.05	1.5
15	0.24	2.14	36.8	305	405	0.67	6.2	1.00	2.26	0.39	1.67	2.08
16	0.35	2.14	40.2	305	432	0.67	4.5	1.00	2.26	0.37	1.4	1.59
17	0.24	2.14	43.1	305	375	0.67	12.6	1.72	1.51	0.56	1.8	2.1
18	0	3.5	53.02	521	450	0.24	1.1	0.27	0	0.55	2.22	3.33

Test No.	$P/(A_g f'_c)$	h_w/l_w	f'_c [Mpa]	f_{yl} [MPa]	f_{ylb} [Mpa]	ρ_{lw} [%]	ρ_{lb} [%]	ρ_{hw} [%]	ρ_{hb} [%]	δ_y [%]	δ_u [%]	δ_c [%]
19	0	3.5	53.64	532	410	0.24	3.7	0.54	0	0.69	2.78	2.89
20	0	3.5	47.3	478	438	0.24	1.09	0.27	1.64	0.55	3.89	4.45
21	0	3.5	45.3	502	444	0.24	3.7	0.54	1.35	0.79	2.74	2.89
22	0.13	3.5	21.9	512	441	0.24	3.7	0.54	0.81	0.72	1.69	1.78
23	0.08	3.5	49.4	490	458	0.24	3.68	0.54	1.35	0.71	2.74	2.83
24	0.09	3.5	42.0	454	447	0.24	3.68	1.38	1.35	0.61	3.33	3.89
25	0.09	3.5	44.1	461	430	0.24	3.68	0.54	1.35	0.67	3.05	3.33
26	0	1	25.5	424	448	0.38	3.11	0.26	0	0.17	0.58	1.49
27	0	1	31.4	424	424	0.38	1.71	0.26	0	0.27	1.30	1.82
28	0	1	31	424	424	0.38	1.71	0.26	0	0.40	1.32	2.2
29	0	1	43.7	424	448	0.38	3.11	0.26	0	0.50	1.17	2
30	0.1	0.9	28.3	424	424	0.26	1.36	0.29	0	0.23	0.58	1.2
31	0.1	0.89	31.4	424	424	0.26	1.36	0.29	0	0.25	0.87	1.25
32	0.05	0.89	31.9	424	424	0.26	1.36	0.29	0	0.21	0.79	1.25
33	0.05	0.89	32.0	424	424	0.26	1.36	0.29	0	0.23	0.88	1.27
34	0	0.89	29.9	424	424	0.26	1.36	0.29	0	0.34	0.78	2.54
35	0	0.89	31	424	424	0.26	1.36	0.29	0	0.25	0.87	1.25
36	0	1.00	31.7	352	352	0.31	1.36	0.31	0	0.20	0.70	1.00
37	0	1.00	31.9	352	352	0.31	1.36	0.31	0	0.20	0.70	1.00
38	0	1.00	33	352	352	0.31	1.36	0.31	0	0.20	0.70	1.00
39	0	1.00	33.6	352	352	0.31	1.36	0.31	0	0.20	0.70	1.00
40	0	2	19.4	392	0	0.25	0	0.13	0	0.23	0.93	0.95
41	0	2	19.6	402	0	0.25	0	0.24	0	0.375	1.25	1.5
42	0	2	19.5	402	0	0.25	0	0.38	0	0.375	0.94	1.8
43	0	1.4	17.6	314	0	0.26	0	0.13	0	0.21	0.75	1.15
44	0	1.4	18.1	471	0	0.13	0	0.25	0	0.208	0.88	1.16

Test No.	$P/(A_g f'_c)$	h_w/l_w	f'_c [Mpa]	f_{yl} [MPa]	f_{y1b} [Mpa]	ρ_{lw} [%]	ρ_{lb} [%]	ρ_{hw} [%]	ρ_{hb} [%]	δ_y [%]	δ_u [%]	δ_c [%]
45	0	1.4	15.7	471	0	0.26	0	0.25	0	0.28	1.13	1.18
46	0	1.4	17.6	366	0	0.26	0	0.25	0	0.198	0.79	0.97
47	0	1.4	16.4	367	0	0.25	0	0.25	0	0.20	0.49	0.83
48	0	1	16.3	362	0	0.25	0	0.13	0	0.24	0.53	0.80
49	0	1	17	366	0	0.13	0	0.25	0	0.25	0.6	0.77
50	0	1	18.1	370	0	0.26	0	0.255	0	0.19	0.68	0.81
51	0	0.7	17.1	366	0	0.25	0	0.125	0	0.08	0.37	0.71
52	0	0.7	19	366	0	0.13	0	0.25	0	0.26	0.44	0.67
53	0	0.7	18.8	366	0	0.25	0	0.25	0	0.17	0.42	0.67
54	0	1.4	24.2	0	0	0	0	0	0	0.13	0.30	0.67
55	0	1.4	17.2	0	0	0	0	0	0	0.17	0.32	0.34
56	0	1.4	24.2	431	0	0	0	0.25	0	0.28	0.67	1.17
57	0	1.4	23.9	431	0	0.25	0	0	0	0.11	0.25	0.47
58	0	1	23.9	0	0	0	0	0	0	0.22	0.51	0.82
59	0	1	17.7	0	0	0	0	0	0	0.18	0.53	0.61
60	0	1	23.9	431	0	0	0	0.25	0	0.21	0.36	0.86
61	0	1	23.3	431	0	0.25	0	0	0	0.14	0.44	0.85
62	0	0.7	23.2	0	0	0.00	0	0	0	0.14	0.29	1.50
63	0	0.7	17.9	0	0	0.00	0	0	0	0.076	0.43	0.76
64	0	0.7	23.3	431	0	0.25	0	0	0	0.32	0.42	1.22
65	0.051	2.3	45	600.7	619.9	0.3	1.6	0.25	1.43	0.27	0.70	1.11
66	0.057	2.3	40.5	534.5	747.4	0.3	1.6	0.25	1.59	0.31	1.12	1.42
67	0.058	2.3	39.2	700.2	725.5	0.54	1.3	0.25	1.21	0.4	2.048	2.05
68	0.057	2.3	40.9	714.4	674.9	0.54	0.0	0.25	0	0.35	1.36	1.71
69	0.14	1.8	87.6	1001	776	0.47	2.36	0.47	2.83	0.6	1.97	3
70	0.13	1.2	93.6	1001	776	0.47	2.4	0.47	2.83	0.7	1.5	2.1

Test No.	$P/(A_g f'_c)$	h_w/l_w	f'_c [Mpa]	f_{yl} [MPa]	f_{ylb} [Mpa]	ρ_{lw} [%]	ρ_{lb} [%]	ρ_{hw} [%]	ρ_{hb} [%]	δ_y [%]	δ_u [%]	δ_c [%]
71	0.17	1.8	55.5	753	840	0.24	2.4	0.23	1.96	0.37	0.99	1.3
72	0.2	1.8	54.6	753	840	0.24	3.1	0.23	1.96	0.5	0.93	1.45
73	0.16	1.8	60.3	753	840	0.47	3.1	0.47	1.96	0.48	1.52	2
74	0.17	1.8	65.2	753	776	0.47	4.0	0.47	1.96	0.63	1.34	1.7
75	0.12	1.2	103.3	1079	761	0.47	2.4	0.47	2.83	0.28	0.73	1.3
76	0.12	1.2	137.5	1079	761	0.47	3.3	0.47	3.33	0.33	0.78	1.18
77	0.17	1.2	65.1	792	1009	0.18	5.3	0.18	2.54	0.29	0.765	0.855
78	0.15	1.2	70.8	792	1009	0.31	5.3	0.31	2.54	0.38	0.75	0.85
79	0.15	1.2	71.8	792	1009	0.47	5.3	0.47	2.54	0.38	0.75	0.85
80	0.18	1.2	103.4	792	1009	0.47	5.3	0.47	2.54	0.3	0.6	0.75
81	0.14	1.8	76.7	792	1009	0.47	5.3	0.47	2.54	0.57	1	1.067
82	0.15	1.2	71.5	792	1009	0.88	5.3	0.88	2.54	0.35	0.8	0.85
83	0.14	1.2	76.1	792	1009	1.29	5.31	1.28	2.54	0.4	0.71	0.825
84	0.35	1.2	62.6	810	848	0.71	5.31	0.707	1.88	0.5	1.85	2
85	0.35	1.2	68.6	810	848	0.71	2.36	0.707	1.88	0.45	1.5	1.7
86	0.35	1.2	66.5	810	848	0.71	2.36	0.707	0.94	0.415	1.45	1.75
87	0.3	1.2	61.4	810	848	0.71	2.4	0.707	1.88	0.415	1.45	1.75
88	0.35	1.2	59.7	810	848	0.71	2.36	0.707	1.88	0.395	1.5	1.7
89	0.04	0.5	58.3	321	389	1.06	7.93	1.05	0.65	0.24	0.64	0.91
90	0.04	0.5	58.1	321	389	1.77	7.9	1.77	0.65	0.24	0.64	0.82
91	0	0.5	83.6	369	377	0.50	2.55	0.50	0.904	0.2	0.86	2.1
92	0	0.5	83.6	369	393	0.50	5.44	0.50	0.904	0.3	0.81	1.2
93	0.2	1.2	72.7	848	385	1.18	2.36	1.18	2.26	0.5	1.5	1.7
94	0.13	1.2	79	848	385	1.18	2.4	1.18	2.26	0.4	2.7	3
95	0.08	1.2	79.4	848	579	1.18	2.4	1.18	2.26	0.4	1.9	2.9
96	0.03	0.4	82.3	560	560	1.31	1.31	1.31	1.50	0.41	1.89	2.12

Test No.	$P/(A_g f'_c)$	h_w/l_w	f'_c [Mpa]	f_{yl} [MPa]	$f_{y lb}$ [Mpa]	ρ_{lw} [%]	ρ_{lb} [%]	ρ_{hw} [%]	ρ_{hb} [%]	δ_y [%]	δ_u [%]	δ_c [%]
97	0.03	0.4	101.8	792	792	1.31	1.31	1.31	1.50	0.61	1.51	1.73
98	0.14	1.4	62.3	413	360	1.02	3.98	1.02	1.21	0.375	1.3	2
99	0.14	1.4	62.3	413	360	1.48	4.0	1.48	1.21	0.3	1.3	1.5
100	0.14	1.4	62.3	413	360	1.02	3.98	1.02	1.21	0.33	1	1.5
101	0.1	3.0	31.6	448	434	0.33	5.86	0.33	1.34	0.46	2.12	2.51
102	0.07	3.0	43.7	448	434	0.33	5.86	0.33	2.01	0.61	2.29	2.35
103	0.075	3.0	41.7	448	434	0.45	2.19	0.45	2.42	1.04	2.19	2.19
104	0.1	2.8	24.1	289	289	1.11	2.53	1.11	1.51	0.39	1.35	2.03
105	0.1	2.8	24.9	289	289	1.11	2.52	1.11	1.51	0.46	1.96	3.11
106	0.25	3.0	17.7	452	365	0.42	9.42	0.42	2.09	0.46	0.73	0.8
107	0.2	3.0	17.7	452	365	0.42	4.71	0.42	3.14	0.73	1.68	1.83
108	0.1	2.5	37.33	345	526.7	0.84	3.72	0.84	1.81	0.64	2.07	2.35
109	0.2	2.5	37.33	345	526.7	0.84	3.7	0.84	1.81	0.79	1.97	2.17
110	0.1	2.5	37.33	345	526.7	0.84	3.72	0.84	1.81	0.61	1.67	1.89
111	0.2	2.5	37.33	345	526.7	0.84	3.72	0.84	1.81	0.8	1.78	1.89
112	0.1	2.0	19.7	392	379	0.36	1.88	0.36	1.096	0.3	1	1.05
113	0.2	2.0	19.7	392	379	0.36	1.88	0.36	1.096	0.35	1.1	1.15
114	0.3	2.0	19.7	392	379	0.36	1.9	0.36	1.096	0.35	1.05	1.15
115	0.4	2.0	19.7	392	379	0.36	1.88	0.36	1.096	0.27	0.6	0.65
116	0.3	1.0	37.7	392	379	0.36	1.88	0.36	1.096	0.27	0.89	0.98
117	0.3	1.5	37.7	392	379	0.36	1.88	0.36	1.096	0.2	0.77	0.92
118	0.3	2.0	37.7	392	379	0.36	1.88	0.36	1.096	0.25	0.675	0.71
119	0.3	2.5	37.7	392	379	0.36	1.88	0.36	1.096	0.392	0.708	0.88
120	0.3	2.0	37.7	392	343	0.36	1.21	0.36	1.096	0.2	0.6	0.63
121	0.3	2.0	37.7	392	352	0.36	1.88	0.36	1.096	0.25	0.5	0.55
122	0.3	2.0	37.7	392	325	0.36	2.70	0.36	1.10	0.33	0.8	0.86

Test No.	$P/(A_g f'_c)$	h_w/l_w	f'_c [Mpa]	f_{yl} [MPa]	f_{y1b} [Mpa]	ρ_{lw} [%]	ρ_{lb} [%]	ρ_{hw} [%]	ρ_{hb} [%]	δ_y [%]	δ_u [%]	δ_c [%]
123	0.3	2.0	37.7	392	379	0.36	1.50	0.36	1.00	0.25	0.6	0.62
124	0.3	2.0	37.7	392	379	0.36	2.50	0.36	1.30	0.3	0.8	0.9
125	0.3	2.0	37.7	392	379	0.36	1.90	0.36	0.50	0.32	0.75	0.92
126	0.3	2.0	37.7	392	379	0.36	1.90	0.36	1.50	0.2	0.95	1
127	0	0.5	27.2	300	300	0.81	2.26	1.68	6.80	0.3	0.93	1.33
128	0	0.5	28	300	300	0.65	2.26	1.49	6.80	0.25	0.92	1.32
129	0	0.5	26	315	300	0.39	1.81	1.68	5.40	0.23	0.39	1.6
130	0	0.5	30.2	315	300	0.39	1.36	0.67	5.40	0.23	1.2	1.73
131	0.1	7.2	49	455	455	0.27	0.67	0.27	1.70	0.44	2.38	2.46
132	0	2.0	36.9	550	500	0.31	2.83	0.39	0	0.55	1.62	1.84
133	0	2.0	31.8	550	530	0.47	2.65	0.35	0	0.46	0.92	2.25
134	0	2.0	38.6	550	500	0.31	2.83	0.35	0	0.58	1.44	1.89
135	0	2.0	32	550	530	0.47	2.65	0.39	0	0.65	1.71	1.88
136	0	2.0	45.8	550	530	0.31	2.9	0.42	0	0.52	2	2.21
137	0	2.0	38.9	550	530	0.31	2.9	0.59	0	0.51	1.97	2.14
138	0.051	2.9	34.5	562	540	0.17	3.1	0.17	0.95	0.65	2.54	2.93
139	0.051	2.9	34.5	562	540	0.17	3.1	0.17	0.95	0.65	1.55	1.63
140	0.098	1.4	36.6	450	473	0.39	2.3	0.52	0	0.32	1.67	2.54
141	0.10	1.4	35.8	450	473	0.52	2.29	0.78	0	0.96	1.57	2.57
142	0.084	3.1	28.1	588	412	0.25	1.27	0.25	0	0.39	2.26	4.30
143	0.083	3.1	28.2	588	412	0.25	1.27	0.25	0	0.53	4.52	4.84
144	0.092	3.1	25.6	588	451	0.25	0.71	0.25	0	0.28	3.68	4.88
145	0.08	3.1	28.7	588	451	0.25	0.71	0.25	0	0.37	0.92	3.13
146	0.11	3.1	20.8	588	451	0.25	0.71	0.25	0	0.2	0.64	2.93

Appendix B COMMUNICATION OF COMPONENT CLASS WITH STRUCTURAL ANALYSIS

This appendix explains the algorithm in Rts for communication of component class with the structural analysis classes. In Rts, all building components either structural or non-structural are modelled with finite elements. These finite elements are generated automatically once an object is instantiated from the component class. The elements are called by the RAssembler, which establishes the stiffness, mass, and damping matrices and the load vectors, which in turn are called by the RStructuralAnalysis to conduct structural analysis. The structural analysis is orchestrated in a model called RComponentResponseModel.

Figure B-1 shows the class map for the building analysis classes in Rts. In Figure B-1, the diamonds indicate the “aggregation” relationship between classes, *i.e.*, the class above the diamond contains the class below. Particularly, it is shown that the RComponentResponseModel class has an RStructuralAnalysis class. On the other hand, the triangles indicate the “inheritance” relationship. That is, the class below the triangle, *i.e.*, subclass, inherits from the class above, *i.e.*, base class. For example, it is shown that the RInelasticStructuralAnalysis is subclass of RStructuralAnalysis. The RComponentResponseModel is located at the most-top level, which indicates that this class contains all classes related to the structural analysis. The class RComponentResponseModel is a subclass of RModel, which means that it can take input from downstream model(s) and return output to upstream model(s). Another subclass of RModel is

RComponentRepairManagerModel. This model basically computes the cost of earthquake and its algorithm is presented in Chapter 4.

The software architecture for structural analysis is designed in the same way as in OpenSees (Haukaas and Der Kiureghian 2007; McKenna *et al.* 2010). The RComponent is the new class, where the performance of building components is assessed. As shown in Figure B-1, RComponent contains elements, from which structural responses are read during analysis to simulate the seismic damage. This chapter only discusses the communication of RComponent with structural analysis as explained in the next paragraphs.

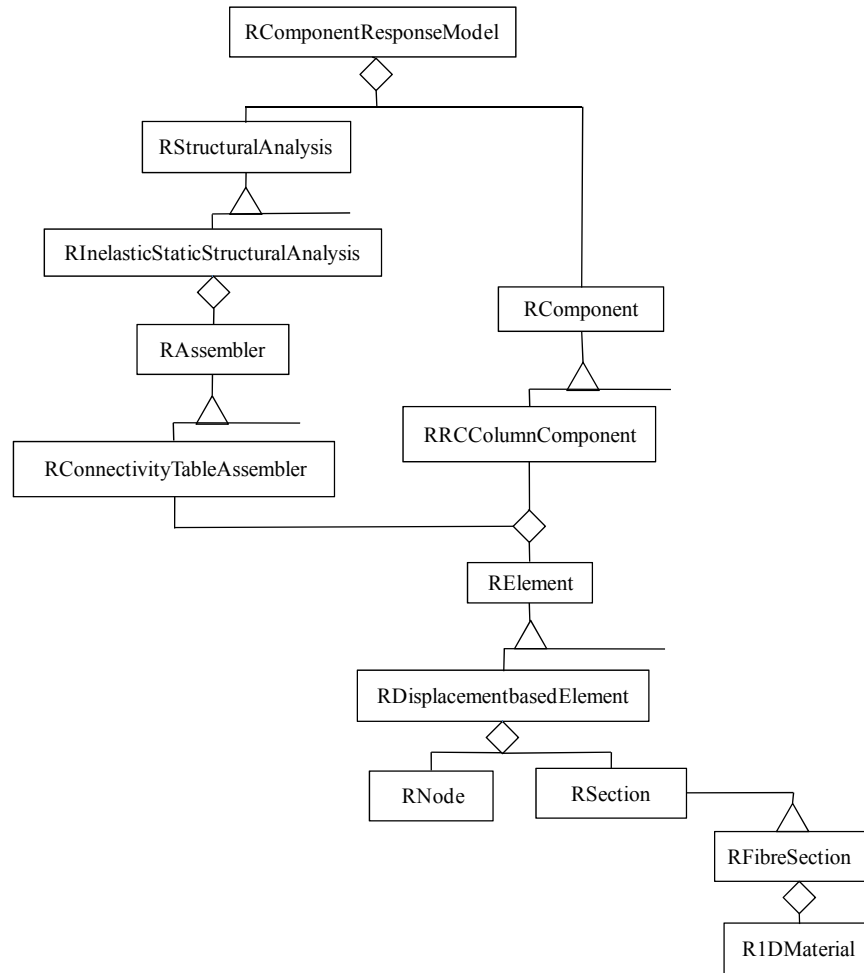


Figure B-1. Class map of Rts building analysis: the inheritance and composition relationship.

The assessment of repair quantities in the RComponent class is conducted with the visualization of the damage to the building components. To visualize the seismic damage, the structural analysis classes are in communication with the RComponent classes to deliver the value of responses that affect the visual damage. The number and type of these responses depend on the component type and its visual damage.

Figure B-2 shows the communication of the RComponent class with the structural analysis classes in Rts. In this figure, the private data members, *i.e.*, the data members that can only be called inside the class, are shown in italic and listed below a dashed line. Also, in Figure B-2 the arrows indicate the calls made from one method to another during the analysis. The numbers on the arrows show the sequence of calls. As stated before, the diamonds indicate the aggregation relationship between classes, *i.e.*, the class above the diamond contain the class below. Particularly, it is shown that RRCShearWallComponent class has an RLinearQuad4Element class.

In Rts, the structural analysis is conducted in the method evaluateModel() in RComponentResponseModel. Once this method is called, call number 1 is made to the method conductStructuralAnalysis() in RInelasticStructuralAnalysis. This is where the structural analysis starts and the displacements and loads are calculated at each time-step. In order to inform the component objects that the updated values of forces and displacements become available, at the end of each time-step call number 2 is made to the method commitState() in RAssembler. Once call number 2 is made, the assembler generates a list of all components and makes call number 3 to the method commitState(). Subsequently, depending on the component type, the method commitState() updates the value of a set of structural responses that affects the visual damage at different parts of the component.

Figure B-2, they are private data members of RC shear wall class. With the exception of *axialLoad*, the value of each data member is updated if the structural response at the time-step exceeds the current value of data member. The value of *axialLoad* is updated at each time-step that the *drift* is updated. This is done by call number 4, 5 and 6. In particular, the axial load and strains for RC shear wall are computed in the method `getResponse()` in the `RLinearQuad4Element` class. However, the displacements are stored in the `RPoint` objects located at the four edges of the component. It is noted that `RPoint` class is used to Hence, `getYDisplacement()` from the points at the top and bottom of shear wall. The method `commitState()` computes drift value using these responses and updates the value of *drift* if the computed drift value is greater.